PRECISION SPRAYER TECHNOLOGIES FOR ENHANCED ORNAMENTAL CROP MANAGEMENT

By

ALEENA RAYAMAJHI

(Under the Direction of Md Sultan Mahmud)

ABSTRACT

Woody ornamentals are essential to landscapes, yet technological advancements in their cultivation often lag behind other agricultural sectors. Traditional spraying methods for ornamental crops can lead to over or under-application of agrochemicals, posing health, environmental, and economic risks. This research aimed to improve precision spraying through advanced technologies, for reducing agrochemical usage while optimizing management practices. This study utilized a high-resolution RGB camera-mounted aerial system and a ground-based LiDAR and depth camera systems to calculate tree characteristics such as height, trunk diameter, and canopy volume, which are crucial for determining precise agrochemical application rates and enabled a comparison between the two methods for assessing canopy characteristics. Additionally, a web application was developed to monitor disease severity and evaluate the efficacy of agrochemicals to quantify disease progression over time. These technologies help enhance agrochemical application efficacy, promoting sustainability, efficiency, and economic viability in ornamental crop management and spraying.

INDEX WORDS: Woody Ornamentals, Precision Spraying, LiDAR, Drone, Deep Learning, Depth Camera, RGB Camera, SAM, Web Application, Canopy Characteristics

PRECISION SPRAYER TECHNOLOGIES FOR ENHANCED ORNAMENTAL CROP MANAGEMENT

By

ALEENA RAYAMAJHI

B.Eng. Institute of Engineering, Tribhuvan University, Nepal, 2018

A Thesis Submitted to the Graduate Faculty of The University of Georgia in Partial Fulfillment of the Requirements for the Degree

MASTER OF SCIENCE

ATHENS, GEORGIA

2024

PRECISION SPRAYER TECHNOLOGIES FOR ENHANCED ORNAMENTAL CROP MANAGEMENT

By

ALEENA RAYAMAJHI

Major Professor:	Md Sultan Mahmud
Committee:	E. W. “Bill” Tollner Jean L. Williams-Woodward Guoyu Lu

Electronic Version Approved:

Ron Walcott
Vice Provost for Graduate Education and Dean of the Graduate School
The University of Georgia
December 2024

ACKNOWLEDGEMENTS

I would like to express my deepest gratitude to my advisor, Dr. Md Sultan Mahmud, for his unwavering support, guidance, and mentorship. His patience and encouragement have been invaluable throughout my journey, and as his first student, I have been fortunate to learn directly from his expertise and work ethic.

I am also deeply thankful to my advisory committee—Dr. E.W. "Bill" Tollner, Dr. Jean L. Williams-Woodward, and Dr. Guoyu Lu—for their valuable suggestions and feedback, which have greatly improved my projects.

A special thanks to my Precision Crop Protection team—Hasan Jahanifar, Muhammad Asif, Muneeb Elahi Malik, Shah Md Abul Hasan, and Md Tauhidul Alam—for their assistance with data collection and thoughtful contributions to my research.

I am immensely grateful to my family—Prava Rayamajhi, Keshab Rayamajhi, and Melina Rayamajhi—for their unwavering love, support, and motivation. Being away from my home country has been challenging, but their encouragement has kept me focused on achieving my goals.

I extend my heartfelt thanks to my confidant, Anjan Dhungana, for his invaluable feedback on my projects and for helping me proofread my thesis.

Lastly, I would like to acknowledge the funding partners of this study: United States Department of Agriculture (USDA)'s National Institute of Food and Agriculture (NIFA) Hatch Project (Accession No. 7007738) and the Startup and Institute for Integrative Precision Agriculture (IIPA) Seed Grant Funds from the University of Georgia.

TABLE OF CONTENTS

LIST OF TABLES

Page

LIST OF FIGURES

Page

CHAPTER 1

INTRODUCTION

Woody ornamental plants beautify indoor and outdoor spaces, adding color, improving air quality, boosting mood, and supporting biodiversity (Huylenbroeck, 2018). They establish vertical layers from the ground upwards, offering several ornamental and environmental advantages. Shrubs play a role in delineating different areas within the landscape. Blooming woody plants contribute vibrant hues and delightful fragrances to outdoor spaces, particularly during spring. The growing economic importance of ornamental plants is evident in numerous countries where international demand has surged significantly (Kleunen et al., 2018). Reflecting this trend, the ornamental plants market, valued at USD 56.8 billion in 2023, is projected to reach USD 98.4 billion by 2032, with a compound annual growth rate (CAGR) of 6.3% (Business Research Insights, 2024). This robust growth reflects the enduring popularity and economic significance of ornamental plants worldwide. Woody ornamentals include a vast array of genera, species, and cultivars, displaying a wide range of phenotypic diversity (Winkelmann et al., 2020) and are commonly used in landscaping, parks, and gardens, improving life quality in urban and rural areas.

The ornamental industry in the United States plays an important role in its economy. Some of the popular ornamental trees in the Southeastern United States are Red Buckeye *(Aesculus pavia)*, Japanese Holly *(Ilex crenata)*, Bottlebrush Buckeye (*Aesculus parviflora*), etc. (Lance, 2004). Ornamental plant cultivation is a major part of the U.S. horticultural industry, however, one of the major issues - disease infections, poses a considerable threat, impacting both the visual appeal and economic viability of crops (Traversari et al., 2021). Woody ornamentals face various biotic and abiotic stresses, which make them susceptible to

disease infestations. Several disease categories, such as powdery mildew, leaf spots, and crown rot, are prevalent among various ornamental plant species (Singh et al., 2012). While they may originate from distinct pathogens, management approaches tend to be similar within each disease category (Singh et al., 2012). Effective management of various pests and diseases is crucial to ensure the production of high-quality ornamental nursery crops meets the standards demanded by the market. Pesticides play a significant role in protecting ornamental plants from pests, diseases, and weeds while also preserving their aesthetic appeal. Ornamental industry heavily relies on pesticides to safeguard these plants from diseases and pests (Carvalho et al., 2019).

The current spraying practice in nurseries primarily involves broadcast applications, where agrochemicals are sprayed uniformly over a large area rather than targeting specific plants. Farmers typically use spraying equipment such as backpack sprayers or tractor-mounted sprayers to uniformly apply pesticides in the crop field (Zwertvaegher et al., 2017). Such conventional pesticide spray technologies exhibit poor application efficiency, leading to the overuse of pesticides across both targeted and unintended areas (Matthews et al., 2014). The inefficiency of conventional spraying methods results in increased production costs, heightened risks of pesticide exposure to workers, and environmental contamination (Matthews et al., 2014). At the same time, over-use of agrochemicals can degrade plant conditions, develop resistance to pesticides, and escalate production expenses (Patle et al., 2019). Conventional air blast sprayers used in tree crops typically distribute less than 30% of the pesticide onto the intended tree canopies, with the majority lost to ground runoff or drift (Zhu et al., 2006). This inefficiency arises from the inability of conventional systems to adapt spray volume based on the size and shape of the tree canopy during application in ornamental nurseries. Additionally, these sprayers dispense a significant amount of agrochemicals in open spaces between trees and into untargeted areas, such as above short trees or around trunks beneath canopies.

Consequently, a large portion of the pesticide is applied inefficiently, increasing production costs without necessarily enhancing pest control, despite following labeling guidelines. To address these challenges and improve profitability in the woody ornamental industry, precise control over pesticide application is imperative. While precision spraying technology may involve initial costs, it can reduce overall pesticide use, minimize environmental impact, and improve application efficiency, potentially offsetting costs over time.

Precision or intelligent spray application, also known as targeted spraying, involves acquiring specific information about the tree, such as its size, shape, structure, and canopy density, and then precisely applying pesticides as required (Maghsoudi & Minaei, 2014). Advanced sensors mounted on drones can provide critical data on tree count, height, canopy area, and volume, enabling growers to make efficient, data-driven decisions (Puliti et al., 2015). However, UAVs with sensors alone are not sufficient to get valuable details of tree structures. In order to get detailed information regarding tree characteristics such as trunk diameter, ground-based sensing is important (Fekry et al., 2022). The ornamental industry can enhance production processes and management practices by leveraging precision technologies such as computer vision and advanced equipment, including sensors and UAVs.

Measuring tree canopy parameters or characteristics is essential to control precision sprayer nozzles automatically and/or variably. This information is usually gathered from various sensors such as cameras, ultrasound devices, and lasers using aerial or ground-based systems. Moreover, assessing the tree canopy parameters such as tree height, canopy structure, and density can help growers accurately estimate expenses for a nursery, mitigate the risks of overuse or underuse due to precise application, enhance resource utilization, and promote sustainable agricultural practices (Maghsoudi & Minaei, 2014; Solanelles et al., 2006).

Various aerial sensing techniques, such as the integration of UAVs equipped with sensors, have been deployed in forest studies (Guimarães et al., 2020; Kwong & Fung, 2020). However, their application in agriculture has commenced only recently (Torres-Sánchez et al., 2015; Weiss et al., 2020). Aerial sensing or aerial surveying refers to the use of various airborne platforms equipped with sensors to collect data about the earth's surface and atmosphere. UAVs are frequently utilized in conjunction with aerial sensing technologies. Human operators remotely control these aircraft or can operate autonomously based on pre-programmed instructions or artificial intelligence algorithms (Internacional, 2011). UAVs serve as versatile platforms for deploying various sensors to collect data over different terrains and environments (Fahlstrom et al., 2022). Equipped with sensors such as cameras, LiDAR (Light Detection and Ranging), multispectral or hyperspectral imagers, thermal sensors, and even radar systems, UAVs enable efficient and cost-effective aerial sensing operations. In contrast to satellite-based operations or conventional manned photogrammetric surveys, UAV flight missions offer significant operational flexibility regarding expenses, locations, platforms, timing, and the ability to repeat missions (Nex & Remondino, 2014). UAVs equipped with RGB sensors can be one of the methods to get information regarding canopy attributes. Several studies that have implemented UAV for canopy parameter measurement using high-resolution imagery (Poblete-Echeverría et al., 2017) which show promise.

While aerial systems are invaluable for surveying vast fields to gather tree attributes, ground-based systems equipped with sensors remain essential for obtaining precise parameters such as tree details, including trunk diameter (Zhou et al., 2022). Ground-based sensing involves the utilization of terrestrial platforms equipped with sensors to acquire data related to target area or phenomena (Sui et al., 2008). These platforms can include fixed installations, mobile vehicles, or even handheld devices. By deploying these sensors close to the target area, ground-based sensing provides valuable information for applications such as environmental

monitoring, surveillance, agriculture, and scientific research (Barber et al., 2008). It has been employed in agriculture and forestry to get detailed information regarding crops (Van der Zande et al., 2006). Ground-based systems equipped with sensors such as LiDAR can provide detailed information regarding tree height and trunk diameter (Henning & Radtke, 2006). LiDAR is a device that emits a laser beam in visible light or near-infrared spectrum towards a target direction. The time taken for the laser pulse to return to the sensor, along with the intensity of the returned signal, is analyzed to determine the distance to objects and the level of scattering in the beam's path. Terrestrial laser scanning (TLS), alternatively known as terrestrial LiDAR, gathers XYZ coordinates of multiple points from the objects by emitting laser pulses towards these points and calculating the distance from the device to the target. Stereo vision, when combined with LiDAR fusion technology, offers a powerful solution for various agricultural applications, such as determining a more accurate and versatile depth estimation of ornamental trees (Jeon & Zhu, 2023).

Assessing the effectiveness of fungicides is important in optimizing precision spray applications, safeguarding ornamental plants against fungal diseases, and preserving their vitality. To evaluate the effectiveness of fungicide treatments, growers often rely on visual observation. They examine disease spots post-application to identify any changes in their size or distribution. This method, however, is inefficient as it is subjective, unquantifiable, and demands significant time and effort.

To address this challenge and minimize reliance on pesticides, there is a growing need for sustainable approaches to pathogen control. In particular, the timely and precise identification of symptoms on a large scale is crucial for achieving effective, energy-efficient, and targeted disease management. Computer vision emerges as a promising solution, offering early and accurate detection of symptoms, thereby supporting the development of more sustainable strategies for managing fungal outbreaks in ornamental plant production. Computer

vision technologies encompass a wide range of methods and tools like deep learning that enable machines to interpret and understand visual information from the real world, relying on algorithms and computational models to analyze and extract meaningful information from images or video data (Chouhan et al., 2020; Hassaballah & Awad, 2020). Deep learning revolutionizes computer vision, empowering machines to perceive and interpret visual data with unparalleled accuracy and efficiency (Voulodimos et al., 2018). Computer vision techniques such as instance segmentation tackle the dual challenges of identifying individual objects within an image while also delineating their precise boundaries (Hafiz & Bhat, 2020). This method integrates object detection and semantic segmentation tasks, allowing for a comprehensive understanding of the visual scene by recognizing distinct objects and providing pixel-level segmentation to distinguish their exact shapes and positions within the image (Hafiz & Bhat, 2020).

The current focus of technological research predominantly centers on agricultural crops, leaving a gap in understanding the needs of ornamental species within the industry. There's a lack of attention to the application of precision sprayer technologies in ornamental tree management (Zhu et al., 2010). Our proposed research aims to address this gap by developing specialized precision techniques tailored to precisely determine the ornamental trees' attributes. Through the integration of computer vision, UAVs, stereo vision, and LiDAR fusion, our research seeks to provide accurate measurements of tree dimensions. These methods will offer professionals in the ornamental industry precise data on tree height, canopy volume, and trunk diameter. Such information is vital for effective management practices, including spraying, disease detection, and pruning. Moreover, the adoption of precision sprayer technologies in the ornamental industry could revolutionize pest and disease management. By accurately targeting pesticide applications based on tree characteristics and pest distribution,

professionals can minimize chemical usage, reduce environmental impact, and improve overall plant health.

1.1 Goals and Objectives

The overall goal of this study was to develop precision sprayer systems to apply agrochemical based on the needs of the ornamental plants and evaluate disease severity overtime using a web application. It can be explained using the flowchart presented in Fig. 2.1. The specific objectives of the study are:

i. Measuring ornamental tree canopy attributes for precision spraying using drone technology
ii. Determination of tree attributes using a ground-based system with LiDAR sensor and depth camera
iii. Development of a web application for monitoring disease dynamics and supporting precision sprayer systems in ornamental crops

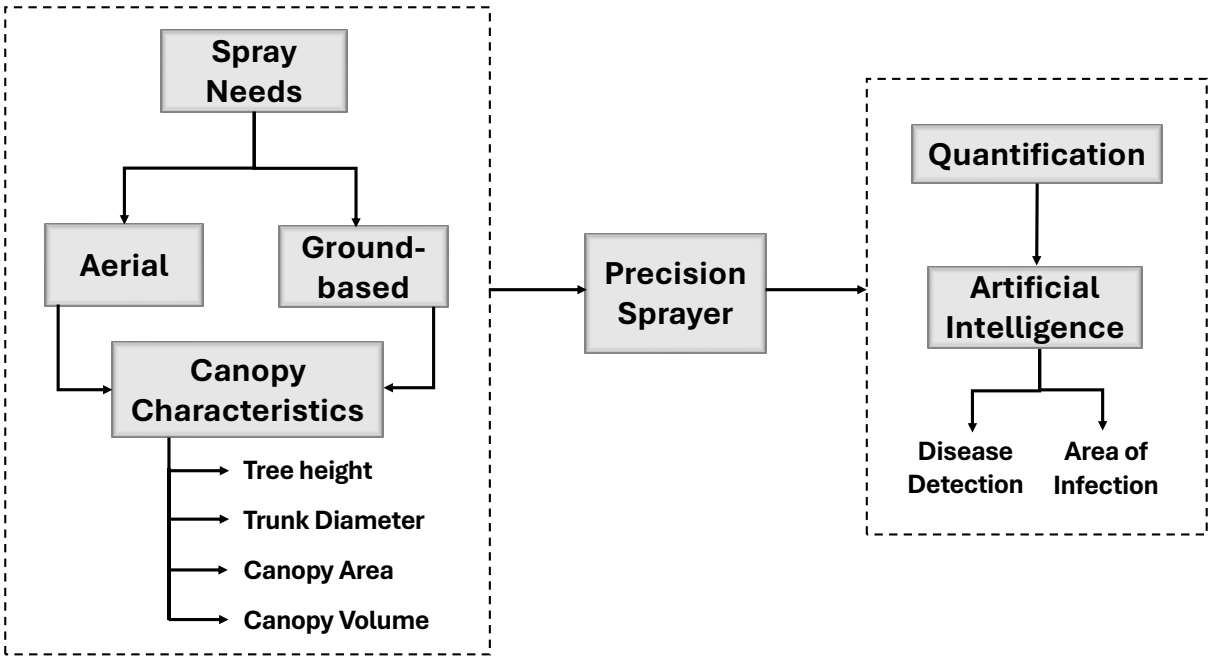

Figure 2.1. Flowchart illustrates the integration of aerial and ground-based technologies to determine canopy characteristics which informs the spray needs for ornamental crop management. These measurements are utilized by precision sprayers to optimize agrochemical applications. Further quantification is achieved through artificial intelligence, which facilitates real-time disease detection and calculates the area of infection.

CHAPTER 2

REVIEW OF LITERATURE

2.1 Significance of the Study

The review of literature emphasizes the pressing challenges in the ornamental plant industry, such as disease prevalence, overuse of agrochemicals, and the environmental and economic consequences of conventional practices. By synthesizing recent advancements in precision agriculture, this study demonstrates the potential of technologies like UAV-RGB systems, LiDAR, depth cameras, and web-based disease monitoring applications to address these issues. The integration of precision spraying techniques promises optimized agrochemical application, reduced environmental impact, and enhanced disease management. This review not only identifies gaps in current practices but also sets the stage for adopting innovative, data-driven solutions tailored to the ornamental plant industry, paving the way for sustainable and efficient production practices.

2.2 Introduction

The ornamental plant industry, encompassing a wide array of species such as floriculture crops, ornamental shrubs, trees, and aquatic plants, is a vital segment within global horticulture, driven by the demand for plants that enhance landscapes, urban spaces, and interior environments. While the sector has flourished in recent years, it faces significant challenges, impacting both productivity and sustainability. Disease management, particularly in controlling fungal pathogens, remains a persistent concern, as ornamental plants are highly susceptible to various microbial threats that can drastically reduce their quality and

marketability. Traditional approaches to disease control, such as broad-spectrum chemical spraying, often lead to overuse of agrochemicals, which increases production costs, elevates environmental risks, and poses health concerns (W. Zhou et al., 2024). Additionally, the industry's reliance on labor-intensive practices for disease monitoring and management has become increasingly difficult due to labor shortages and the variable demands of different plant species (Charania & Li, 2020).

In response, precision agriculture technologies are emerging as a promising solution, offering targeted approaches for enhancing crop health and optimizing resource use. Techniques such as precision spraying and canopy monitoring through UAV-mounted sensors, LiDAR, and depth cameras are transforming traditional practices by enabling growers to apply agrochemicals more efficiently and manage plant health on an individualized basis (Farhan et al., 2024; Lefsky et al., 2002; Pederi & Cheporniuk, 2015; Sankaran et al., 2010). These advancements not only improve the efficiency of chemical use but also reduce the need for intensive manual inspections and labor, helping to mitigate the environmental and economic pressures associated with conventional methods (Charania & Li, 2020). This literature review explores the current landscape of ornamental horticulture, the specific challenges it faces, and the role of precision agriculture in creating more sustainable and efficient practices, paving the way for a modernized approach to ornamental plant production.

2.3 Current Status of Ornamental Plants

The horticultural sector cultivates plants primarily for their visual appeal, encompassing diverse species. Over 2,000 genera of ornamental plants, including floriculture crops, shrubs, trees, and ornamental aquatic plants, contribute to the vibrant diversity of ornamental horticulture (Chen, 2021). The aesthetic value of ornamental plants is determined by their appealing visual characteristics, including the color, shape, and fragrance of their

flowers and leaves, as well as the texture, variegation, and overall architecture of the plants. The cultivation of ornamental plants is a flourishing and financially rewarding segment within the field of plant production. The global market for flowers and ornamental plants is on the rise (Business Research Insights, 2024); however, the industry's future remains uncertain amid the ongoing energy crisis, lasting impacts of the pandemic, and global political turbulence (Salachna, 2022). The growing global demand and diverse applications of ornamental plants call for extensive research into their growth, development, and characteristics although current efforts largely focus on advancing propagation, cultivation techniques, and postharvest handling (Chen, 2021). Modern ornamental plant production necessitates solutions that integrate enhanced production efficiency with a more rational and environmentally sustainable resource utilization. Embracing the principle of sustainable development offers a viable approach to addressing these challenges, facilitating the more efficient utilization of production resources while safeguarding the surrounding environment.

2.4 Existing Challenges in Ornamental Plants

The ornamental industry faces numerous challenges, with diseases being a significant concern. Managing plant health involves complexities such as the potential for contamination during inspections and the shortage of skilled labor for manual disease management. Limited access to advanced diagnostic facilities can delay timely interventions, prompting reliance on conventional practices such as pesticide applications. However, current pesticide spraying methods often result in excessive usage, which may inadvertently increase production costs and pose risks to human health and the environment. Addressing these interconnected challenges requires a proactive and strategic approach to safeguard the health and sustainability of ornamental crops.

All the issues stem from challenges related to agrochemical use. Ornamental plants are vulnerable to various microbial organisms, including bacteria, fungi, and viruses, which can detrimentally affect their growth and commercial value (Singh et al., 2012). Fungi are considered the primary threat and leading cause of pathogen-driven losses among ornamental plants (Fisher et al., 2012). Fungal diseases account for approximately 70% of plant diseases, with bacteria, viruses, and viroid contributing to the remaining cases (Mekapogu et al., 2021). These fungal infections often lead to substantial crop quality and yield reductions, sometimes amounting to up to 40% of the potential yield (Punja, 2006). Visual disease symptoms significantly impact the quality and marketability of ornamental plants, especially cut flowers and potted varieties. Fungal diseases are often controlled using chemical fungicides. However, overreliance or excessive use of these chemicals can lead to the development of pathogen resistance and raise concerns about health and environmental safety (Gavrilescu & Chisti, 2005). Effective disease control can be achieved through host plant resistance, which can reduce the need for pesticide application. However, not all ornamental plants possess natural disease resistance.

2.5 Application of Chemicals in Disease Management

The application of chemicals is one of the most effective methods for controlling plant diseases. The primary aim of applying chemicals is to mitigate losses caused by plant pathogens, ensuring they remain below a specified threshold level. These chemicals directly inhibit pathogen growth on plant surfaces or within host tissues, exerting adverse effects on their life cycle or causing injury, and are widely adopted for their effectiveness in disease control (Ul Haq et al., 2020). Liquid sprays are frequently utilized to treat the foliage of actively growing plants. The manifestation of disease infections is characterized by dynamic changes, and achieving complete control over disease pathogens remains elusive (McQuilken &

Hopkins, 2004). Failure to adequately manage disease infections in densely populated areas can lead to a significant risk of widespread infection. Conventional methods, such as broadcast applications, involve applying chemicals to entire fields once diseases become visually apparent, presenting several challenges. Over usage of the required agrochemicals can inflate production costs and pose risks to trees, while under application may lead to inadequate disease control. Additionally, manual disease inspections may lack accuracy and consistency across individuals. Amin and Islam (2022) conducted a study using seven chemical pesticides to control arthropod pests on ornamental plants and found that using recommended pesticide doses was significantly more effective in reducing pest populations compared to the doses typically applied by farmers, which may not always align with labeled recommendations. In contrast, agrochemicals play a vital role in safeguarding plant health; both overdosing and underdosing of pesticides not only impact plant health but also contribute to increased production costs. An emerging solution for accurately estimating the precise amount of agrochemicals required for individual trees is through advanced precision technology.

2.6 Precision Agriculture

Precision agriculture (PA) refers to the utilization of technologies and methodologies to address the spatial and temporal variations inherent in agricultural production to enhance crop productivity and environmental sustainability. Central to precision agriculture is its reliance on technological advancements. The integration of specific technologies empowers the assessment and management of variability at unprecedented levels of granularity, facilitating improvements in both precision and quality. When implemented adeptly, precision agriculture holds the promise of achieving outcomes of unparalleled excellence, owing to its ability to harness cutting-edge technologies in the service of agricultural optimization (Sishodia et al., 2020). Over the past decade, precision agriculture has garnered significant attention and

recognition within the agricultural sector (Stafford, 2000). As a crop management concept, precision agriculture can potentially address a substantial portion of the growing environmental, economic, market, and public pressures faced by crop farming (Bhakta et al., 2019).

2.7 Role of Precision Spraying

Precision spraying is part of PA, commonly described as a farm management system that relies on information and technology to identify, analyze, and manage variability within fields to achieve optimal profitability, sustainability, and preservation of land resources. Precision spraying can help address the existing challenge of excessive use of agrochemicals in ornamental plants by providing more efficient and accurate ways to monitor plant health, detect pests and diseases early, sense the required amount of chemicals needed, and optimize irrigation and nutrient management (Banu, 2015). Instead of applying a uniform amount of agrochemicals across entire fields based on generalized assumptions, which may not accurately represent the conditions throughout the field (Shanwad et al., 2004), precision spraying acknowledges and addresses site-specific variations within fields, determining the need for chemicals for individual trees, thereby optimizing the use of agrochemicals. Additionally, precision spraying can improve resource utilization, reduce waste, and enhance overall productivity and profitability in the ornamental industry (Thompson et al., 2019). However, implementing precision spraying may require technologies that can provide information regarding plant health, disease detection (Pedersen & Lind, 2017), canopy characteristics, and monitoring disease dynamics. Several studies have indicated that implementing precision spraying techniques in ornamental crops has reduced agrochemical usage while simultaneously enhancing plant productivity. For example, Fessler et al. (Fessler et al., 2022) developed and tested an intelligent, laser-guided, variable-rate spray system for pest control in nurseries and

orchards, which adjusts spray volume based on plant characteristics in real time, finding that the new system provided comparable or better pest control while reducing spray volume by significant percentages, and observed that anthracnose severity was greater in the constant-rate treatment. Wei et al. (Wei & Khachatryan, 2021) evaluated the efficacy of precision sprayers compared to traditional radial air blast sprayers for pesticide applications in specialty crop production, finding that precision sprayers reduced chemical wastage and off-target drift by approximately 40% and 15% of the total applied spray volume, respectively, compared to traditional radial air blast sprayers (Amin & Islam, 2022). With the application of precision spraying, the loss of agrochemicals will be reduced. And for precision spraying, it is important to have information on tree and canopy attributes.

2.8 Ornamental Tree Canopy Characteristics with UAV-RGB

Canopy characteristics, such as height, crown size, and density, play an important role in trees by influencing their aesthetic appeal, health, and growth. These traits determine light capture (Lambers et al., 2008), competition among plants, and water or nutrient uptake (Kohyama, 1993), making them essential for managing the beauty and vitality of ornamental landscapes. Conventional ground-based methods for assessing canopy structures in large ornamental nurseries are often challenging to implement due to difficulties in achieving accuracy and distinguishing overlapping canopies. The advent of UAVs, has enabled the rapid collection of detailed, high-resolution remote sensing data (Anderson & Gaston, 2013). For instance, Vinci et al. (2023) developed and validated a UAV-based method for canopy characterization in hazelnut orchards, comparing parameters like canopy radius, height, and volume to manual measurements, achieving high accuracy except for trunk height. Over the past few decades, researchers have increasingly employed UAVs outfitted with different sensors to evaluate various canopy attributes. Gallardo-Salazar and Pompa-García (2020)

employed a UAV with six sensors (five multispectral and one RGB to extract tree characteristics like height, crown diameter, and trunk diameter with high accuracy by combining high-resolution orthomosaics, Normalized Difference Vegetation Index (NDVI), image analysis, and field validation. Similarly, Young et al. (2022) utilized drone imagery and structure-from-motion (SfM) photogrammetry to create 7,568 individual tree maps of a mixed-conifer forest, testing various flight, imagery processing, and tree detection parameters, and achieved high accuracy for mapping canopy-dominant trees. RGB cameras are widely used for capturing high-resolution images of tree canopies, delivering detailed visual data that can be processed into comprehensive 3D (three-dimensional) models. When mounted on UAVs, these cameras offer a cost-effective solution, providing high-quality imagery and enabling faster data acquisition compared to traditional methods, making them an essential tool for ornamental nursery management and canopy analysis (Birdal et al., 2017). Many studies have utilized UAVs equipped with RGB sensors in agriculture and forestry to gather detailed data on individual tree attributes, such as canopy structure, height, and health, enhancing precision in tree monitoring and management (Jayathunga et al., 2023; Kulhandjian et al., 2024; Lee et al., 2023). For instance, Zhou et al. (2023) demonstrated the potential of UAV RGB images for automated afforestation evaluation, achieving high accuracy in monitoring sapling growth and extracting tree heights with R^2 values up to 0.99 and RMSE (Root Mean Square Error) as low as 0.16 using the divide-and-conquer method, and R^2 of 0.95 with RMSE of 0.33 for the canopy height model. Thus, these studies suggest that UAVs equipped with RGB sensors offer a precise method for determining canopy characteristics.

2.9 Tree Attributes with Ground-based LiDAR and Depth Camera System

Ground-based sensing offers finer insights into tree features like trunk diameter and structure, complementing UAV sensor data by capturing details that might have been

overlooked from aerial perspectives. Recent studies have explored various methodologies and technologies to build upon the advancements in tree parameter estimation using terrestrial lidar. LiDAR, ultrasonic sensing, and optical sensing have been evaluated to measure tree canopy geometric characteristics. Certain studies have utilized tractor-mounted LiDAR systems for measuring tree attributes (Siefen et al., 2023). Lovell et al. (2011) demonstrated the effectiveness of automated methods utilizing scanning LiDAR data for tree stem identification and diameter measurement in forests, achieving high success rates and closely matching field data. Watt and Donoghue (2005) utilized ground-based laser scanning to quantitatively measure trees in densely stocked forests, highlighting the potential for accurate measurements of tree diameter and other parameters from laser scan data, albeit with limitations based on scanning resolution and tree density. Additionally, Hu et al. (2020) developed a novel method using multi-station terrestrial laser scanning for accurate tree parameter estimation and trunk model establishment, achieving mean relative errors of 1.89% for tree height, 1.74% for trunk diameter, and 2.91% for CBH, meeting accuracy standards and outperforming previous approaches. Stovall et al. (2023) compared tripod-mounted TLS and mobile MLS for diameter measurements along tree stems, with TLS showing overall higher accuracy, especially at greater heights. Despite limitations, MLS proved effective for certain applications. Furthermore, Eliopoulos et al. (Eliopoulos et al., 2020) developed an algorithm utilizing stereo camera footage to efficiently identify the ground and measure trunk diameter or any height along the stem. Their approach significantly reduced data acquisition and processing times while maintaining relatively accurate trunk diameter estimates, offering computational efficiency and cost reduction compared to traditional methods like terrestrial laser scanning and other photogrammetry techniques. Building on these advancements, Brack et al. (Brack et al., 2020) compared TLS instruments, including Zebedee and DWEL, with traditional methods for measuring tree parameters at the National Arboretum Canberra. TLS instruments showed

high accuracy in height and growth rate measurements, with potential to enhance forest inventory, but challenges exist in defining new parameters for historical comparisons. In a study assessing an MLS with simultaneous localization and mapping (SLAM) technology for tree inventory in a historic garden, Pérez-Martín et al. (2021) evaluated trunk diameter estimation accuracy using three fitting algorithms: RANSAC, Monte Carlo, and Optimal Circle. The study utilized a reference sample of 378 trees. MLS data acquisition took 27 minutes and 37 seconds to cover 2.38 hectares. The Monte Carlo fitting algorithm yielded the best results, estimating trunk diameter for 77% of the trees with an RMSE of 5.31 cm and a bias of 1.23 cm. This methodology enabled supervised tree detection and automatic trunk diameter estimation, offering a valuable tool for historic garden management and conservation. These studies suggest that significant progress has been made in tree parameter estimation using terrestrial LiDAR technology. From automated methods for tree stem identification to innovative approaches utilizing multi-station terrestrial laser scanning, researchers have demonstrated the potential to improve accuracy and efficiency in forest inventory processes. LiDAR's strength lies in scanning expansive areas, making it particularly useful for creating detailed representations of tree canopies in nurseries. For instance, the Velodyne VLP-16 uses 16 laser channels spaced in 2° intervals from −15° to +15°, providing a 30° vertical field of view. However, LiDAR's lower resolution for smaller details, such as young tree trunks, presents challenges, as gaps in the point cloud can lead to inaccuracies (Lassiter et al., 2020).

Depth cameras offer a better solution for measuring smaller objects like young tree trunks. With their higher resolution at close range, depth cameras can capture fine surface details, resulting in more accurate trunk diameter measurements (Andújar et al., 2016). Stereo depth cameras, for example, generate detailed depth maps by calculating the disparity between two image sensors, enabling precise measurements of small features (Zhang et al., 2015). This makes depth cameras ideal for younger trees, where the increased point density and

measurement accuracy ensure reliable trunk diameter estimations, overcoming the limitations of LiDAR in such cases. Sankari (2022) presented an automated method to estimate tree trunk width in a commercial apple orchard using RGB-D images, which combined color data with point clouds from a depth camera. A Mask RCNN deep learning network was trained to detect tree trunks in the images, producing usable results for 71 of 100 images. The most accurate measurement method, "width 3," utilized the depth data to triangulate the trunk width, achieving an average error of 0.56 cm per tree, 8.4% of the average trunk width (6.7 cm). This study suggested the use of depth camera for determining the trunk diameter of trees successfully.

However, challenges such as defining new parameters for historical comparisons and addressing limitations in scanning resolution and tree density persist. As technology continues to evolve and methodologies are refined, the integration of terrestrial LiDAR with depth camera into forest management practices holds promise for more precise and sustainable resource assessments.

2.10 Web-Based Application for Monitoring Disease Dynamics

Accurately estimating the necessary agrochemical dosage is crucial for disease control, yet monitoring its impact on plant health is equally vital. Human assessments of disease progression post-agrochemical application can be subjective. A web app can be designed to identify disease infections and map their spread, facilitating continuous monitoring after treatment. By harnessing computer vision technology, a specialized model can be integrated into the web application, offering growers real-time updates on disease status for effective disease management and crop health tracking. Across numerous computer vision applications, CNNs have achieved remarkable success, particularly in the realm of image classification and instance segmentation (Bello et al., 2019). Mask RCNN (He et al., 2017), utilizing the strengths

of CNNs, is a powerful instance segmentation method that independently generates binary masks for each class. However, Mask RCNN can struggle with capturing fine-grained details in small or overlapping objects, limiting its effectiveness in certain complex segmentation tasks (Wang et al., 2022). On the other hand, MaskFormer (Cheng et al., 2021) presents an innovative framework for instance segmentation, seamlessly combining semantic and instance-level segmentation into a unified model. It supports diverse backbone architectures such as ResNet and Swin Transformer (Swin T) (Liu et al., 2021). Instead of traditional approaches, it predicts binary masks associated with global class labels, streamlining the segmentation process while maintaining high accuracy and reliability. Some studies have explored the application of MaskFormer with transformer-based backbones in agriculture (Chen et al., 2024). Earlier studies by Shinoda et al. (2023) and Wang et al. (2023) demonstrated the superiority of Swin T in instance segmentation on tomato datasets over CNN-based models. Building on these advancements in model performance, the demand for web-based applications in agriculture arises from their remote accessibility, and while real-time disease detection using deep learning algorithms has been explored, only a few studies have focused on deploying these models to web or mobile platforms. Nag et al. (2023) developed a mobile app-based system for intelligent detection of diseases on tomato leaves using DenseNet-121 for a user-friendly mobile application. Although CNN architecture has been widely compared for accuracy, transformer-based models remain underexplored for web applications, leaving the ornamental industry behind in adopting advanced disease detection tools.

Precision technologies have been utilized in various agricultural sectors, including row crops and forestry. However, their application in the ornamental industry remains relatively scarce. Despite the wealth of studies demonstrating the effectiveness of precision agriculture techniques, there is a notable gap in research focused on ornamental crops. There is a pressing need for innovative solutions in disease management and canopy characterization within the

ornamental industry. Challenges such as disease prevalence, overuse of agrochemicals, and limited accessibility to advanced technologies highlight the urgency for proactive measures. This study seeks to address these challenges by leveraging precision agriculture techniques to accurately estimate agrochemicals needed in the ornamental plants for precision spraying and provide real-time disease detection, which can be useful in monitoring disease dynamics.

CHAPTER 3

MEASURING ORNAMENTAL TREE CANOPY ATTRIBUTES FOR PRECISION SPRAYING USING DRONE TECHNOLOGY [1]

---

[1] Rayamajhi, A., H. Jahanifar, and M.S. Mahmud. 2024. *Computers and Electronics in Agriculture*. 225:109359.

Abstract

Tree canopy attributes or characteristics, such as canopy volume and density, are important parameters for calculating the precise quantity of agrochemicals required in each tree. Assessing the agrochemical needs in a nursery can help growers effectively estimate expenses, mitigate the risks of overuse or underuse, enhance resource utilization, and promote sustainable agricultural practices. This study aimed to develop a UAV-based system to measure tree canopy attributes like tree height, tree count, canopy area and canopy volume using an image processing and self-supervised zero-shot segmentation approach. A high-resolution red-green-blue (RGB) sensor mounted on a drone captured three aerial image datasets, D1 and D2 from the first experimental plot and D3 from the second experimental plot. The acquired aerial images were stitched together and processed to generate a digital surface model (DSM) and a digital terrain model (DTM). A self-supervised zero-shot segmentation model, Segment Anything Model (SAM), was applied for tree segmentation and counting. The tree canopy area was calculated by segmenting individual trees and applying a conversion factor to convert pixelwise areas into square meters. Height calculation was done using elevation data of each pixel from DSM-DTM imagery within SAM-derived bounding box coordinates, and the highest pixel was considered as the height of the tree. The drone-calculated heights of 24 randomly selected trees were compared with manually measured heights in all datasets. The results showed an average absolute error of 2.43% in D1, 7.09% in D2 and 12.58% in D3. The Mean Absolute Error (MAE) and RMSE were noted to be 0.09 m and 0.23 m in D1, 0.13 m and 0.25 m in D2, and 0.16 m and 0.21 m in D3, respectively. In D3, manual area and volume calculations were performed for validation. The RMSE and MAE for area calculation were calculated as 0.18 m^2 and 0.15 $m^{2,}$ respectively, and the RMSE and MAE for volume measurements were calculated as 0.33 m^3 and 0.26 m^3 respectively, which indicated the level of agreement between manual and drone measurements. Using canopy volume information,

calculated by summing pixel heights within each tree's bounding box and multiplying by the ground sample distance (GSD) of 0.025 meters per pixel, the average quantity of agrochemicals needed for a Maple tree was estimated at 0.20 liters. These results underscore the high potential of this method for accurate canopy characteristic calculations and precision spray applications in the ornamental industry.

Keywords: Nursery Crops, Segment Anything Model, Canopy Volume, Tree Height Measurement, Precision Spray Applications

3.1 Significance of the Study

This chapter focuses on measuring ornamental tree canopy attributes using UAV-based RGB imagery combined with self-supervised segmentation, marking the first instance in this study where drones are utilized for this purpose. Understanding canopy characteristics of tree canopy volume is critical for determining the precise quantity of agrochemicals. By integrating drone technology with SAM, this study enhances the accuracy and efficiency of tree monitoring and agrochemical estimation. It addresses limitations in traditional methods by offering cost-effective, scalable solutions tailored to woody ornamental nurseries. The study's ability to automate the segmentation and measurement process using zero-shot learning demonstrates the potential for reducing labor-intensive manual work while increasing precision in agrochemical application. Furthermore, the findings demonstrate how UAV-based systems can aid growers in decision-making processes, such as planning harvests, optimizing pruning schedules, and reducing agrochemical waste. The methodology presented in the chapter aligns with sustainable agricultural goals and sets a benchmark for leveraging advanced AI-driven technologies in the ornamental and broader agricultural sectors. This chapter lays the groundwork for subsequent analyses, where ground-based systems were explored to complement UAV surveys.

3.2 Introduction

Ornamental plants are valued for their aesthetic importance, spiritual symbolism, and emotional significance (Chowdhuri & Deka, 2019). The United States horticulture sector achieved sales of USD 13.8 billion from floriculture, nursery, and specialty crops in 2019 (USDA, 2020). However, the Census of Horticultural Specialties indicated a notable decline in the number of producers in that year, while sales experienced a minor reduction from 10 million USD in the same timeframe (USDA, 2020). The reduction in ornamental tree production may be ascribed, in part, to several factors, including increased expenses for disease and pest management (Beverly et al., 1997). Pesticides play a crucial role in protecting ornamental plants from pests, diseases, and weeds while also preserving their aesthetic appeal (Pereira et al., 2021). Knowing tree canopy details, such as tree count, tree height, and canopy volume, assist in determining the accurate amount of agrochemicals needed to protect trees from disease and pest attacks (Maghsoudi & Minaei, 2014; Solanelles et al., 2006).

Precision spray application minimizes resource usage, reduces environmental impact and optimizes crop protection by accurately targeting and applying pesticides or agrochemicals to specific areas (Bonicelli et al., 2010). Numerous studies have explored the precise application of agrochemicals in agriculture, examining aspects such as crop yields, leaf nutrients, and soil nutrients (López-Granados et al., 2004; Salazar-García & Lazcano-Ferrat, 2003). For example, Zaman et al. (Zaman et al., 2005) employed ultrasonic sensors and a differential global positioning system to calculate citrus canopy volume, subsequently creating maps for site-specific nitrogen applications through variable rate application and concluded that applying a variable rate of nitrogen on individual trees resulted in a significant 40% reduction in granular fertilizer usage for the examined orchard. Similarly, Pascual et al. (Pascual et al., 2009) used a non-destructive LiDAR system to assess canopy volume and tree shape, suggesting the applicability of LiDAR in analyzing the effects of fertilization strategies

on productivity. Canopy geometric attributes or characteristics serve as key indicators for biomass, growth, yield prediction, water consumption, health assessment, and long-term productivity monitoring (Lee & Ehsani, 2009). In addition to determining the optimal amount of agrochemical requirement for ornamental plants, canopy characteristics provide valuable information for various other purposes. For example, understanding the height and trunk diameter of the Maple tree dictates the ideal time for harvesting. Optimal harvest time is defined by the peak quality of the wood for timber purposes (Kozakiewicz & McKinney, 2021). Additionally, utilizing canopy volume or growth information for Maples allows growers to implement effective thinning and pruning techniques, enhancing the trees' survival rates (Lamson, 1988). Overall, managing the ornamental trees in large fields poses difficulties in tracking readiness for harvest, especially with the constraints of manual inspections and limited labor (Hertz & Zahniser, 2013). However, the geometric characterization of trees is both a significant and complex task (Sanz-Cortiella, Llorens-Calveras, Rosell-Polo, et al., 2011). Among many precision technologies, UAVs, commonly known as drones, can offer a solution by providing valuable information such as tree count, height, canopy area, and canopy volume, aiding growers in efficient and informed decision-making (Mahmud et al., 2023).

Methods, including ground-based scanning LiDAR, ultrasonic sensing, and optical sensing, have been tested for measuring tree canopy geometric characteristics, including crop height, canopy volume and cover. Some studies used ground-based systems with LiDAR mounted on tractors for tree characteristics measurement (Palleja et al., 2010; Polo et al., 2009; Sanz-Cortiella, Llorens-Calveras, Escolà, et al., 2011). However, ground-based sensing systems face challenges in hilly landscapes, rendering them less effective for canopy measurements in undrivable areas where row spacing is narrow between trees. Furthermore, their travel speed limitations hinder efficiency, particularly in large-scale orchards and nurseries with varying slopes. More recently, UAVs with sensors and LiDAR systems have

been used in tree characteristics measurement (Liao et al., 2022), which usually covers a huge area. Though LiDAR delivers precise depth details, it has limited vertical and horizontal resolution (Fu et al., 2019). On the contrary, a high-resolution RGB camera offers rich texture and, when mounted on a UAV, can capture images that can be processed to form a complete model, offering comprehensive visual details of tree canopies. In fact, RGB sensors with drones are gaining popularity because of their cost-effectiveness, high-resolution imagery, and quicker operational pace compared to traditional photogrammetric methods and UAV-LiDAR (Birdal et al., 2017).

An important step in the measurement of the canopy area involves choosing a suitable algorithm for tree segmentation (Dalponte et al., 2014). Some studies have performed segmentation in ornamental trees for various precision technologies (Bayraktar et al., 2020; Rayamajhi & Mahmud, 2023). In image processing, segmentation involves dividing an image into different regions or segments, often based on certain criteria like color, intensity, or texture. The aim is to establish a clear association between each segment and a specific object or class within the image. Segment Anything Model (SAM) is a pioneering self-supervised image segmentation approach known for its outstanding generalization across various image datasets, demonstrating the unique capability to segment unfamiliar objects without the need for additional training (Kirillov et al., 2023). Trained on an extensive dataset of 11 million images and 1 billion masks, the fast and adaptable SAM demonstrates exceptional segmentation capabilities across diverse scenarios, contributing innovations to image segmentation and computer vision. The implementation of SAM provides significant advantages over traditional segmentation methods. The speed at which SAM operates, thanks to its zero-shot learning capabilities, allows for the rapid processing of images. Zero-shot learning refers to the model's ability to correctly make predictions for new, unseen classes without any specific training for those classes. This is a substantial improvement over the typically time-consuming

segmentation methods. Furthermore, SAM's advanced algorithms drastically reduce the need for manual annotation by quickly recognizing and segmenting new images without specific training, which is often a bottleneck in image analysis workflows. This efficiency is particularly beneficial in large-scale environmental projects where timely and accurate segmentation of numerous images is paramount. A study (Mazurowski et al., 2023) has investigated the assessment of SAM in the field of medical imaging for segmenting medical images, using 19 datasets from various modalities and anatomies. The study found that SAM demonstrated impressive segmentation for certain medical imaging datasets, suggesting a potential impact in automated medical image segmentation. Carraro et al. (Carraro et al., 2023) explored SAM's semi-automatic segmentation modes on the crop/weed field image dataset (CWFID), finding they accelerate ground-truth annotation while maintaining accuracy.

Although ground-capture imagery is high in resolution compared to UAV-captured imagery, several attempts have been reported in UAV-based canopy parameter measurement due to the capacity of drones covering large areas in a brief period of time with fairly good resolution. Poblete-Echeverría et al. (Poblete-Echeverría et al., 2017) detected vine canopy in a vertical trellis system using low-cost UAV-captured RGB images and assessed the effectiveness of different classification methods. The results demonstrated that while spectral indices excel in detecting the plant class (vine canopy), they struggled to discriminate between soil and shadow classes, and the study relied on human intervention for machine-learning model training. Our study overcomes these limitations by employing a self-supervised zero-shot learning model, SAM, specifically adept at detecting tree canopies, thus providing a more robust and automated solution for accurate segmentation.

This study aimed to use a cost-effective and quick operational approach to measure ornamental tree attributes or characteristics for precision spray applications using an RGB sensor-equipped drone with advanced application of SAM. The specific objectives of this study

were to (i) count the number of ornamental trees in a nursery using SAM, (ii) measure the height of the trees with DSM-DTM imagery, (iii) calculate the tree canopy area using SAM and volume using GSD and pixel height values and (iv) estimate the optimum quantity of agrochemicals required in the trees using volume information and standard chemical application rate. This study offers several significant contributions to the precision ornamental sector, with the primary ones being:

- Enhancement of visual data analysis by SAM, overcoming the limitations of traditional models in handling complex or overlapping objects to count ornamental trees and calculate their canopy volume individually
- Evaluation of the applicability of drone technologies in counting trees and calculating the height of the trees and canopy volume in woody ornamental nurseries
- Calculation of tree-based agrochemical requirements using a UAV-based system to estimate agrochemical expenses for ornamental growers and conduct precision spray applications

3.3 Materials and Methods

3.3.1 Study Site

The first experimental site was located on Smith Farm, McMinnville, TN (35° 41' 20.616" N, 85° 46' 50.556" W), a private property with a total area of approximately one hectare (under experimental consideration), featuring more than 350 strategically planted red maple trees spaced in rows (Fig. 3.1). During data collection, it was observed that some trees had been previously harvested, leaving noticeable potholes in the landscape. The terrain exhibited a gentle, uneven slope. The field was mowed carefully before collecting the first dataset to reduce interference in the images, and the grass was kept short to limit visual distractions. In the aerial image collection for the second dataset, the grass was comparatively taller than the first time.

Most of the trees were trimmed on the crown by a few centimeters (up to 0.1 m) by the grower to shape them and make them market-ready, and some trees were harvested, leaving behind potholes. The second experimental site was located in Watkinsville, GA (33° 45' 22.6" N, 83° 25' 58.4" W). The third dataset was collected from this experimental plot, which had more than 400 trees spaced in rows.

Figure 3.1. Experimental plot of red maple trees located at Smith Farm, McMinnville, TN. The plot serves as the first experimental site for evaluating UAV-based methodologies for canopy and tree characteristic measurements.

3.3.2 Field Measurement

On July 6, 2023, July 24, 2023, and May 28, 2024, the height of 24 trees (randomly selected) was measured using a measuring tape before aerial images were collected using a drone. D1 and D2 were collected from the first experimental site, while D3 was collected from the second experimental site. The weather was sunny, with no wind or rain at all measurements. To establish reference points, 12 randomly placed whiteboards (each measuring 0.51 × 0.76 square meters) with numbers from 1 to 12 were utilized, with one board assigned to two

adjacent trees (from rows at the left and right of the board). Each of the 24 trees was tagged with ribbons for identification, and precise height measurements were conducted using a centimeter-unit measuring tape. Trees were labeled with unique IDs, like R2T14, denoting the tree's location as the 14^{th} in the second row.

3.3.3 Aerial Data Collection and Preparation

The data collection was performed on the same days after manual height measurements using DJI Matrice 300 RTK (SZ DJI Technology Co., Ltd, Shenzhen, China) for first and second dataset and DJI Matrice 350 RTK (SZ DJI Technology Co., Ltd, Shenzhen, China) for third dataset, both equipped with an RGB camera (DJI Zenmuse H20, SZ DJI Technology Co., Ltd, Shenzhen, China). A flight plan for autopilot flight was created in DJI Flight Planner (SZ DJI Technology Co., Ltd, Shenzhen, China). It created optimum flight lines based on the polygon selected. Some of the trigger points which were outside the experimental area were removed manually. The images were captured with 80% forward and side overlap with constant time intervals, making the consistent distance between images. An optimal 12.19 m (40 ft) flying altitude was used to capture high-resolution canopy images. At higher altitudes, image resolution decreases, making it harder to capture tree canopy details. At lower altitudes, each image covers less ground, requiring more images and flights to cover the same area, increasing data collection time. Additionally, flying at lower altitudes creates turbulence, affecting the quality of the images. A total of 764 images on the first flight, 765 images on the second flight, and 670 images on the third flight were efficiently captured during a single flight. The first, second, and third datasets were named D1, D2, and D3. The two sets of data were collected to compare the results and observe differences in tree growth and canopy characteristics. An additional dataset was used for validation with ground truth and to get the average basal height for all maple trees. The images were stitched together to get a complete field image. Agisoft Metashape Professional version 2.0.2 (Agisoft LLC, Petersburg, Russia) was used for image

stitching. First, images were aligned, and then a dense point cloud was generated. Gradually, mesh, textured mesh, digital elevation model (DEM) and orthomosaic (Fig. 2) were built to reflect the topography of the captured terrain.

The final orthomosaic image was exported in GeoTIFF (Geographic Tagged Image File Format). Digital surface model (DSM) and digital terrain model (DTM) were computed to represent the elevation data of the surface and the terrain, respectively. They were then imported into QGIS (Quantum Geographic Information System, Quebec, Canada). The DSM includes elevation information of the trees and ground relative to the mean sea level. The DTM included elevation information for only ground relative to the mean sea level. The DTM was subtracted from the DSM, which provided only heights for all Maple trees in the experimental nursery. This process yielded the DSM-DTM image (Fig. 3.3), serving as the foundation for the subsequent analysis. The white segments in this image represent the tree canopy areas, which were the focal points in this study.

Figure 3.2. Orthomosaic generation process showing individual aerial images collected during data acquisition (left) and the final stitched orthomosaic image (right) created from the D1 dataset.

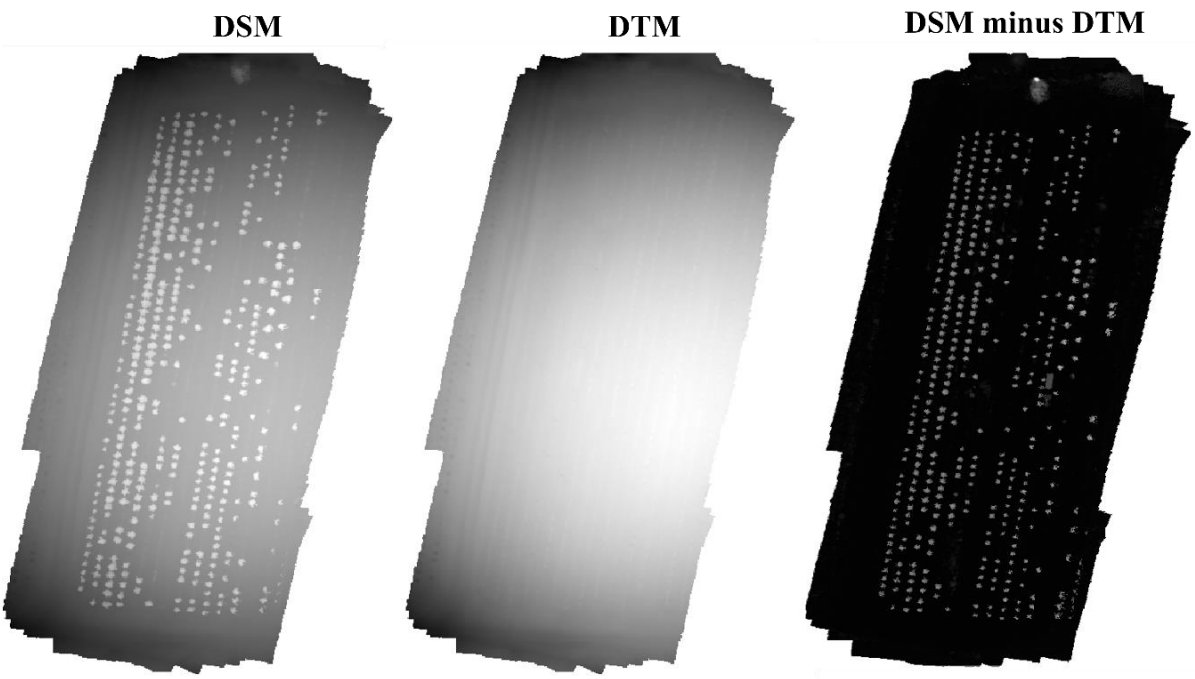

Figure 3.3. Generation of DSM minus DTM image (right) using QGIS. The DSM (left) captures all surface features, the DTM (center) represents the bare ground elevation, and their difference highlights tree heights in white color.

3.3.4 Segment Anything Model for Segmentation and Pixel-wise Area Measurement

The SAM, Segment Anything Model developed by the FAIR team at Meta AI (Astor Place, New York City, New York, US), is a self-supervised zero-shot image segmentation model capable of generating high-quality masks. It operates through both automatic processes and interactive prompt-based instructions. Designed to produce high-quality masks from a single foreground point, SAM can be applied to a variety of segmentation tasks. A key feature of SAM is its ability to generalize new tasks and image domains without the need for custom image annotation or intensive retraining, facilitating zero-shot transfer to new image distributions and tasks. This significantly enhances the segmentation process, as SAM can segment objects in images, detect edges, and perform segmentation tasks on new image distributions and tasks that it has not encountered during training.

SAM's architecture is presented in Fig. 3.4, illustrating the hierarchical structure and functional components.

The SAM comes in three different versions, each with a different backbone size to accommodate various computational power and performance needs:

Default or ViT H: ViT stands for Vision Transformer, and H refers to the 'huge' model, which offers the most powerful architecture suitable for tasks requiring extensive detail and complexity in image segmentation.

ViT L: The 'large' model provides a balance between performance and computational demand, which is recommended if a computer has adequate resources.

ViT B: The 'base' model is the smallest and least resource-intensive, providing a lighter option without significantly compromising performance.

The choice of the ViT-H model for this project was driven by its exceptional ability to handle complex segmentation tasks, such as detailed tree canopy analysis, supported by its more robust architecture compared to the other versions. In addition, the performance difference between the 'large' (L) and 'huge' (H) models is reportedly minimal, suggesting that the 'large' model could be an efficient alternative for adequately resourced machines. Conversely, the 'base' (B) model, while lighter, does not lag far behind in performance, offering a viable option for environments with more limited computational capacity.

In Fig. 3.4, the image encoder can be any network that outputs an image embedding with dimensions C×H×W, where C denotes the number of color channels (e.g., Red-Green-Blue), H is the height, and W is the width of the image. The DSM minus DTM (DSM-DTM) input image was split into smaller, non-overlapping patches, e.g., 16×16 pixels each. Each patch represented a specific region of the image, allowing for detailed local feature extraction. A linear projection was then applied to each flattened patch to transform it into a feature-

embedded space. This process enabled the encoder to capture and embed fine-grained details from each part of the image efficiently. These patch embeddings were then processed by the transformer network. After the transformer, unlike the original ViT architecture, there was a neck module that consisted of a sequence of a 1x1 convolution to get to 256 channels, followed by layer normalization, and then a 3x3 convolution also with 256 channels, followed by another layer normalization. The prompt encoder was responsible for interpreting and encoding various types of input prompts, which can be sparse (like points, boxes, text) or dense (such as masks). We utilized sparse prompts, specifically a grid of points, to guide the segmentation. The mask decoder maps the image embedding, prompt embeddings, and an output token to a segmentation mask. It incorporates a modified Transformer decoder block, which employs prompt self-attention and cross-attention mechanisms in both directions—from prompt to image embedding and from image embedding to prompt—to update all embeddings. After processing through two such blocks, the image embedding was upscaled, and a multilayer perceptron (MLP) mapped the output token to a dynamic linear classifier. This classifier then computed the foreground probability of the mask at each location in the image, which was used to generate the final segmentation mask.

This study employed SAM with an automatic approach for mask generation. This involved prompting the model with a grid of 100×100 points, totaling 10,000 points, to systematically scan the entire image and automatically generate masks. The default grid size for this approach in SAM was 32×32. However, the large, stitched image with dimensions of 3011×5898 pixels increased this value to better accommodate our dataset. The overall utilization of SAM in this study is presented in Fig. 3.5.

To prepare the image for segmentation using SAM, a copy of the original DSM-DTM image, which contained elevation data, was used. It was converted to BMP (Bitmap) format with the same resolution as the original image and then treated as an RGB image, retaining its

three channels ($F \in R^{H \times W \times 3}$: indicates that the image data F is an array with real number values (R), having a height of H pixels, a width of W pixels, and three color channels) (Fig. 3.6). However, by converting the image to BMP format, the elevation data inherent to the original image were discarded, as they were not required for the segmentation process. A binary thresholding operation was applied to the BMP image with a threshold value of 127 to reduce noise and focus on the relevant features, namely the canopies. This operation converted the image into a binary format where pixels with values of 127 or above were set to 255 (white), representing the canopies, and those below 127 were set to 0 (black), representing the background. This step was essential for isolating the canopies and enabled more precise subsequent processing. The SAM was used to leverage its capabilities for segmentation, mask generation, as well as pixel-wise area generation. It also provided bounding box coordinates for each segmented area, which is often an important step in calculating the area of each tree.

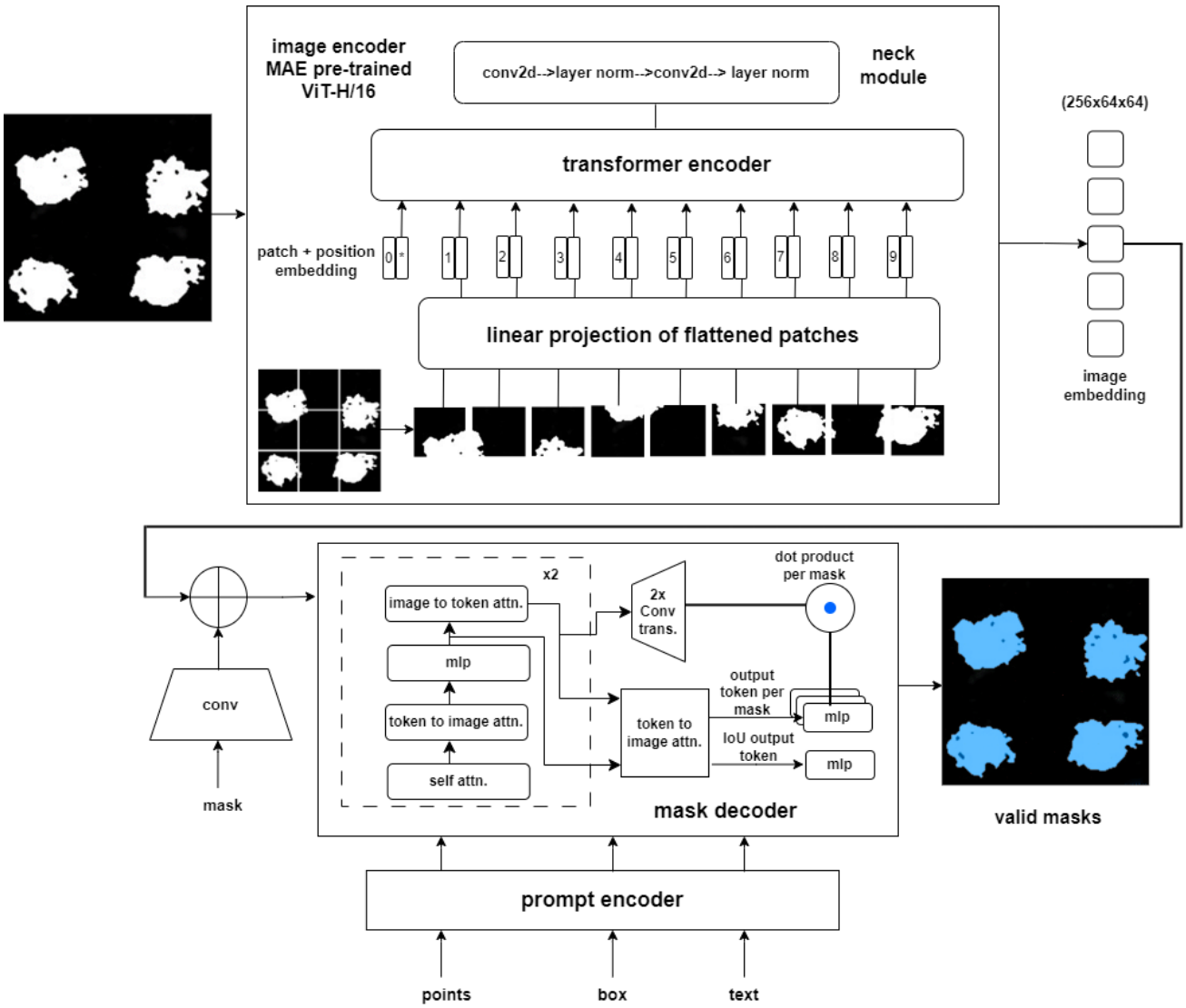

Figure 3.4. Overview of SAM's hierarchical architecture showing the integration of the image encoder, prompt encoder, and mask decoder modules.

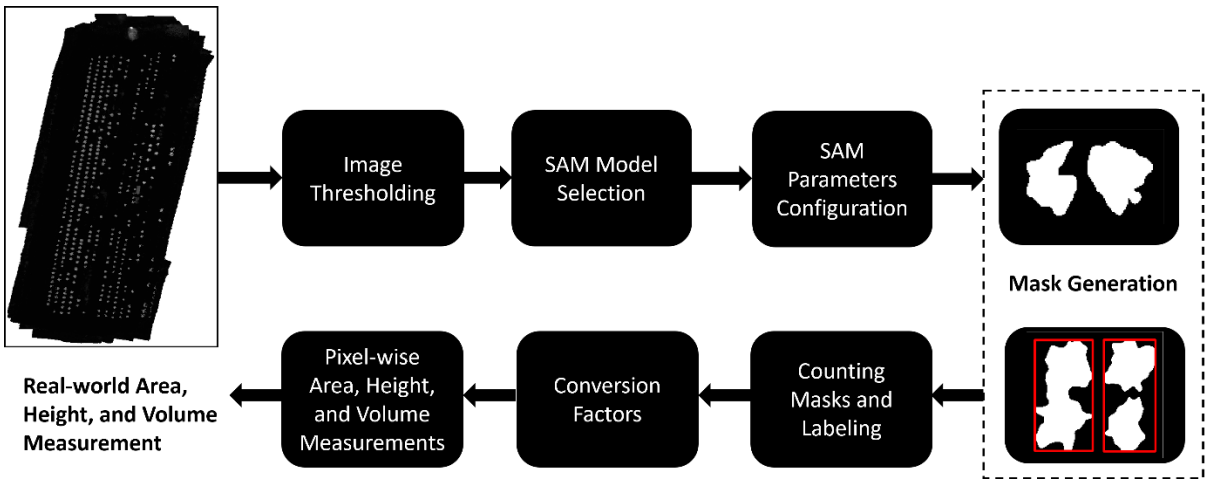

Figure 3.5. Flowchart illustrates the measurement workflow for tree height, canopy area, and volume using SAM.

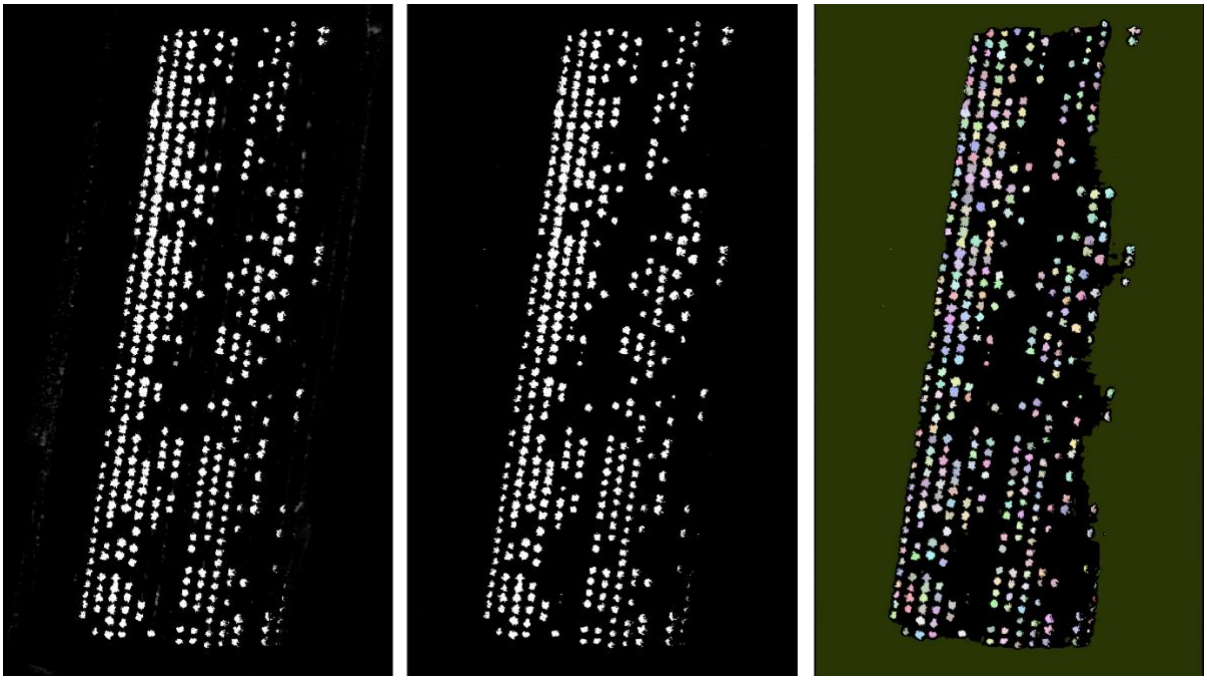

Figure 3.6. Visualization of processing stages in the canopy height model analysis. From left to right: Original DSM-DTM image showcasing the canopy height model, thresholded image isolating canopy features, and segmented image highlighting individual trees or canopy sections for further analysis.

3.3.5 SAM Configuration

To optimize the segmentation of individual trees, several parameters in the SAM algorithm were finetuned. This finetuning approach was aimed at enhancing the precision of tree segmentation. The parameters applied in this step are discussed in Table 3.1.

The values for parameters such as IOU threshold, stability score threshold, NMS threshold, overlap ratio, and downscale factor were carefully chosen based on empirical testing and best practices in image segmentation. The quality of the mask generated is primarily controlled by two hyperparameters: pred_iou_thresh and stability_score_thresh. Higher values for these parameters result in fewer masks with fewer artifacts and higher overall quality. However, care was taken not to set them too high, as this could eliminate actual object masks as well.

The prediction IOU threshold (pred_iou_thresh) ensures that only masks with an IOU equal to or higher than this value are selected. By increasing this value from the default of 0.88 to 0.92, we ensured that the retained masks were of high quality and accuracy.

The stability score threshold of 0.97 ensures that only masks with high stability are retained. This is an additional parameter that allows us to generate better-quality masks. This threshold filtered masks based on their stability under changes to the cutoff used to binarize the model's mask predictions, ensuring that the retained masks are consistent and reliable. Choosing the higher value generated fewer masks but with higher quality and less noise and artifacts.

The NMS (Non-Maximum Suppression) threshold of 0.8 allows for a higher tolerance to overlapping boxes, facilitating the removal of duplicate masks. NMS is a

technique used to select the best bounding box among overlapping boxes by keeping the one with the highest score and suppressing the others.

The points per side (points_per_side), considering the stitched image size of 3011×5898, was set to 100 to ensure a dense sampling of points along each side of the image. This parameter determined the number of points sampled along one side, with the total number of points being the square of this value (i.e., 100^2=10,000 points). By setting points_per_side to 100, we ensured that a high-resolution grid of points was used for segmentation, which helped in accurately capturing detailed features of the image.

The downscale factor (crop_n_points_downscale_factor) was set to 2 to balance the resolution and computational load effectively. This parameter determined how the number of points per side decreased as the image was processed through multiple crop layers. By reducing the number of points per side by a factor of 2 for each subsequent layer, we confirmed that the segmentation process remained efficient without compromising the accuracy and quality of the masks generated. This downscale factor helped manage computational resources while maintaining sufficient detail in the segmentation. A higher downscale factor reduced the number of points sampled, which led to a decrease in computational load.

The crop overlap ratio (crop_overlap_ratio) was set to 0.2 to ensure sufficient coverage and continuity in segmentation across crops. This parameter determined the degree to which crops overlap in each layer. By setting the overlap ratio to 0.2, we checked that crops in the first layer overlap by 20% of the image length. In subsequent layers with more crops, this overlap was scaled down, ensuring that the segmentation process captured details at the boundaries between crops effectively. A higher overlap ratio ensured that important features near the edges of each crop were not missed, leading to more accurate

and seamless segmentation results. However, this value was sufficient in our case while taking the computational cost into account as well.

SAM offers multiple methods (automatic, from bounding boxes, from points, and from points and boxes) for generating segmentation masks. The automatic mask generator was utilized, which is preferable for its speed and self-supervised approach, and it was applied to segment individual tree canopies within converted DSM-DTM imagery without any user prompts. Some of the masks generated using SAM of red maples in the experimental plot can be visualized on Fig. 3.7.

Table 3.1. Configuration details for the SamAutomaticMaskGenerator parameters, describing the function of each parameter, its value, and its role in enhancing segmentation quality and efficiency.

Parameter	Value	Description
points per side	100	Number of points sampled along each side of the bounding box during the segmentation process.
points per batch	20	Number of points processed per batch, adjusted based on the available GPU memory.
pred iou thresh	0.92	Threshold for stricter mask quality, ensuring only masks with a higher predicted IoU are considered.
stability score thresh	0.97	Threshold for stricter mask stability, filtering out unstable predictions.
box nms thresh	0.8	Threshold for non-max suppression, facilitating the filtering of duplicate masks with a higher tolerance to overlapping boxes.
crop n layers	2	Number of layers in the crop pyramid used during the segmentation process.
crop nms thresh	0.8	Threshold for stricter suppression between different crops, aiding in removing duplicate masks arising from different crops.
crop overlap ratio	0.2	Dictates the overlap ratio between different crops, assisting in maintaining continuity and coherence in the segmentation across different crops.
crop n points downscale factor	2	Influences the downscaling factor for the number of points in the crop pyramid.
min mask region area	200	Parameter pivotal in removing noise by discarding regions in the masks smaller than the expected smallest tree area.

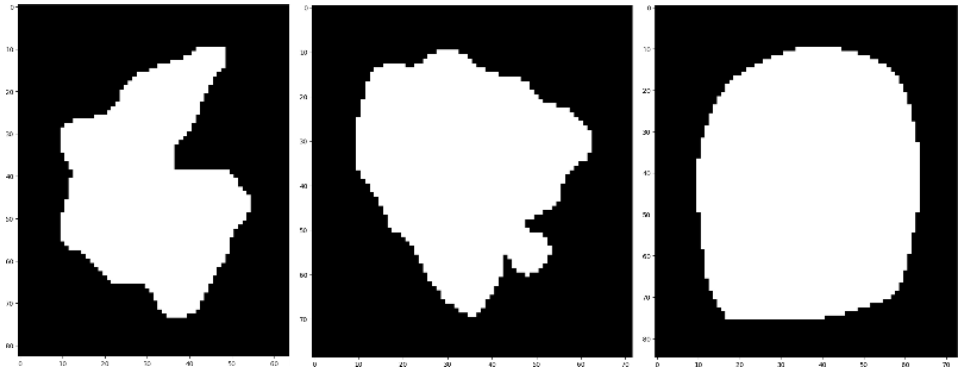

Figure 3.7. Visualization of generated masks for trees, showing distinct segmentation results used for further canopy analysis and feature extraction.

3.3.6 Filtering Irrelevant Masks and Removing Duplicate Bounding Boxes

After running SAM on the converted DSM-DTM imagery, a list containing dictionaries with details for each mask, such as bounding box coordinates and mask area, was obtained. The use of different threshold values for mask filtering serves specific purposes at various stages of the process. Initially, the SAM model is executed with a minimum mask region set to 200 pixels. This initial threshold is set relatively low to perform preliminary filtering, removing small and irrelevant masks without needing to run the model multiple times. After obtaining the initial set of masks, a secondary, more stringent filtering process is applied with thresholds of 300 and 8000 pixels. This second step fine-tunes the results by removing masks that are either too small or excessively large, ensuring the remaining masks are within the desired size range for accurate analysis. This dual-step filtering approach optimized computational efficiency by avoiding multiple runs of the SAM while achieving high-quality and accurate segmentation results. These thresholds were established through trial and error.

The bounding boxes were selectively removed based on their coordinates and the pixel-wise area of each tree. Specifically, if a bounding box included more than one other bounding box within it (Fig. 3.8), it was marked for removal under the assumption that it was likely to be an erroneous detection. Additionally, if a bounding box was entirely enclosed in another and

there was only one such enclosure, the areas of the two bounding boxes were compared. The smaller of the two bounding boxes was then marked for removal, operating under the assumption that the larger detection was more likely to be corrected. This process helped to reduce false positives by ensuring that each tree detection was distinct and not a subset of another.

Through this filtering process, we reduced the number of masks, and the remaining masks were then indexed, allowing us to label and count each tree within our study. Fig. 3.9 provides the pseudo code for handling the issue of overlapping between trees during segmentation.

Figure 3.8. Visualization of overlapping masks of red maple trees under different conditions: (a) and (b) illustrates a single bounding box containing one mask, (c) and (d) illustrates a larger bounding box containing more than one smaller bounding box.

```
Data: SAM generated masks (List of binary masks which has been generated by SAM)
Result: Filtered Masks with non-overlapping bounding boxes to remove ← empty set;
for each data1 in SAM generated masks do
      inside count ← count how many bbox are inside each bounding boxes;
      if inside count > 1 then
            Add the index of data1 to remove;
      else
            for each data2 in SAM generated masks do
                  if data2's bbox is inside data1's bbox then
                        Add index of smaller area between data1 and data2 to remove;
                  end
            end
      end
end
Filter masks by removing indices in to remove;
```

Figure 3.9. Pseudo code for handling overlapping issues during the segmentation process using SAM.

3.2.7 Measuring Tree Canopy Area, Height, and Volume

Tree Detection and Counting

The process of detecting and counting trees within the datasets transforms segmentation masks generated by the SAM into quantified and identifiable tree data. This procedure ensures that each tree is accurately detected and counted for further analysis.

Detecting Trees:

- **Unique Identifiers:** Each tree is assigned a unique identifier in the form of "T" followed by an index number (e.g., T1, T2, etc.). This identifier is used not only for labeling trees on the image but also serves as a reference in the generated dataset for tree attributes such as area, volume, and height.
- **Centroid Calculation for Label Placement:** For each tree mask within its bounding box, the centroid was calculated to serve as the anchor point for the label after removing duplicates. By doing so, the label was positioned in a visually coherent location that corresponds to the central point of the tree mask. The largest contour detected within

the binary segmentation was used for centroid calculation. The centroid (cx, cy) of the contour was determined using the moments of the contour. It was calculated using the following formulas:

$$(a)\ cx = \frac{M_{10}}{M_{00}}$$
$$(b)\ cy = \frac{M_{01}}{M_{00}} \quad \text{(Eq. 3.1)}$$

where:

M_10 and M_01 represent the first-order spatial moments.

M_00 represents the area of the contour.

Spatial moments are statistical measures that provide information about the shape and pixel intensity distribution of the contour. By calculating the centroid this way, we ensured that the label was placed accurately based on the actual shape and area of each tree mask, improving the clarity and reliability of the annotated image.

Counting Trees:

The counting of trees is directly linked to the detection process. Giving each tree mask a unique identifier allowed us to detect and count the trees effectively. We determined the total number of trees in the dataset by iterating through all the masks and labeling each one.

Canopy Area Measurement

To translate the pixel-wise area to the real-world area, some white paper boards placed within the imaging area, served as the reference object. The board's real-world dimensions were 0.76 meters in length and 0.51 meters in width. The area of the board, as captured in the image, was determined to be 620 pixels. From these values, we derived a conversion factor using the formula:

$$\text{Conversion Factor } (m^2/\text{pixel}) = \frac{Real\ world\ area}{Pixel\ wise\ area} \quad \text{(Eq. 3.2)}$$

Applying the whiteboard's dimensions to this formula, we calculated the conversion factor that would be used to convert pixel-wise areas into square meters. Using this conversion, we then translated the area of each tree, as derived from SAM, into its real-world area.

For validating the area of drone measurements, ground truths for one out of three datasets, i.e. D3, were calculated manually. For manual area calculation, each experimental tree was divided into three sections from the canopy starting point (Fig. 3.10). Two diameters for each section (measured parallel and perpendicular to the row) were measured using a measuring tape. The area for manual measurement was calculated by considering the tree in the canopy region as a circle. All six diameters were averaged, and the formula for the area of a circle (Eq. 3.3) was applied to calculate the canopy area.

$$Manual\ canopy\ area\ (\mathrm{m})^2 = \pi((d1 + d2 + d3 + d4 + d5 + d6)/12)^2 \qquad \text{(Eq.3. 3)}$$

where d1, d2, d3, d4, d5, and d6 are the diameters of the tree at different sections of the canopy region.

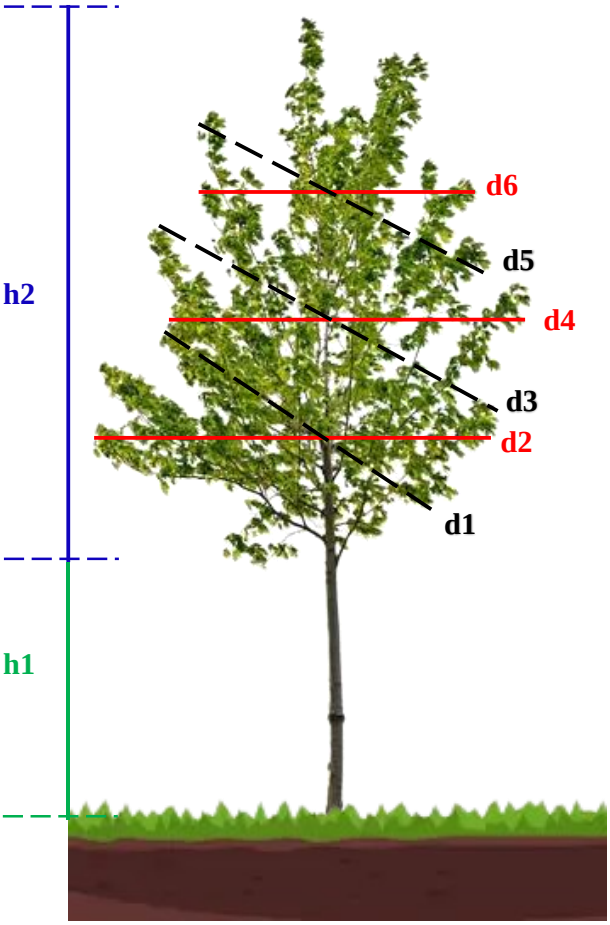

Figure 3.10. The tree is divided into three sections to measure six diameters of the canopy (d1, d2, d3, d4, d5, and d6). h1 and h2 represent the height of a tree below the canopy start point and after the canopy start point, respectively.

Tree Height Measurement

After successfully segmenting individual trees and measuring their areas, we determined each tree's height. The primary source for height data was DSM-DTM imagery, which provides elevation data for each pixel. This dataset is particularly valuable as it directly measures elevation above the terrain, which is essential for accurate tree height calculation. To estimate the height of each tree, we analyzed the elevation data within the bounding box coordinates of each segmented tree mask, which was derived from SAM. The process involved

identifying the pixel with the maximum elevation value within this bounding box if this point represents the tree's height.

The validation of tree height was performed using manual heights measured using a measuring tape for all three datasets.

Canopy Volume Measurement

The final step in our quantitative analysis was to estimate the volume of each individual tree. The ground sample distance (GSD) was used to compute the volume of the individual tree. This value was derived from the measurements of a reference sheet with a length of 0.76 meters and a width of 0.51 meters, giving it an area of 0.3876 square meters (0.76 m × 0.51 m). The area of this sheet in pixels was 620. Therefore, dividing the paper's real-world area (0.3876 m^2) by its area in pixels (620 pixels) gave us the area per pixel, which is the square of the Ground Sample Distance (GSD^2), calculated as 0.00062903 m^2/pixels. The canopy volume was then multiplied by the total height (in intensity) from each pixel within the boundary of a tree segmented by SAM by GSD^2.

$$Canopy\ volume\ (m^3) = (\sum_{i=0}^{n} Height\ of\ the\ pixel_i \times GSD^2) - (Avergae\ trunk\ height\ from\ ground\ to\ canopy\ starting\ point \times Total\ number\ of\ pixels\ from\ a\ tree \times GSD^2) \quad \text{(Eq. 3. 4)}$$

The drone-measured volume was validated using the ground truth of volume measured manually. The canopy part of the tree was considered a cylinder, and the volume formula for the cylinder was applied to calculate the manually measured volume using Eq. 3.5.

$$Manual\ canopy\ volume\ (\mathrm{m})^3 = \pi * h2 * (d1 + d2 + d3 + d4 + d5 + d6)/12^2 \quad \text{(Eq. 3.5)}$$

where h2 is the height of the tree canopy

Estimation of Agrochemical Requirement

Estimating the agrochemical needs for ornamental trees is essential for growers to calculate production expenses accurately and avoid the unnecessary or inadequate use of agrochemicals in the field. This study utilized volume information to calculate the required agrochemicals, with chemical amounts established considering the trees' maximum capacity to retain liquid spray. This study followed the standard practice suggested by Furness et al. (Furness et al., 1998), which involves using 80 liters of spray volume for every 1000 cubic meters of tree canopy volume, accounting for the maximum canopy retention volume. Therefore, this study employed a chemical application rate of 0.08 liters per cubic meter of tree canopy volume when determining the spray volume for the 24 selected experimental trees.

3.3.8 Statistical Analysis

A paired t-test was conducted to evaluate the agreement between drone and manual measurement methods for tree height calculation in all three datasets. The paired t-test aimed to discern whether there were statistically significant differences between the drone and manual height measurements. Subsequently, performance metrics, including the RMSE and MAE, were computed for all three parameters to quantify the accuracy of the drone-derived measurements relative to the manual values in all datasets. The statistical analyses were conducted using R software (Team, 2010), employing appropriate functions and packages to execute the paired t-tests and compute the RMSE and MAE values. The RMSE and MAE formulas are given by:

$$RMSE = \sqrt{\frac{\sum_{i-1}^{n}(y_i - \hat{y}_i)^2}{n}} \quad \text{(Eq. 3.6)}$$

$$MAE = \frac{\sum_{i-1}^{n} | y_i - \hat{y}_i |}{n} \quad \text{(Eq. 3.7)}$$

where y_i represents the manually measured height, $\hat{y}_i$ denotes the corresponding drone-measured height, and n signifies the total number of measurements.

3.4 Experimental Results and Discussion

3.4.1 Tree Detection and Counting

The segmented image displayed each tree labeled with an identifier and a corresponding number (e.g., identifier: T322), as shown in Fig. 3.11. The tree count was conducted manually using the orthomosaic images, revealing 373 trees in D1, averaging 34 trees per row, 361 trees in D2, averaging 33 trees per row, and 423 trees in D3, averaging 71 trees per row (Fig. 3.12). The SAM identified 370 trees in D1, 367 trees in D2, and 420 trees in D3. The algorithm missed three trees in D1, overestimated six trees in D2, and missed three trees in D3 analysis. The overestimation of six trees in D2 could be due to tall vegetation in the field while capturing D2 data (Fig. 3.14b). This observation implies that SAM's performance might be optimized in environments with a well-maintained, mowed nursery, such as in D1 and D3 as opposed to those lacking such grooming such as in D2. Notably, in D2, SAM encountered challenges distinguishing between grass and potholes, resulting in misclassifications where these non-tree elements were identified as trees. The resolution of stitched images could also be one of the possible factors for misclassifications. It is one of the limitations of the SAM as per this experiment. Strategies to enhance results include reducing noise in aerial images through pre-data collection measures like mowing vegetation. Despite these challenges, it is important to note that SAM exhibited good accuracy and holds the potential for further improvements by minimizing noise in the data. Many studies have used UAVs for data collection and deep learning or segmentation algorithms for counting trees in forests or orchards (Bazi et al., 2014; Chen & Shang, 2022; Yao et al., 2021). Santoro et al. (Santoro et al., 2013) developed a tree counting algorithm and spatial transforms for individual fruit tree identification using Very High Spatial Resolution (VHSR) satellite imagery. Our approach introduced a self-supervised deep learning approach for segmenting and counting trees that reduces reliance on manual

image annotation. It used aerial images captured using an RGB camera attached to a drone, and SAM was employed to count trees and calculate tree canopy area.

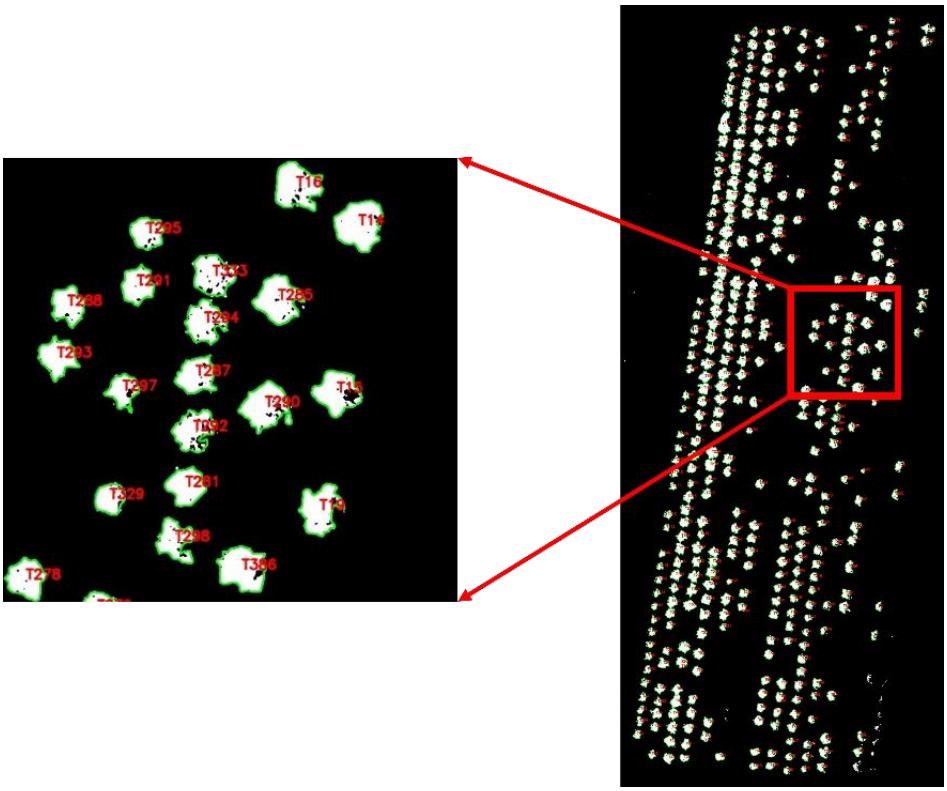

Figure 3.11. Processed image from SAM shows individual tree counts. The inset zooms into a section of the processed data, where trees are distinctly segmented in green and labeled in red for further analysis.

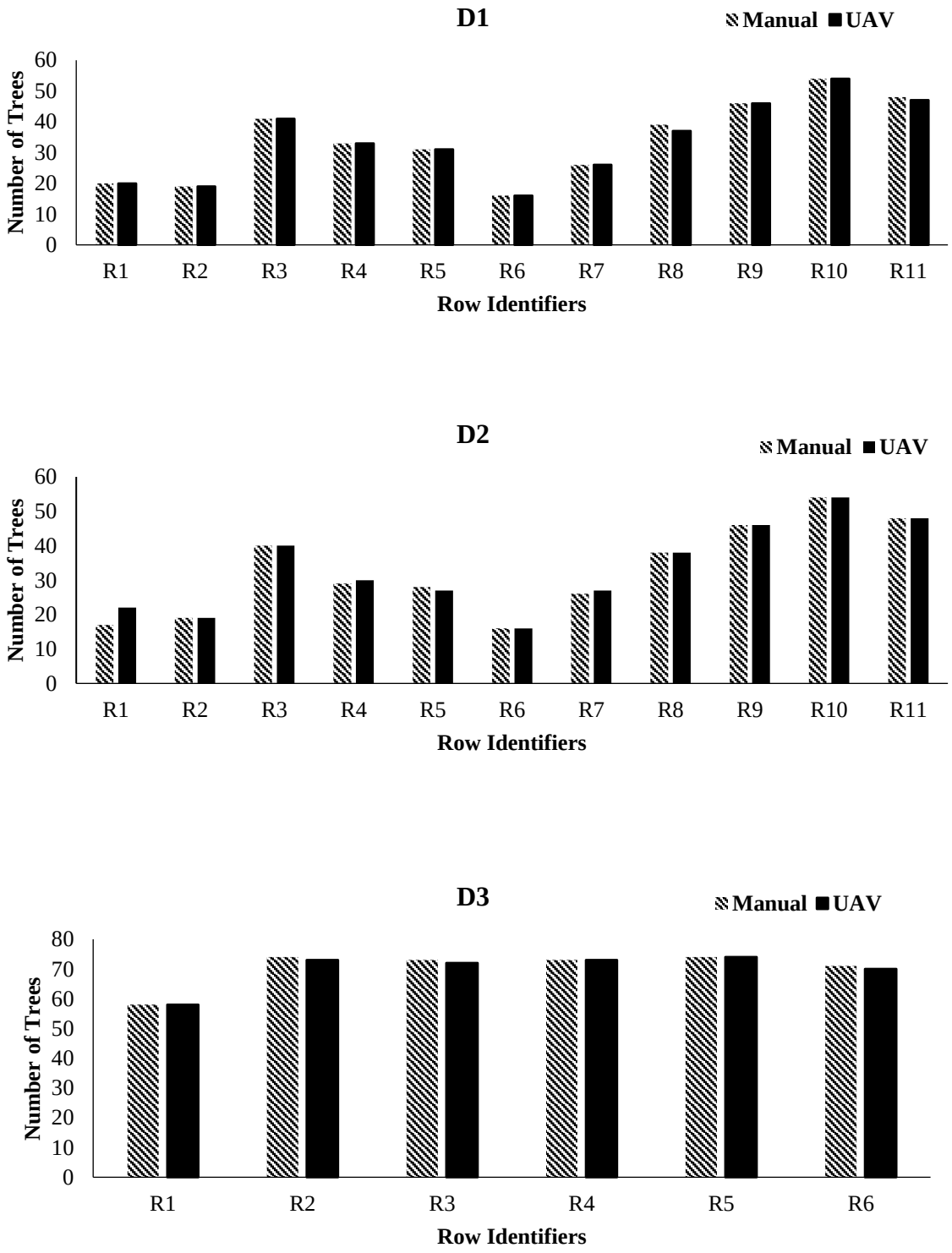

Figure 3.12. Row-based comparison of tree counts obtained manually and using a UAV-based approach for datasets D1 (top), D2 (middle), and D3 (bottom). The figure shows variations in tree counts for each row (R1 to R11 for D1 and D2, and R1 to R6 for D3).

3.4.2 Tree Height Measurement

The tree height measured manually and using UAV for 24 trees under experiment in D1, D2, and D3 are presented in Table 3.2, along with the absolute error, and Fig. 3.13 shows their comparison. A paired t-test ($p \leq 0.05$) comparing drone-based and manual measurements of tree heights across datasets D1, D2, and D3 revealed high agreement between the methods. In D1, a non-significant p-value of 0.27 and an R^2 value of 0.57 indicate no significant difference. For D2, despite a highly significant p-value (6.078e-11), the mean difference is minor (-0.23), and a high R^2 value of 0.86 suggests strong agreement. In D3, a non-significant p-value of 0.87 and an R^2 value of 0.37 confirm the consistency and reliability of drone-based measurements. These results underscore the reliability of drone-based data collection for measuring tree height across all datasets. The average tree height in D1 for manual and UAV-based measurements was 3.62 m and 3.65 m, respectively. For D2, it was 3.30 m and 3.53 m, respectively, and for D3, it was 2.94 m and 3.31 m, respectively. The height of trees in D2 was comparatively lower because growers trimmed the top canopies of trees of the experimental nursery. The average absolute error of the height measurement was 2.43% in D1, 7.09% in D2, and 12.58% in D3. The MAE and RMSE obtained for D1 were 0.09 m and 0.13 m, respectively. For D2, they were 0.23 m and 0.25 m, respectively, and for D3, they were 0.16 m and 0.21 m, respectively. The poorer results for D2 compared to D1 can be attributed primarily to the significant growth of grass/vegetation within the 18 days between data collection. The presence of tall or dense grass (Fig. 3.14b) can interfere with UAV imagery and subsequent data analysis, leading to decreased accuracy in measurements and assessments. The tall vegetation provided an inaccurate DTM for D2 (it was difficult to determine the surface ground of the experimental nursery); thus, height measurement errors were higher. In order to reduce the error due to vegetation, it is suggested that the plot be mown before data collection. Fields with tall vegetation need to capture some portion of bare soil that could be from outside of the field

during drone imagery collection to minimize errors. As results show, in most of the trees, the UAV-based measurement was more than the manual-based measurement, which means overestimated, which can be ascribed to both coarser spatial resolution and elevation differences within the ornamental field. However, in R2T14 (identifier: T366), the height was underestimated by 0.45 m. This might be due to human error during manual measurement. The underestimation was not observed in the D2 measurement for this tree. In the case of D3, which was a different experimental plot (Fig. 3.14c) as compared to D1 and D2, the absolute error ranged from 0.01 m to 0.91 m, with a percentage error ranging from 0.36% to 31.28%. The larger percentage errors were observed in trees with smaller manual measurements, as seen in R6T62, where the manual measurement was 2.91 m, and the drone measurement was 3.82 m, resulting in a 31.28% error. Despite these individual discrepancies, the overall average absolute error of 0.37 m and percentage error of 12.58% in D3 still indicate a general alignment between the two methods. The higher average error in D3 compared to D1 and D2 might be attributed to factors such as the presence of dense canopy cover or irregular tree shapes, which can affect the accuracy of drone-based measurements. Additionally, human error in manually measuring height might arise from the challenge of estimating height variations caused by visible slope changes in certain trees. Lim et al. (2015) performed a similar study for tree height extraction using drone images and achieved RMSE values of 0.84 m in test area 1 (coniferous trees) and 2.45 m in test area 2 (deciduous coniferous trees) (Lim et al., 2015). Our study achieved better accuracies with an improved segmentation approach.

Table 3.2. Calculation of absolute error for manual and UAV-based tree height measurements across datasets D1, D2, and D3. D1, D2, and D3 exhibited average absolute errors of 0.09 m (2.43%), 0.23 m (7.09%), and 0.37 m (12.58%), respectively.

Tree No.	D1				D2				D3				
	Height Measured (m)		Absolute Error		Height Measured (m)		Absolute Error		Tree No.	Height Measured (m)		Absolute Error	
	Man-ual	UAV	(m)	(%)	Man-ual	UAV	(m)	(%)		Man-ual	Drone	(m)	(%)
R2T3	3.77	3.87	0.1	2.65	3.66	3.91	0.25	6.83	R1T3	2.65	2.94	0.28	10.59
R3T3	3.7	3.87	0.17	4.59	3.73	3.9	0.17	4.56	R2T3	3.23	3.21	0.01	0.36
R2T14	3.85	3.4	0.45	11.69	3.93	3.95	0.02	0.51	R1T10	3.05	3.21	0.17	5.45
R3T13	3.66	3.66	0	0	3.65	3.79	0.14	3.84	R2T10	2.79	2.94	0.15	5.35
R3T10	3.73	3.99	0.26	6.97	3.7	3.83	0.13	3.51	R1T22	3.00	3.30	0.30	10.17
R4T10	3.75	3.82	0.07	1.87	3.15	3.41	0.26	8.25	R2T22	2.54	2.87	0.33	12.95
R3T17	3.59	3.7	0.11	3.06	3.1	3.67	0.57	18.39	R1T48	2.74	3.12	0.38	13.86
R4T17	3.71	3.84	0.13	3.5	3.17	3.46	0.29	9.15	R2T48	3.11	3.33	0.22	6.92
R4T1	3.29	3.41	0.12	3.65	3.1	3.36	0.26	8.39	R3T5	2.78	3.00	0.21	7.72
R5T1	3.46	3.42	0.04	1.16	2.98	3.24	0.26	8.72	R4T5	2.84	3.07	0.22	7.89
R4T14	3.76	3.8	0.04	1.06	3.19	3.41	0.22	6.9	R3T16	2.74	3.11	0.37	13.44
R5T14	3.45	3.42	0.03	0.87	3.4	3.58	0.18	5.29	R4T16	3.01	3.21	0.20	6.50
R8T2	3.6	3.55	0.05	1.39	3.29	3.52	0.23	6.99	R3T33	3.09	3.39	0.30	9.78
R9T2	3.45	3.49	0.04	1.16	3.19	3.48	0.29	9.09	R4T33	3.00	3.45	0.46	15.25
R8T11	3.94	3.96	0.02	0.51	3.3	3.47	0.17	5.15	R3T46	2.74	3.33	0.58	21.27
R9T13	3.64	3.82	0.18	4.95	3.22	3.42	0.2	6.21	R4T46	2.84	3.46	0.61	21.45
R9T3	3.64	3.66	0.02	0.55	3.27	3.45	0.18	5.5	R5T17	3.20	3.67	0.47	14.77
R10T3	3.41	3.41	0	0	3.05	3.31	0.26	8.52	R6T17	3.07	3.64	0.56	18.38
R9T20	3.64	3.67	0.03	0.82	3.38	3.5	0.12	3.55	R5T24	2.95	3.23	0.28	9.56
R10T21	3.7	3.72	0.02	0.54	3.18	3.44	0.26	8.18	R6T24	3.20	3.60	0.40	12.36
R10T6	3.68	3.78	0.1	2.72	3.18	3.41	0.23	7.23	R5T35	3.19	3.45	0.26	8.08
R11T5	3.51	3.45	0.06	1.71	3.14	3.42	0.28	8.92	R6T35	3.05	3.58	0.54	17.58
R10T12	3.53	3.55	0.02	0.57	3.04	3.26	0.22	7.24	R5T62	2.92	3.53	0.61	20.84
R11T11	3.39	3.31	0.08	2.36	3.17	3.46	0.29	9.15	R6T62	2.91	3.82	0.91	31.28
Avg.	**3.62**	**3.65**	**0.09**	**2.43**	**3.3**	**3.53**	**0.23**	**7.09**		**2.94**	**3.31**	**0.37**	**12.58**

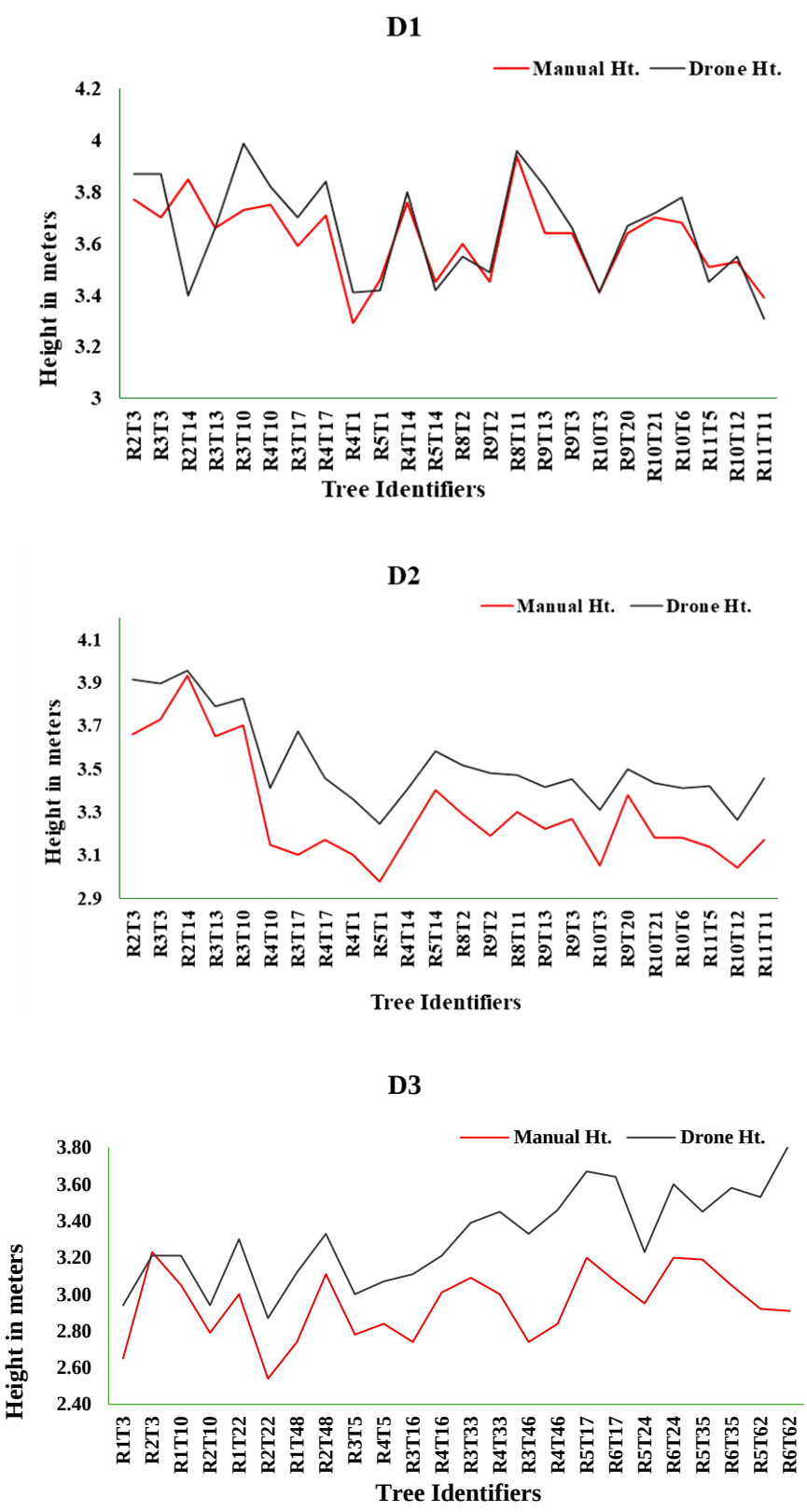

Figure 3.13. Comparison of tree heights measured manually and using a drone for datasets D1, D2, and D3. The red line represents the manually measured heights, while the black line represents heights measured using the UAV.

(a) **(b)** **(c)**

Figure 3.14. Comparison of the two experimental plots during data collection. D1 and D2 are presented in (a) and (b), which are from the first experimental plot and (c) represents the second experimental plot used for D2; the grass is short in (a) and (c) and long in (b).

3.4.3 Canopy Area Measurement

In D1, the average tree area was 1.6 m^2 among the 24 trees under the experiment. R11T11 (identifier: T107) covered a minimum area of 0.85 m^2, and R3T10 (identifier: T85) covered a maximum area of 2.23 m^2. Similarly, in D2, the average tree area was 3.52 m^2 among 24 trees. R3T17 (identifier: T307) covered a minimum area of 2.38 $m^{2,}$ and R9T13 (identifier: T36) covered a maximum area of 5.99 m^2. In the case of D3, the average tree canopy area was 1.18 m^2 for manual measurement and 1.27 m^2 for drone measurement among 24 trees under the second experimental plot (Table 3.3). The tree with the largest canopy area was R3T33 (identifier: T305), with measurements of 1.95 m^2 manually and 2.05 m^2 by drone. Tree R5T24 (identifier: T557) exhibited the highest absolute error at 0.34 m^2, while tree R2T3 (identifier: T159) had the lowest absolute error at 0.1 m^2. The significant absolute errors in tree canopy area measurements were primarily due to human error in the manual calculations. This error stemmed from the assumption that the tree canopy area was circular, whereas tree canopies are irregularly shaped, leading to slight overestimations or underestimations in some cases. The

RMSE and MAE were calculated as 0.18 m^2 and 0.15 $m^{2,}$ respectively, which indicated the degree of discrepancy between the manual and drone measurements in the D3 dataset. These relatively low error values suggest that, while there are some differences between the methods, both manual and drone measurements were reasonably consistent with each other.

As reported in the previous research (Panagiotidis et al., 2017), one of the challenges in the canopy area calculation was overlapping. This issue was handled through the filtering process. Initially, the number of masks was more than 400 in D1 and D2 and 665 in D3. However, the numbers decreased to 370 in D1, 367 in D2, and 641 in D3, with each mask representing a distinct tree. For each mask, the pixel area generated by SAM is multiplied by the GSD value. This conversion provides the area in real-world measurements. The dual-step filtering approach (section 2.4.2) optimized computational efficiency by avoiding multiple runs of the SAM while achieving high-quality and accurate segmentation results. The thresholding values refined the measurements by excluding noise and ensuring an accurate representation of tree canopies, thereby significantly improving the reliability and consistency of our measurements across different datasets.

Table 3.3. Comparison of tree canopy area and volume measurements obtained manually and using drone-based methods for dataset D3. The average absolute error for canopy area was 0.16 m^2 (14.94%), while for canopy volume, it was 0.13 m^3 (17.88%).

ID	Area		Absolute Error		Volume		Absolute Error	
	Manual	Drone	(m)	(%)	Manual	Drone	(m)	(%)
R1T3	1.11	1.16	0.05	4.26	1.28	0.84	0.44	34.30
R2T3	0.89	0.88	0.01	1.56	1.43	0.80	0.63	44.36
R1T10	0.81	1.10	0.29	35.81	1.21	0.99	0.23	18.55
R2T10	0.58	0.79	0.20	34.85	0.70	0.62	0.08	10.92
R1T22	1.45	1.42	0.03	2.28	2.17	1.63	0.54	25.08
R2T22	0.94	0.65	0.29	31.06	0.86	0.68	0.18	21.06
R1T48	1.35	1.26	0.09	6.65	1.65	1.64	0.01	0.50
R2T48	1.27	1.45	0.18	14.22	1.95	1.95	0.00	0.23
R3T5	1.20	1.25	0.05	3.77	1.64	1.57	0.07	4.54
R4T5	0.69	0.65	0.04	5.83	0.90	0.78	0.12	13.70
R3T16	1.02	1.26	0.24	24.02	1.37	1.85	0.48	35.00
R4T16	1.38	1.22	0.16	11.38	1.84	1.70	0.13	7.30
R3T33	1.95	2.05	0.10	5.36	2.99	2.96	0.03	1.08
R4T33	1.17	1.20	0.04	3.05	1.99	1.57	0.41	20.69
R3T46	1.48	1.36	0.13	8.77	1.77	1.45	0.32	18.14
R4T46	0.81	1.07	0.26	31.65	1.07	0.90	0.17	15.98
R5T17	1.38	1.57	0.19	13.93	2.38	2.01	0.37	15.51
R6T17	1.24	1.54	0.30	23.93	1.77	1.64	0.13	7.22
R5T24	0.94	1.27	0.34	35.95	1.19	0.90	0.28	23.96
R6T24	1.42	1.61	0.19	13.49	2.10	1.80	0.29	13.95
R5T35	1.54	1.61	0.07	4.54	2.25	2.02	0.23	10.42
R6T35	1.07	1.39	0.32	29.82	1.47	2.19	0.72	48.87
R5T62	1.49	1.44	0.04	2.90	2.00	2.00	0.00	0.14
R6T62	1.18	1.29	0.11	9.40	1.49	1.94	0.45	30.41
Average	**1.18**	**1.27**	**0.16**	**14.94**	**1.64**	**1.52**	**0.13**	**17.58**

3.4.4 Measurement of Canopy Volume and Agrochemical Requirement

The average volume of the tree was 2 m^3 in D1, 3.82 m^3 in D2, and 1.52 m^3 in D3 (Table 3.3). As previously noted, during the collection of D2, the terrain was obscured by tall and dense grasses, potentially contributing to errors in the DTM generation and subsequent volume estimations. Additionally, the observed increase in tree volume from D1 to D2 may be

attributed to natural growth over the 18-day interval between data collection periods. The average tree height from the ground to the canopy starting point (the height at which canopies started growing), which was calculated as 1.54 m, was subtracted from volume calculation to calculate accurate tree canopy volume. In the case of D3, the drone measurement of the volume of tree canopies was compared with the manual measurements. The RMSE and MAE for volume measurements were calculated as 0.33 m^3 and 0.26 $m^{3,}$ respectively, which indicated the level of agreement between manual and drone measurements. These error values suggested that while there were discrepancies between the two methods, both manual and drone measurements of volume were fairly consistent with each other.

Cunha et al. (2019) measured tree canopy volume using UAV-mounted cameras, creating 3D models, which were then compared with TRV measurements for validation. This study introduced the utilization of canopy attributes or characteristics, particularly volume, as a valuable parameter for estimating the precise quantity of agrochemicals needed in ornamental trees. Following the standard practice mentioned in section 2.6, the volume of agrochemicals for each experimental tree was calculated using D1 information (Table 3.4). In the same manner, the chemical requirement in all the trees can be calculated with this approach. For D1, the range of the chemicals lay between 0.07 l to 0.25 l, with 0.16 l being the average volume. Likewise, for D2, the range of the chemicals lay between 0.18 l and 0.49 l, with 0.31 l being the average volume. For D3, the range of the chemicals lay between 0.05 l and 0.24 l, with 0.12 l being the average volume. In future studies, the estimated agrochemical quantity per tree will be compared with the actual application in red maple nurseries of the same age and variety. A precision air blast sprayer for ornamental tree spraying will be utilized, adjusting the application quantity based on tree canopy volume. The application quantity for individual trees using the precision sprayer will be compared with the agrochemical requirement calculated by UAV to evaluate the potential of this technology.

Table 3.4. Calculation of agrochemicals required for individual trees based on their canopy volume for datasets D1, D2, and D3. The average agrochemical requirements across datasets were as follows: D1 - 0.17 l, D2 - 0.31 l, and D3 - 0.14 l

Tree No.	D1		D2		Tree No.	D3	
	Volume (m^3)	Agrochemical Req.	Volume (m^3)	Agrochemical Req. (l)		Volume (m^3)	Agrochemical Req. (l)
R2T3	1.47	0.12	3.10	0.25	**R1T3**	0.84	0.07
R3T3	1.42	0.11	3.80	0.30	**R2T3**	0.80	0.06
R2T14	1.48	0.12	3.41	0.27	**R1T10**	0.99	0.08
R3T13	1.89	0.15	3.74	0.30	**R2T10**	0.62	0.05
R3T10	1.67	0.13	3.39	0.27	**R1T22**	1.63	0.13
R4T10	1.57	0.13	2.87	0.23	**R2T22**	0.68	0.05
R3T17	2.28	0.18	3.41	0.27	**R1T48**	1.64	0.13
R4T17	2.43	0.19	2.69	0.21	**R2T48**	1.95	0.16
R4T1	1.56	0.12	2.30	0.18	**R3T5**	1.57	0.13
R5T1	1.29	0.10	2.74	0.22	**R4T5**	0.78	0.06
R4T14	2.44	0.20	2.92	0.23	**R3T16**	1.85	0.15
R5T14	1.60	0.13	3.68	0.29	**R4T16**	1.70	0.14
R8T2	2.21	0.18	4.85	0.39	**R3T33**	2.96	0.24
R9T2	2.74	0.22	3.78	0.30	**R4T33**	1.57	0.13
R8T11	2.99	0.24	6.10	0.49	**R3T46**	1.45	0.12
R9T13	3.10	0.25	5.33	0.43	**R4T46**	0.90	0.07
R9T3	2.78	0.22	5.29	0.42	**R5T17**	2.01	0.16
R10T3	1.63	0.13	3.33	0.27	**R6T17**	1.64	0.13
R9T20	2.42	0.19	5.13	0.41	**R5T24**	0.90	0.07
R10T21	2.44	0.19	4.59	0.37	**R6T24**	1.80	0.14
R10T6	2.17	0.17	4.81	0.39	**R5T35**	2.02	0.16
R11T5	1.31	0.10	3.57	0.29	**R6T35**	2.19	0.18
R10T12	2.20	0.18	4.13	0.33	**R5T62**	2.00	0.16
R11T11	0.92	0.07	2.76	0.22	**R6T62**	1.94	0.16

3.4.5 Discussion and Future Directions

This study introduced a UAV-based method for assessing ornamental trees, encompassing parameters such as tree count, tree height, crown area, and canopy volume. The results demonstrated the precision of this approach for effective tree monitoring and approximate agrochemical calculations. A common traditional practice of measuring tree

volume is Tree Row Volume (TRV) (Byers et al., 1984). It refers to measuring or evaluating the volume occupied by trees in a row, typically in agricultural settings such as nurseries, orchards, or plantations. It entails computing the volume of the canopy by assuming it has a prismatic shape (Sutton & Unrath, 1984). Da Cunha et al. (da Cunha et al., 2019) developed a UAV-based method for determining coffee crop vegetation volume from digital images and compared its efficacy with the TRV method. Anifantis et al. (Anifantis et al., 2019) compared three methods for evaluating TRV in a super-high-density olive orchard using UAV photogrammetry and 3D modeling against manual and traditional TRV detection methods. Our study calculated the canopy volume of individual trees as it is important for precision spraying.

Factors like flying altitude, image resolution, and overlap were identified to enhance accuracy (Kyriou et al., 2021). This research utilized an 80% forward and side overlap during aerial data collection for both flights. In these future studies, different flying altitudes and image overlapping values will be explored to determine the optimal settings for improved accuracy in different kinds of ornamental crops. Torres-Sánchez et al. (2015) achieved high accuracy in the geometrical characterization of woody crops using 60% lateral overlap, while Torres-Sánchez et al. (2018) suggested a 95% forward overlap when flying at 100 m altitude. Using a large number of images increases processing times while using fewer images reduces accuracy. The reliability of results, including orthomosaic, DSM, and DTM, relies on image quality affected by weather and sunlight.

This study overcame the overlapping of trees' canopy challenge effectively using the filtration approach to ensure accuracy. However, the presence of tall vegetation can obstruct the view of the tree’s basal region, causing slight variations in the measurement of canopy characteristics. Additionally, aerial images might have a lower resolution in some cases. Ideally, image resolution should remain consistent across all images captured at a particular altitude, ensuring uniform quality and detail. However, variations in factors such as

atmospheric conditions, in particular, wind speed and direction, while in flight missions could lead to the movement of canopies, resulting in some images being less clear or detailed than others due to factors like suboptimal camera settings, which can reduce the clarity and detail of the images. Despite some minor challenges, the study proved successful and serves as a foundational resource for researchers, growers, and industries. The methodology initially applied to red maple highlights adaptability for various ornamental and fruit trees.

The SAM is a great advancement in computer vision technology, primarily due to its varied capability to identify and segment different objects in images, regardless of their complexity. This innovation is crucial as it enables more accurate and detailed analysis of visual data, thus overcoming the limitations of traditional models that often struggle with complex or overlapping objects. Additionally, SAM's advanced learning algorithms significantly reduce the need for extensive labeled datasets, which traditionally pose a challenge in machine learning. This efficiency not only accelerates the development cycle but also opens new possibilities in fields where data shortage is a bottleneck.

The approach developed in this study can be put together in a computer application, where the aerial images will be provided, and it will provide the height of the tree. Wu et al. (Wu et al., 2023) developed ARTreeWatch, an AR-based mobile app for Android smartphones to measure tree height and diameter and found it to be an efficient, accurate, and cost-effective alternative to traditional ground surveys, saving half the labor and time. The next step of this study is to generate real-time tree counting and tree height by incorporating the final SAM algorithm into the edge device attached to the drone system. Salamí (Salamí et al., 2019) presented a novel approach to utilize UAS for real-time aerial sensing for olive tree counting. This would be helpful for growers, researchers, and industries to get information for precision spray applications instantly. Moreover, this approach can be applied to generate agrochemical charts for growers, facilitating the estimation of the appropriate chemical quantities based on

factors such as growth, season, and field conditions. This method can serve as a standardized practice for ornamental and fruit trees cultivated with row spacing.

Looking ahead, advancements in AI can be implemented to achieve better and quicker results. Particularly, OpenAI's technologies could aid in developing user-friendly interfaces for the envisioned computer application, allowing seamless integration of SAM algorithms, aerial images, and data outputs for real-time tree counting and height estimation, offering a more accessible and efficient tool for growers, researchers, and industries involved in precision agriculture.

3.5 Conclusions

Accurate estimation of agrochemical needs in the ornamental industry helps growers calculate expenses prudently, preventing the overuse of chemicals and promoting sustainable agricultural practices. This study employed a drone-based method with an RGB sensor to accurately measure ornamental tree canopy attributes with the aim of calculating tree count, tree height, canopy area, canopy volume, and agrochemical requirements. The drone-calculated heights of 24 randomly selected trees in two experimental plots were compared with manual measurements. The average absolute error was 2.43% in D1, 7.09% in D2, and 12.58% in D3. The MAE and RMSE were 0.09 m and 0.23 m in D1, 0.13 m and 0.25 m in D2, and 0.16 m and 0.21 m in D3. In D3, manual area and volume calculations validated the drone data, with area RMSE and MAE of 0.18 m^2 and 0.15 m^2 and volume RMSE and MAE of 0.33 m^3 and 0.26 m^3. The canopy volume calculation estimated the average value of the agrochemical needs from all three datasets of a maple tree to be 0.20 liters. The results indicate the potential for precise agrochemical estimation during precision spray applications and proper crop management. Although there was a slight overestimation of tree height and tree count, these discrepancies can be mitigated by reducing noise during data collection, improving the

generation of orthomosaic images, and selecting appropriate weather conditions. Notably, tree canopy area measurements using SAM yielded outstanding results. The study addressed the issue of overlapping canopies through an effective filtration process using SAM. This approach has the potential to enhance overall efficiency and productivity in both the ornamental and tree fruit industries and can serve as a benchmark for future research related to the measurement of canopy attributes in the ornamental and tree fruit sectors.

Acknowledgements

This study was supported by the USDA's NIFA Hatch Project (Accession No. 7007738) and the Startup and Institute for IIPA funds from the University of Georgia. The authors would like to give special thanks to Otis L. Floyd Nursery Research Center and Smith Farm for providing field access and necessary resources.

CHAPTER 4

DETERMINATION OF TREE ATTRIBUTES USING A GROUND-BASED SYSTEM WITH LIDAR SENSOR AND DEPTH CAMERA [2]

[2] Rayamajhi, A. and M.S. Mahmud. To be submitted to a peer-reviewed journal.

Abstract

Understanding and accurately measuring key tree characteristics, such as canopy volume and trunk diameter, is essential for improving resource management and sustainability in ornamental nurseries. These parameters help in the precise calculation of agrochemical requirements and in assessing tree maturity for market readiness. This study utilized a ground-based LiDAR system and a depth camera to measure these parameters. Canopy volume was estimated using a convex hull algorithm on processed point clouds through point cloud registration, ROI clipping, downsampling, and denoising whereas trunk diameter was calculated using a circle-fitting algorithm on point clouds at 0.15 m (6 in) above ground, derived from depth images and binary masks isolating the trunk region. Thirty-two trees were randomly selected in pairs from two plots (Plot-1 and Plot-2) with varying terrains for this experiment. The results for canopy volume of Plot-1 indicated an average absolute error percentage of 10.99%, with RMSE and MAE values of 0.37 m^3 and 0.33 m^3, respectively, while Plot-2 showed an error percentage of 13.01%, with an RMSE of 0.27 m^3 and MAE of 0.24 m^3. Similarly, the trunk diameter results in Plot-1 exhibited an average absolute error percentage of 0.33%, with an RMSE of 0.028 m and MAE of 0.020 m, whereas Plot-2 showed an error percentage of 1.11%, with an RMSE of 0.078 m and MAE of 0.065 m. The canopy volume measured using the LiDAR system was further used to estimate agrochemical needs, with results indicating an average requirement for one tree as 0.22 l in Plot-1 and 0.14 l in Plot-2. Likewise, the trunk diameter measured using the depth camera system was further analyzed for tree maturity analysis, revealing that Plot-1 had 10 mature trees while Plot-2 had only 5, indicating a more advanced growth stage in Plot-1. These findings demonstrate the feasibility and accuracy of integrating LiDAR and RGB-D technologies for efficient nursery management, offering a scalable solution for precision agrochemical application and maturity assessment, supporting sustainable practices in ornamental horticulture.

Keywords: LiDAR, RGB-D, Depth Camera, Canopy Volume, Trunk Diameter, Precision Spraying

4.1 Significance of the Study

In contrast to the UAV-based approach discussed in the previous chapter, this chapter introduces a ground-based system for measuring tree attributes, addressing specific limitations of aerial methods while offering distinct advantages. UAVs are ideal for quickly covering large areas and estimating agrochemical requirements before mixing, thereby reducing wastage. However, they face challenges such as occlusions, limited precision for detailed trunk measurements, and constraints on carrying significant agrochemical loads. The ground-based system, equipped with LiDAR and depth cameras, overcomes these limitations by providing high-resolution data for both canopy volume and trunk diameter. Additionally, its capacity to carry larger amounts of agrochemicals enables better spray deposition across different parts of the trees, making it more practical for precision spraying in densely planted nursery settings. This method demonstrated exceptional accuracy and agreement with manual measurements, complementing UAV systems by offering unmatched detail and practicality for on-ground operations in ornamental nurseries.

4.2 Introduction

Woody ornamental plants, especially ornamental trees, are an integral part of landscaping, valued for their ability to provide structure, longevity, and aesthetic appeal in various environments. Despite their environmental, decorative and economic benefits, challenges such as disease control, labor shortages, and ensuring plants are market-ready have threatened the industry's ability to meet production demands and sustain continued growth (Traversari et al., 2021). Tree characteristics such as canopy volume, height, and trunk diameter are important for assessing tree growth and biomass (Yin et al., 2011). Managing ornamental

trees in nurseries is both labor-intensive and costly, with tasks such as frequent spraying and growth assessment (Xun et al., 2023). Currently, most nurseries use broadcast spraying methods, with equipment like backpack or tractor-mounted sprayers to apply pesticides uniformly (Zwertvaegher et al., 2017) which have low efficiency. For instance, only 29% to 56% of the sprayed chemicals reach the target when using traditional air-blast and boom sprayers, leading to significant drift losses (Perry et al., 2013). To address these, advanced technologies, such as sensor-guided systems, offer greater precision, with the intelligent sprayer reducing spray volume and drift by up to 71% while maintaining efficacy (Boatwright et al., 2020). Another challenge faced by growers is assessing trunk diameter, a key factor in determining market readiness, which is typically done manually with calipers. Accurate measurements are important for optimal harvest timing and profit maximization (Grella et al., 2020); however, labor shortages hinder consistent monitoring.

Recent advancements in automation, such as precision spraying and sensor-based monitoring, have the potential to improve ornamental nursery operations, and address labor shortages. Various sensors, including time-of-flight cameras and ultrasonic transducers, improve precision. However, they may struggle with complex plant structures, leading to challenges in accurately capturing the three-dimensional geometry of trees (Li & Liu, 2019) (Miller et al., 2015). Meanwhile, LiDAR, which emits laser pulses to create detailed 3D models of vegetation, provides precise measurements of tree characteristics (Srinivasan et al., 2015). LiDAR's precision address the challenges seen with other methods, such as the inaccuracies in measuring slender branches (Jin et al., 2021). LiDAR is increasingly utilized to measure tree attributes through methods like Terrestrial Laser Scanning (TLS) and UAV-based LiDAR. TLS generates dense point clouds for highly detailed tree analysis (Xu et al., 2021). While UAVs offer speed and large-area coverage (Bartholomeus et al., 2022), they often struggle with occlusion, making it difficult to capture fine details like trunk diameters (Roşca et al., 2018;

Yrttimaa et al., 2020). Even though TLS data collection is time-consuming and requires manual setup (Dalla Corte et al., 2020), it is well-suited for smaller areas like ornamental nurseries, where its precision and detail outweigh the logistical challenges.

Many studies have successfully employed TLS for accurate canopy volume measurement, highlighting its effectiveness in capturing detailed tree canopy structures (Demol et al., 2021; Gao et al., 2021; Jacobs et al., 2020). It excels in scanning broad areas, making it an ideal tool for generating detailed models of tree canopies in nurseries. Bornand et al. (2023) applied TLS for non-destructive volume estimation of individual trees and identified that combining stem diameters and convex hull volumes around tree crowns can effectively model entire tree volumes. However, LiDAR's lower resolution for smaller features makes it less effective for measuring narrow objects, such as young tree trunks (Lassiter et al., 2020). In contrast, depth cameras offer a more suitable alternative for measuring thin tree trunks. With finer resolution at close range, depth cameras can capture the detailed surface geometry of narrow objects (Andújar et al., 2016) making them ideal for younger trees. In a study by J. Zhou et al. (2024), a non-invasive system was developed using RGB-D cameras to measure maize stem diameter. The system demonstrated a MAPE (Mean Absolute Percentage Error) of 3.01%, MAE of 0.75 mm, RMSE of 1.07 mm, and R^2 of 0.96, offering a precise and efficient method for crop phenotyping and advancing precision agriculture.

Thus, this study utilized advanced sensors for accurate tree characteristic assessments of young oak trees in a nursery environment. Despite the widespread use of such technology in forestry, research specifically focusing on ornamental nurseries remains limited. While ornamental nurseries may not present the same complexities as forest environments, precise measurement of parameters like trunk diameter and canopy volume is critical due to their direct impact on market value. These gaps emphasize the need for improved methodologies. To address this, the study aimed to implement a cost-effective and efficient approach for

measuring ornamental tree characteristics, optimizing crop management and precision spraying applications using LiDAR, RGB-D sensors, and 3D point cloud processing techniques. The specific objectives of this study were to (a) calculate trunk diameter at six inches above ground using an RGB-D sensor, (b) calculate the canopy volume of the trees using LiDAR-based point cloud data, and (c) calculate the optimal amount of agrochemicals needed for the trees by using canopy volume data and standard application rates.

4.3 Materials and Methods

4.3.1 Study Site

The study was conducted at a nursery located in Watkinsville, GA, featuring two distinct experimental plots (Plot-1 and Plot-2) with Quercus nuttallii (Nuttall oak) trees. Plot-1, located at coordinates 33°44'43.0" N, 83°25'15.3" W, consisted of 511 trees arranged in 11 rows and was planted 3.5 years ago (Fig. 4.1). Plot-2, situated at 33°45'22.6" N, 83°25'58.4" W, contained 266 trees across 8 rows. The terrain in both plots exhibited varying inclines, influencing elevation from the start to the end of each plot along tree columns. In Plot-1, slope inclination began at 1.95°, shifted direction multiple times, and ended with an inclination of 3.35° toward the last tree, leading to a cumulative elevation drop of approximately 43 cm (1.41 ft) from the first to the last tree. Plot-2 displayed more pronounced undulations, with slope inclinations between 1.7° and 3.6°, resulting in a cumulative elevation rise of about 166 cm (5.44 ft) along the column. Additionally, moving horizontally across Plot-2 from C1 to C8 showed a steady downward incline, with C8 positioned 113.68 cm (44.76 in) lower than C1, highlighting the steeper and more variable terrain of Plot-2 compared to Plot-1.

Trees in both plots were planted to achieve a target trunk diameter range of 6.35 cm (2.5 in) to 13.97 cm (5.5 in) at 15.24 cm (6 in) above ground, based on recommendations from

the farm's growers (personal communication with grower) to meet the ornamental nursery standards for their nursery.

Plot-1

Plot-2

Figure 4.1. Oak experimental plots in Watkinsville, GA: Plot-1 located on plain terrain with well-structured rows of oak trees, and Plot-2 situated on hilly terrain, providing contrasting landscape features.

4.3.2 Statistical Analysis for Field Conditions

This analysis aimed to investigate the variability of trunk diameters in both experimental plots. Assessing trunk diameter variability is important because it indicates whether each tree's trunk diameter must be manually measured to determine its readiness for sale from the nursery. Furthermore, if significant variability is found, which is expected, it highlights the need for a system that can efficiently measure trunk diameters for all ornamental farms with oak nurseries.

Field Measurement

Data collection for Plot-1 and Plot-2 was carried out on August 26 and 27, 2024, respectively. Trunk diameters were collected from 511 trees in Plot-1 and 266 trees in Plot-2, both recorded in inches. Some trees from the rows were avoided during data collection due to their small size or because they were of a different variety. The trunk diameter measurements were converted from inches to centimeters for analysis. The collected data were systematically organized into datasheets prepared, ensuring accurate recording and easy access for further statistical evaluation.

4.3.3 Data Collection

Ground Truth Collection

On October 17, 2024, the trunk diameter and canopy volume of 16 randomly selected oak trees in both plots P1 (plot first) and P2 (plot second) were manually measured from the study site. A caliper, with a scale ranging from 1 to 7 inches divided into four increments, was used to measure trunk diameter. A measuring pole with a foot scale (with 12 divisions) was employed for measuring tree height above ground, canopy height, and cross-sections to calculate canopy volume, providing essential ground truth data. Both plots had mowed grounds. Some trees had recently been harvested, leaving behind potholes. The trees were

planted with an alternating row spacing of 3 m (10 ft) and 1.8 m (6 ft). A total of 32 trees were selected for the experiment, labeled P1-C1T6, where "P1" indicates the first plot, "C1" signifies the column number, and "T6" denotes the tree number within the respective column. The slope increased as one moved northward from the front face of the field in P1 and eastward from the front face of the field in P2.

Ground Truth Measurement

The RGB-D system measured trunk diameter and LiDAR system measured canopy volume were validated using the respective ground truth of trunk diameter and canopy volume measured manually. For trunk diameter, a caliper was used to measure the diameter at 15.24 cm above the ground and for canopy volume, a measuring pole was used to measure different parameters of tree such as height, and cross-sectional lengths as shown in Fig. 4.2. The canopy part of the tree was considered a cylinder, and the volume formula for the cylinder was applied to calculate the manually measured volume by using Eq. 4.1.

$$Manual\ canopy\ volume\ (\mathrm{m})^3 = \pi \times\ h_b\ \times (d_1 + d_2 + d_3 + d_4 + d_5 + d_6)/12^2 \quad \text{(Eq. 4.1)}$$

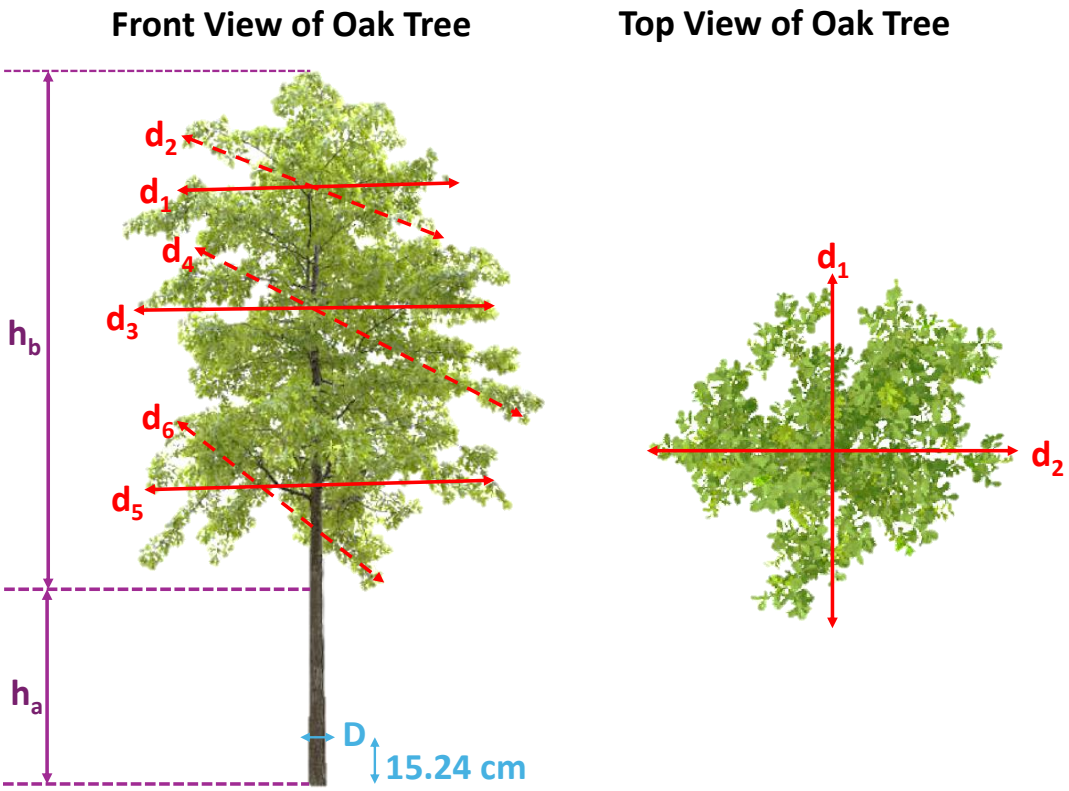

Figure 4.2. The tree canopy is divided into three sections to measure six diameters (d_1, d_2, d_3, d_4, d_5, and d_6). h_a and h_b represent the height of a tree below the canopy start point and after the canopy start point, respectively. D represents trunk diameter at 15.24 cm (6 in) above ground.

Experimental Setup and Ground-based Data Acquisition

For the LiDAR-based canopy volume measurement, a Velodyne Puck Hi-Res (VLP-16) (Velodyne Lidar, Inc., San Jose, CA) was mounted on a tripod in a horizontal orientation (rotated left) at a height of approximately 1 m, as shown in the image (Fig. 4.3). This orientation was specifically chosen to maximize the vertical field of view, allowing for comprehensive coverage of the tree canopy. The tripod legs were adjustable, which allowed for precise leveling of the LiDAR even on sloped surfaces. By independently adjusting the length of each leg, the LiDAR sensor was kept stable and free of tilt, ensuring accurate and consistent data collection across varying terrain. The tripod's bubble level was used to ensure the setup was perfectly level, providing visual confirmation of the tripod's alignment during adjustments. The

Velodyne VLP-16 sensor, with a 30° vertical and 360° horizontal field of view, was configured to operate with a *Dual* return type for capturing both first and second returns, allowing for a more detailed representation of the canopy structure. The motor was set to a rotation rate of 600 RPM (rotations per minute) which is equivalent to 10 Hz (Hertz) providing a horizontal resolution of 0.2° and a complete 360-degree sweep during each revolution. The FOV was configured to start at 0° and end at 359°, ensuring nearly full horizontal coverage. The LiDAR data were recorded in real-time using a Dell Precision 3570 laptop (Intel Core i7-1255U, 32GB RAM, Windows 11). Data capture and visualization were performed using VeloView version 5.1.0 (Velodyne Lidar, Inc., San Jose, CA), which allowed both real-time visualization and storage of the point clouds in PCAP format. Each recording session lasted approximately 15 seconds, generating 130 to 160 frames per session.

For the trunk diameter measurement, a ZED 2 AI Stereo Camera (Stereolabs, San Francisco, CA) was mounted on a tripod and positioned horizontally to capture RGB and depth images of the tree trunks as shown in Fig. 4.4. Just like the LiDAR system, the tripod for the depth camera had adjustable legs, allowing for precise leveling on uneven or sloped surfaces. This ensured the camera remained stable and captured accurate depth data without tilt distortion. The depth camera was connected to an onboard personal computer running Windows 11 Enterprise 64-bit, powered by a 12th Gen Intel® Core™ i7-1255U processor (12 cores) with a clock speed of approximately 1.7GHz. This setup ensured full coverage of each tree's trunk within the camera’s FOV (Field of View). The ZED Depth Viewer software (ZED SDK version 4.0.8, Stereolabs, San Francisco, CA) provided real-time depth information alongside 3D visualization, enabling precise analysis of the spatial relationships in the scanned scenes. The left lens of the stereo camera was utilized for image acquisition, providing high-resolution images of 2208 × 1242 pixels (HD2K standard). The imaging sessions took place during late afternoon hours (between 4:00 PM and 7:00 PM) to minimize harsh lighting and

ensure consistent image quality. During data collection, depth maps were generated and processed to address non-numeric values and eliminate outliers to improve data reliability. Camera intrinsic parameters for each camera (left camera: fx: 1906.29, fy: 1906.29, cx: 1099.99, cy: 619.98 and right camera: fx: 1906.29, fy: 1906.29, cx: 1099.99, cy: 619.98), distortion coefficients for each camera (left camera: [0. 0. 0. 0. 0. 0. 0. 0. 0. 0. 0. 0.] and right camera: [0. 0. 0. 0. 0. 0. 0. 0. 0. 0. 0. 0.]), extrinsic parameters (Tx: 119.96, Ty: 0.00, Tz: 0.00) and horizontal FOV (field of view) for left camera (60.15) were automatically computed through a custom Python script.

Figure 4.3. LiDAR system setup for tree canopy data collection, featuring a Velodyne VLP-16 LiDAR sensor mounted on a tripod for stable positioning. A laptop, placed on a mobile lab workstation, is used for recording and visualizing the LiDAR data streams in real-time.

Figure 4.4. Depth camera setup for capturing RGB and depth images of oak tree trunks. The camera is mounted on a tripod to ensure stability. A laptop is used for real-time data capture and visualization, facilitating immediate review of images for quality and consistency in research applications.

4.3.4 Data Preparation

LiDAR Point Clouds Stitching with Point-to-Plane Iterative Closest Point Algorithm

Robust registration of two 3D point sets is widely used in computer vision, especially when constructing a full 3D model of an object. Since capturing an object's shape generally requires multiple scans from different angles, these point sets must be accurately aligned to form a complete representation of the 3D object (Levoy et al., 2000). 3D point cloud registration and stitching involve combining multiple point clouds, often from different viewpoints or times, to reconstruct a complete 3D scene or model. In real-world applications such as robotics, autonomous vehicles, and surveying, point clouds captured from sensors like LiDAR often come from different angles or positions. Registration algorithms are used to align these point clouds by finding the relative transformation between them (rotation and translation). Once aligned, the individual point clouds are stitched together to form a more

comprehensive, global point cloud representation of the environment or object. The challenge in point cloud registration lies in the fact that different point clouds may overlap only partially, have different levels of noise, and may need precise transformations to align accurately. Registration algorithms such as Iterative Closest Point (ICP), introduced by Chen and Medioni (1992) and Besl and McKay (1992), often employed for this purpose, are important for ensuring the accurate alignment of point clouds before stitching. Point-to-Plane ICP is a specific variant of the ICP algorithm used for 3-D point cloud registration. The general ICP algorithm iteratively refines the alignment between two point clouds by minimizing the distance between corresponding points. However, Point-to-Plane ICP goes a step further by minimizing the distance between points in one cloud (the "moving" cloud) and the planes formed by the local neighborhoods of points in the other cloud (the "fixed" cloud). This ICP variant tends to converge faster and provide more accurate results than the standard point-to-point ICP, especially in cases where the scene contains large flat surfaces (e.g., walls, roads, or the ground). This is because point-to-plane ICP considers not only the distances between points but also the surface normals, which provides additional geometric information about the underlying shape.

For each tree, approximately 130 to 160 frames of LiDAR data were collected and processed for stitching. All frames were utilized to ensure comprehensive coverage of the tree structure. The data processing began with the conversion of raw PCAP files into PCD (Point Cloud Data) format to facilitate smoother integration with point cloud processing tools. Point-to-Plane ICP registration was applied to align and merge each frame into a single cohesive point cloud. During this process, each frame was downsampled to expedite processing while maintaining essential structural details. This alignment minimized positional discrepancies across frames, resulting in a unified, high-resolution point cloud for each tree. Once the frames were merged, the entire point cloud was clipped to isolate each individual tree based on

manually set ROI coordinates, ensuring that only the desired tree structure was retained. Outliers and noise were subsequently removed using statistical outlier filtering to improve data quality. Further refinement was achieved through a voxel grid filter, which downsampled the data while preserving spatial characteristics. Ground points were excluded by setting a Z-value threshold, leaving only the tree structure for analysis. A final transformation was applied as necessary to standardize the orientation and alignment of the trees, ensuring consistency across datasets. This processed point cloud was then used to calculate canopy volumes, with the data preparation steps for Tree C6T1 of Plot-1 illustrated in Fig. 4.5.

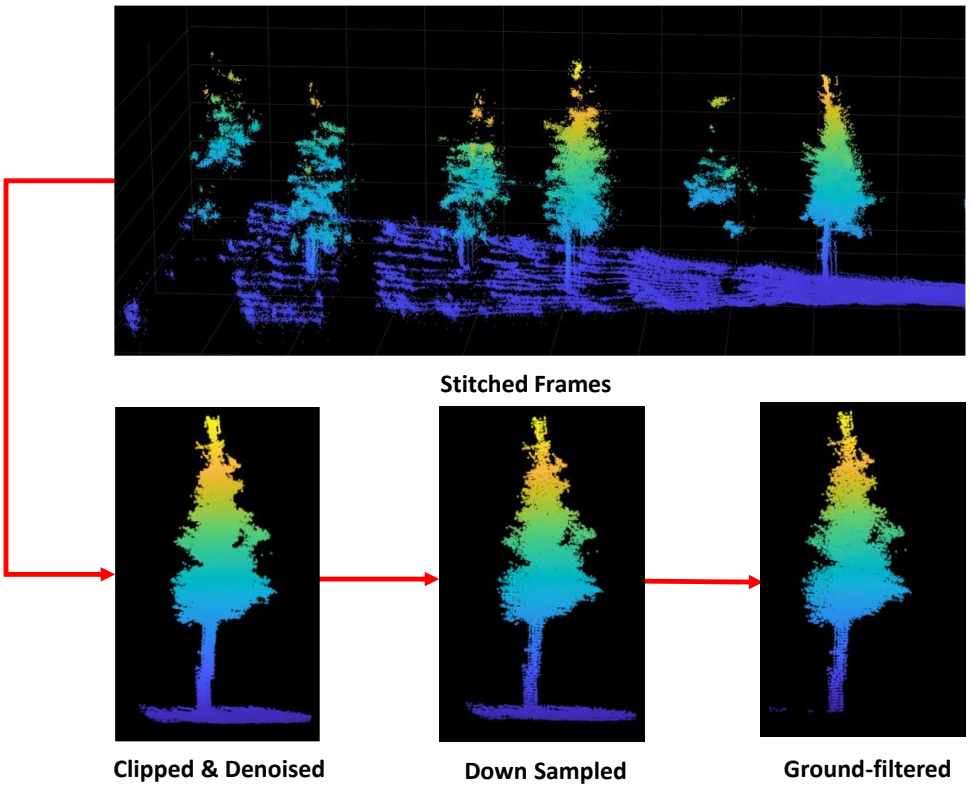

Figure 4.5. Workflow for processing oak tree point cloud data, including LiDAR stitching, tree clipping, denoising, downsampling, and ground filtering to retain tree structures for analysis. The illustrated example corresponds to sample C8T17 from Plot-1.

RGB-D Stereo Vision Data

In the process of generating 3D point clouds from stereo image pairs, depth maps played an important role by providing pixel-wise distance information. The camera's left lens was used

to capture high-resolution RGB and depth images, where the depth map was aligned with corresponding RGB-derived ROIs. A binary mask was applied to isolate specific objects, such as tree trunks. These binary masks, generated using polygon annotations on RGB images, were used to filter the depth maps, allowing only relevant sections to be retained for further analysis. The calibration parameters of the camera, including focal lengths (fx, fy) and optical centers (cx, cy), were essential for converting 2D-pixel data into real-world 3D coordinates.

Using the formula:

$$\begin{Bmatrix} (a) & X = (u - cx) \times \frac{Z}{fx} \\ (b) & Y = (v - cy) \times \frac{Z}{fy} \\ (c) & Z = \text{ depth value from depth map} \end{Bmatrix} \quad \text{(Eq. 4.2)}$$

where u, v are the pixel coordinates in the image, cx, cy are the optical centers of the camera, fx, fy are the focal lengths of the camera, and Z is the depth value at the pixel. This transformation enabled the generation of 3D point clouds that precisely represented the trunk structures in the scene. To enhance the reliability of the 3D reconstructions, the noise reduction technique – Statistical Outlier Removal (SOR) was applied. This method assessed the mean distance between points and their neighbors, excluding those that deviated significantly as outliers. These processed 3D point clouds, free from noise and outliers, provided a reliable representation of the trunks, which was necessary for further analysis, including trunk diameter measurements and structural assessments. Fig. 4.6 shows the process of generating point clouds of the segmented region of the trunk after overlaying polygon coordinates on the depth image and generating a binary mask of the trunk region of C6T1 of Plot-1.

Data preparation and parameter calculations for processing the LiDAR and depth camera data, including point cloud extraction and geometric transformations, were all performed using MATLAB R2023a (version 9.14), developed by MathWorks (Natick, MA).

MATLAB provided essential functions for 3D data processing and visualization. Key functions and libraries used in the study included *pointCloud* for point cloud processing, *pcdenoise* for noise reduction, *convhull* for defining boundary points, and custom circle-fitting functions for calculating trunk diameters. These tools, combined with custom scripts, ensured reliable computation and visualization of results, facilitating accurate canopy volume and trunk diameter measurements.

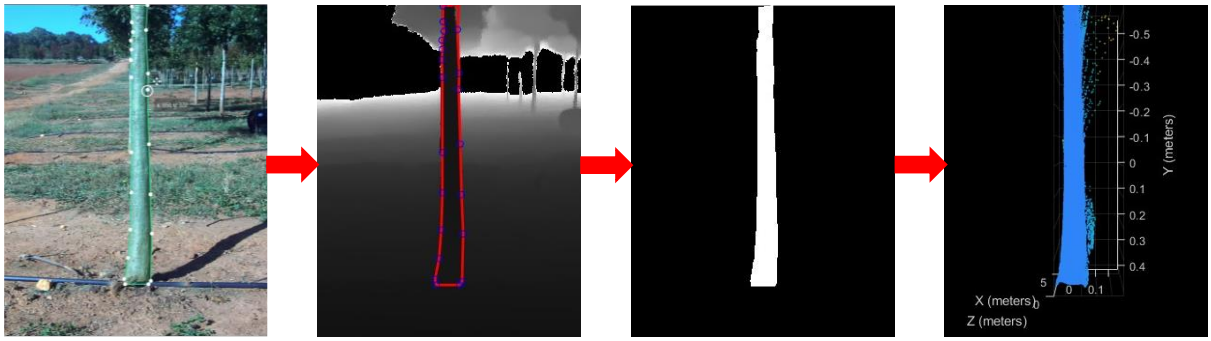

Figure 4.6. Illustration of trunk segmentation and point cloud generation process: starting with an annotated RGB image, overlaying trunk polygon coordinates on the depth image, creating a binary trunk mask, and generating a 3D point cloud. The example shown corresponds to C6T1 of Plot-1.

4.3.5 Measuring Trunk Diameter

After isolating the ROI based on defined polygon coordinates, the depth values were converted to real-world dimensions in inches. To ensure accurate spatial representation, the point cloud was oriented by adjusting the axes to correct any discrepancies in the initial camera alignment. A clipping process was then applied to retain only the relevant portion of the tree trunk, focusing on points located approximately 15.24 cm (6 in) from the ground.

To define the outer boundary of the points in this cross-section, the convex hull method was employed. The convex hull is the smallest convex polygon or shape that encloses all the points in a set. Mathematically, given a set of points P, the convex hull is defined as the minimal convex set $C(P)$ such that all points in P lie within or on the boundary of $C(P)$. The convex hull is essential for this analysis as it isolates only the boundary points that are relevant for fitting, ensuring that internal points or noise do not distort the trunk's outer structure. The next step was using the convex hull, a circle was fitted to these points using the least-squares method through the CircleFitByPratt function. This method applies a least-squares approach to fit a circle to the boundary points identified by the convex hull. The function minimizes the squared residuals between the observed boundary points and the equation of the circle. The least-squares fitting minimizes the sum of squared residuals between the observed boundary points (x_i, y_i)) and the equation of the circle, which can be written as:

$$(x - x_c)^2 + (y - y_c)^2 = r^2 \quad \text{(Eq. 4.3)}$$

where (x_c, y_c) are the coordinates of the circle's center and r is the radius. The least-squares method seeks to minimize the objective function:

$$S = \sum_{i=0}^{n} [(x_i - x_c)^2 + (y_i - y_c)^2 - r^2]^2 \quad \text{(Eq. 4.4)}$$

By solving for x_c, y_c, and r, the method determines the best-fitting circle that approximates the trunk's shape at the selected height. The trunk diameter was calculated as 2r, providing an accurate measurement of the tree's trunk diameter at the specified height.

To verify the accuracy of this process, the fitted circle was visualized alongside the cross-sectional points, ensuring that the circle closely followed the boundary of the trunk. This visual confirmation helped validate that the least-squares fitting produced an accurate

representation of the trunk's cross-sectional shape, resulting in a reliable calculation of the trunk diameter.

4.3.6 Measuring Canopy Volume

For the canopy volume calculation, the point cloud data above a specific Z-axis threshold (determined uniquely for each tree) was selected to isolate the canopy points. Points above this threshold represented the canopy, while those below it was excluded from the analysis. The convex hull algorithm was then applied to these isolated canopy points, constructing the smallest convex shape that encloses all canopy points. Each point in the point cloud was assigned to its spatial coordinates (x, y, z) based on its location in the canopy structure. These coordinates served as the foundational values for the convex hull calculation. The convex hull algorithm used these coordinates to create a boundary that wraps around all canopy points, forming the smallest convex shape possible. The convex hull provides a simple and efficient method to approximate the overall volume of a tree's canopy. Since it encapsulates all the points in the canopy, it offers a reliable way to estimate the tree's volume, even when dealing with irregularly shaped or sparse point cloud data. This method offers a standardized approach to quantify canopy volume, which is essential for determining the agrochemical needs and other management decisions for individual trees. This convex shape was used to estimate the total canopy volume, providing a three-dimensional representation of the tree's upper structure.

Mathematically, the convex hull volume V can be calculated as:

$$V = \sum_{i=0}^{n} \frac{1}{3} A_i h_i \qquad \text{(Eq. 4.5)}$$

where A_i represents the area of the triangular face of the convex hull, and h_i is the perpendicular height from the centroid of the triangle to the origin.

The convex hull algorithm calculates the surface area and volume of the canopy's 3D structure. By visualizing this convex hull, the total canopy volume was determined, providing an accurate estimation of the tree’s canopy size.

4.3.7 Estimation of Tree Maturity

As mentioned earlier in section 4.1, according to ornamental tree grower, oak trees are considered mature and ready for the market once their trunk diameter at 15.24 cm (6 in) above ground reaches 6.35 cm (2.5 in). Using this benchmark, tree maturity was assessed based on trunk diameter measurements obtained from the depth camera system. The trunk diameters were classified into three categories: mature, semi-mature, and young. Trees with trunk diameters measured at 15.24 cm above ground which were equal to or exceeding 6.35 cm (2.5 inches) were classified as mature, while those with diameters around this threshold were classified as semi-mature and below this threshold were categorized as young. This classification provided a clear distinction between trees that were ready or near ready for market and those still in earlier growth stages. The use of depth camera measurements allowed for consistent and precise evaluation of trunk diameters, facilitating efficient maturity assessment across the nursery. This method helped identify trees that required further growth, optimizing management and resource allocation for young and mature trees alike.

4.3.8 Estimation of Agrochemical Requirement

Accurately estimating the agrochemical requirements for ornamental trees is important for growers to manage production costs and ensure the optimum use of chemicals in the field. In this study, the necessary amount of agrochemicals was calculated based on tree volume, with the chemical application rates determined by the trees' capacity to retain liquid sprays. The methodology followed guidelines from Furness et al. (1998), recommending 80 l of spray per 1,000 m^3 of canopy volume, which represents the maximum canopy retention capacity. As a

result, the application rate used in this study was 0.08 l of spray per m^3 of canopy volume to determine the appropriate spray volume for the experimental trees.

4.3.9 Statistical Analysis

A paired t-test was performed to assess the consistency between ground-based and manual methods for calculating tree canopy volume and trunk diameter across both plots' data. The goal was to determine if there were any statistically significant differences between the two measurement approaches. Additionally, accuracy metrics such as RMSE and MAE were calculated to quantify how closely the systems-derived measurements matched the manual values in each dataset. The statistical analysis was carried out using R software (Team, 2010), utilizing relevant functions and packages to perform the paired t-tests and compute the RMSE and MAE.

The RMSE and MAE formulas are given by:

$$RMSE = \sqrt{\frac{\sum_{i-1}^{n}(y_i - \hat{y}_i)^2}{n}} \quad \text{(Eq. 4.6)}$$

$$MAE = \frac{\sum_{i-1}^{n} | y_i - \hat{y}_i |}{n} \quad \text{(Eq. 4.7)}$$

where y_i represents the manually measured height, $\hat{y}_i$ denotes the corresponding drone-measured height, and n signifies the total number of measurements.

4.4 Experimental Results and Discussion

4.4.1 Data Analysis for Trunk Diameter

The summary statistics for trunk diameters revealed information about the variability within each plot. In Plot-1, which included measurements from 511 trees, the minimum trunk diameter recorded was 6.43 cm (2.54 in), while the maximum reached 30.65 cm (12.07 in). The first quartile was at 16.13 cm (6.35 in), the median was 19.34 cm (7.62 in), and the mean was 18.84 cm (7.42 in). The variance for Plot-1 was calculated to be 2.94, with a standard

deviation of 1.71, indicating moderate variability in trunk diameters. In Plot-2, containing 266 trees, the trunk diameters ranged from a minimum of 7.74 cm (3.05 in) to a maximum of 22.60 cm (8.89 in). The first quartile was at 13.23 cm (5.21 in), the median at 14.50 cm (5.72 in), and the mean at 14.89 cm (5.86 in). The variance for Plot-2 was found to be 0.94, with a standard deviation of 0.97, suggesting lower variability compared to Plot-1, although some degree of variation still existed. In summary, trunk diameters in both plots exhibited variability. In Plot-1, the average difference from the mean diameter was approximately 1.70 cm (0.67 in), reflecting greater variation among the measurements. Conversely, Plot-2 showed less variability, with an average difference of around 1 cm (0.39 in) from the mean. This indicated that while the trunk diameters in both plots differed, the extent of variability was more pronounced in Plot-1 than in Plot-2. Fig. 4.7 displays boxplots of trunk diameters across columns in Plot-1 and Plot-2, comparing size distribution and variability within each plot. Plot-1 (top panel) shows a broader range of trunk diameters with wider interquartile ranges (IQRs) and some outliers, indicating higher variability across columns. Conversely, Plot-2 (bottom panel) has a more compact diameter distribution, with narrower IQRs and fewer outliers, reflecting greater consistency. These findings illustrate that Plot-1 exhibits greater trunk diameter variability, while Plot-2 shows a relatively uniform distribution.

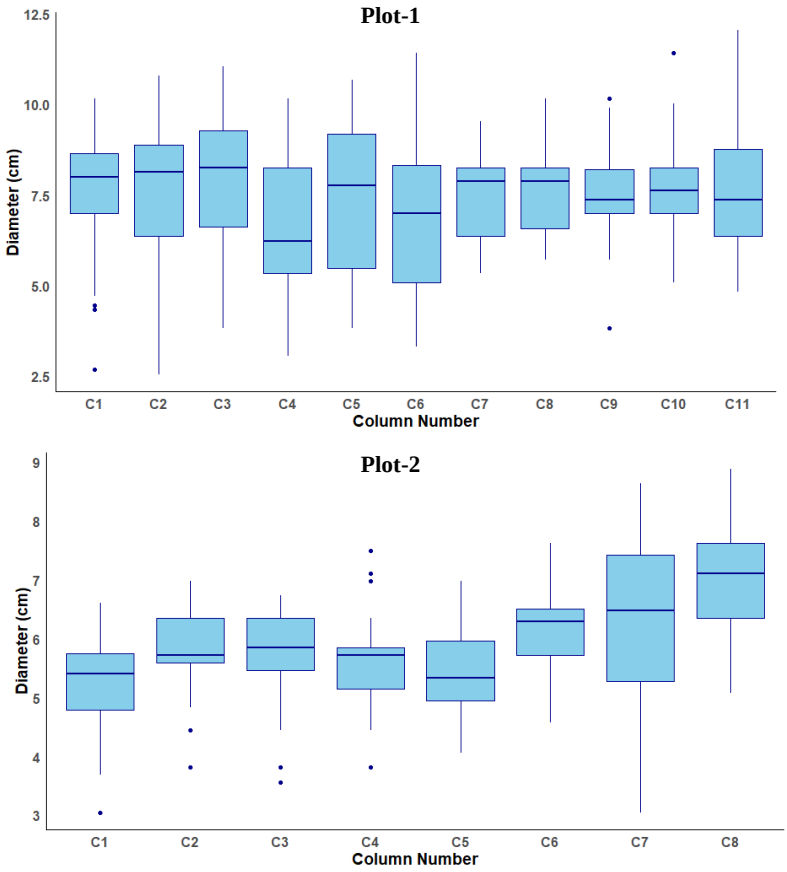

Figure 4.7. Boxplots illustrate tree trunk diameter measurements across different columns for Plot-1 and Plot-2. The upper panel shows the diameter distribution in centimeters for each column in Plot-1 (C1 to C11), while the lower panel represents the diameter distribution in Plot-2 (C1 to C8). Each boxplot indicates the median (central line), interquartile range (box), and the spread of data (whiskers), with individual outliers displayed as dots.

4.4.2 Trunk Diameter

The trunk diameter of each experimental tree was calculated and visualized with a red circle fitted on the point clouds along with their trunk diameter in meters. Fig. 4.8 visualizes results for C6T1, C6T2, and C8T17 of Plot-1 and C4T12, C2T3, and C4T7 of Plot-2.

The absolute error analysis (Table 4.1) for trunk diameter measurements reveals that for Plot-1, the absolute trunk diameter error ranges from 0% to 1.48%, with the smallest error observed for trees like C6T1 and C6T14 and the largest error for C6T2. For Plot-2, the error

ranges from 0.19% to 2.72%, with the smallest error observed for C2T5 and the largest for C2T9. This minimal range of errors signifies a strong agreement between manual and RGB-D measurements. The average absolute error percentage across all trees is 0.33% for Plot-1 and 1.11% for Plot-2, further supporting the reliability of the RGB-D method in measuring trunk diameters. The RMSE for Plot-1 is 0.028 m, and the MAE is 0.020 m, while Plot-2 shows a slightly higher RMSE of 0.078 m and an MAE of 0.065 m. These metrics reflect small yet consistent discrepancies between manual and RGB-D-derived trunk diameter measurements, likely due to several factors, including the limited number of point clouds generated from the depth images and potential biases in the circle-fitting algorithm as seen in the comparison graphs presented in Fig. 4.9.

The paired t-test results indicate no statistically significant difference between manual and RGB-D-derived measurements for Plot-1 ($p = 0.12$), suggesting that the RGB-D system performs comparably to manual measurements in this plot. However, for Plot-2, a statistically significant difference was observed ($p = 5.301 \times 10^{-5}$). Despite this difference in Plot-2, the high R^2 values of 0.9997 for Plot-1 and 0.9988 for Plot-2 indicate a strong correlation between the two methods, affirming the accuracy and reliability of the RGB-D system in measuring trunk diameters with minimal deviation from manual measurements across both plots.

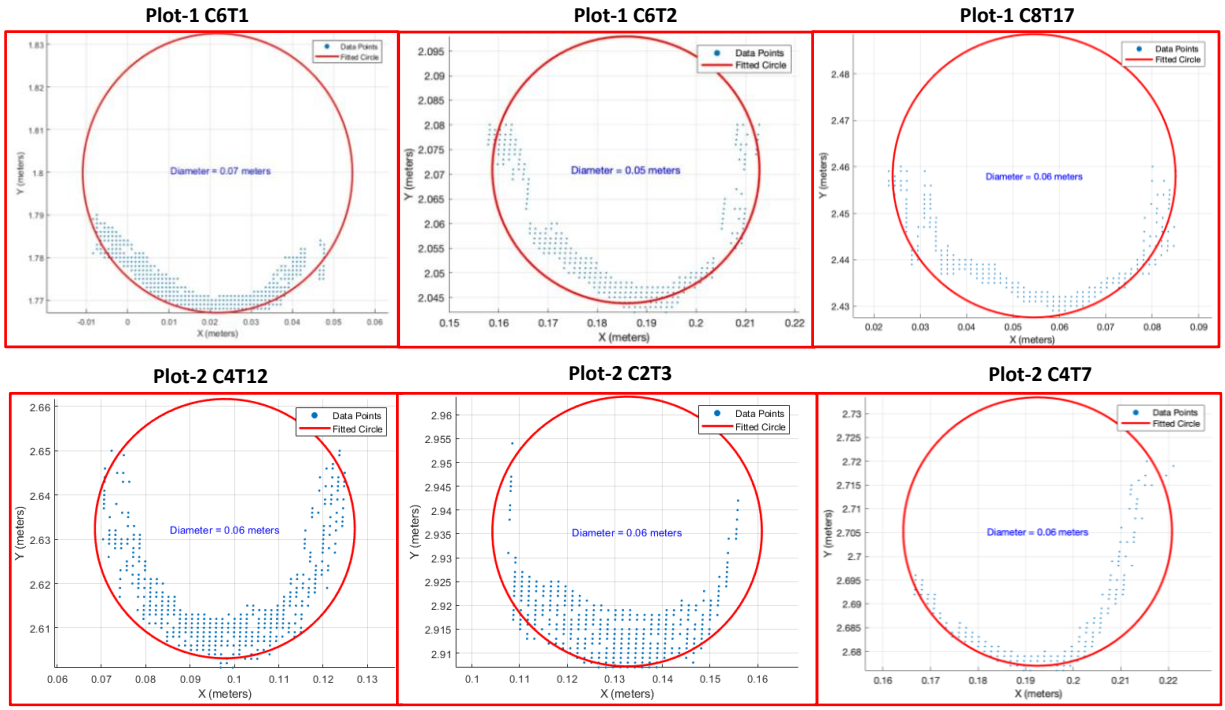

Figure 4.8. Trunk diameter estimation for selected trees from Plot-1 and Plot-2 using circle fitting. The top row illustrates trunk diameters for trees from Plot-1: C6T1 (0.07 m), C6T2 (0.06 m), and C8T17 (0.08 m). The bottom row shows trunk diameters for trees from Plot-2: C4T12 (0.06 m), C2T3 (0.06 m), and C4T7 (0.06 m). Data points represent the segmented trunk region, and the fitted circle demonstrates the calculated diameter, ensuring precise measurement from ground-based LiDAR data.

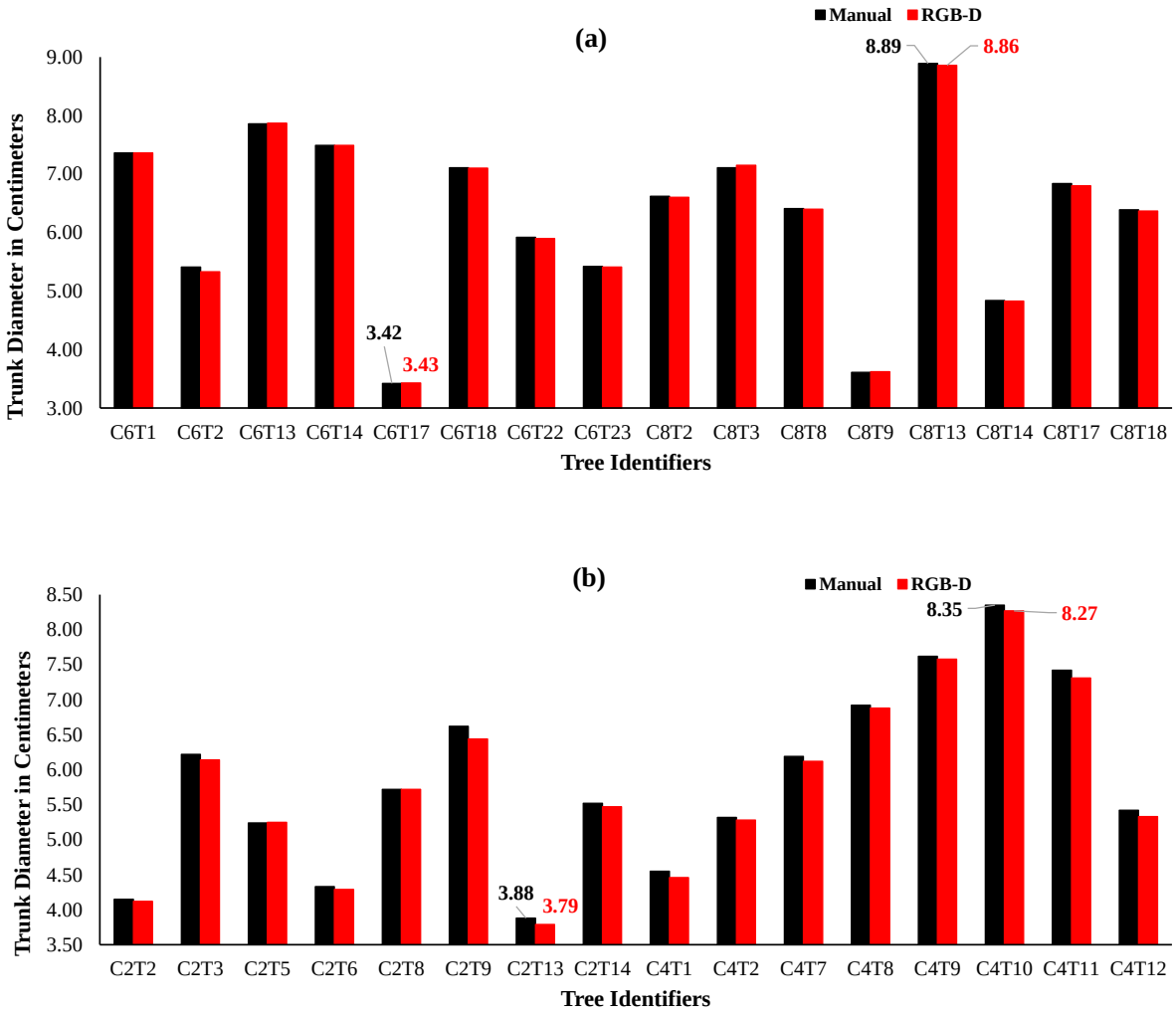

Figure 4.9. Comparison of trunk diameter measurements obtained through manual methods (black bars) and RGB-D camera data (red bars) for selected trees in (a) Plot-1 and (b) Plot-2. In Plot-1 (a), the highest diameter recorded was for C8T13 (manual: 8.89 cm, RGB-D: 8.86 cm), and the lowest was for C6T14 (manual: 3.42 cm, RGB-D: 3.43 cm). In Plot-2 (b), the highest diameter was C4T11 (manual: 8.35 cm, RGB-D: 8.27 cm), and the lowest was for C2T6 (manual: 3.88 cm, RGB-D: 3.79 cm).

Table 4.1. Calculation of absolute errors for manual and RGB-D-based trunk diameter measurements of oak trees in Plot-1 and Plot-2. The average absolute error for trunk diameter measurements was 0.06 cm (0.33%) in Plot-1 and 0.06 cm (1.13%) in Plot-2, demonstrating high consistency between manual and RGB-D measurements.

Plot 1					Plot 2				
Tree ID	**Trunk Diameter (cm)**		**Absolute Error**		**Tree ID**	**Trunk Diameter (cm)**		**Absolute Error**	
	Manual	**RGB-D**	**(cm)**	**(%)**		**Manual**	**RGB-D**	**(cm)**	**(%)**
C6T1	7.36	7.36	0.00	0.00	**C2T2**	4.15	4.12	0.03	0.72
C6T2	5.41	5.33	0.08	1.48	**C2T3**	6.22	6.14	0.08	1.29
C6T13	7.86	7.87	0.01	0.13	**C2T5**	5.24	5.25	0.01	0.19
C6T14	7.49	7.49	0.00	0.00	**C2T6**	4.33	4.29	0.04	0.92
C6T17	3.42	3.43	0.01	0.29	**C2T8**	5.72	5.72	0.00	0.00
C6T18	7.11	7.10	0.01	0.14	**C2T9**	6.62	6.44	0.18	2.72
C6T22	5.92	5.90	0.02	0.34	**C2T13**	3.88	3.79	0.09	2.32
C6T23	5.42	5.41	0.01	0.18	**C2T14**	5.52	5.47	0.05	0.91
C8T2	6.62	6.61	0.01	0.23	**C4T1**	4.55	4.46	0.09	1.98
C8T3	7.11	7.15	0.04	0.56	**C4T2**	5.32	5.28	0.04	0.75
C8T8	6.41	6.40	0.01	0.16	**C4T7**	6.19	6.12	0.07	1.13
C8T9	3.61	3.62	0.01	0.28	**C4T8**	6.92	6.88	0.04	0.58
C8T13	8.89	8.86	0.03	0.34	**C4T9**	7.62	7.58	0.04	0.52
C8T14	4.84	4.83	0.01	0.21	**C4T10**	8.35	8.27	0.08	0.96
C8T17	6.84	6.80	0.04	0.58	**C4T11**	7.42	7.31	0.11	1.48
C8T18	6.39	6.37	0.02	0.31	**C4T12**	5.42	5.33	0.09	1.66
Avg.	**0.06**	**0.06**	**0.02**	**0.33**	**Avg.**	**0.06**	**0.05**	**0.06**	**1.13**

4.4.3 Canopy Volume

The canopy volume of each experimental tree was calculated after clipping the canopy region of individual trees and visualized with sky blue color representing the 3D structure of the canopy along with their canopy volume in cubic meters. Fig. 4.10 visualizes results for C8T2, C8T9 and C8T17 of Plot-1 and C2T3, C2T2, and C4T2 of Plot-2.

The absolute error analysis (Table 4.2) for canopy volume measurements in Plot-1 revealed an average absolute percentage error of 10.99%, demonstrating relatively strong agreement between manual and LiDAR measurements. The smallest error was observed for C6T2 (0.06 m^3), while the largest error was recorded for C8T9 (0.82 m^3). In Plot-2, the average absolute percentage error of 13.01% indicates moderate variability in LiDAR performance across different trees and conditions. The smallest error was found for C4T8 (0.10 m^3), while the largest was for C2T13 (0.29 m^3). The variability in error rates between manual and LiDAR measurements for canopy volume in both plots may be attributed to slight misalignments in point cloud registration can introduce inaccuracies, especially when individual tree structures overlap with adjacent trees (Hu, 2023). The comparison of canopy volume measured manually and using LiDAR system for both plots are visualized using bar graphs in Fig. 4.11.

The paired t-test further reinforced the findings. In Plot-1, the t-test yielded a p-value of 0.0022, signifying a statistically significant difference between manual and LiDAR canopy volume measurements ($p < 0.05$). The R-squared value was 0.87, indicating a strong correlation between the two methods, while the RMSE and MAE were 0.37 m^3 and 0.33 m^3, respectively. In contrast, Plot-2 exhibited no statistically significant difference, with a p-value of 0.36 ($p > 0.05$). However, the R-squared value was 0.91, demonstrating a high level of agreement between the manual and LiDAR measurements. The RMSE and MAE were 0.27 m^3 and 0.24 m^3, respectively, reflecting a close match between the two methods in Plot-2.

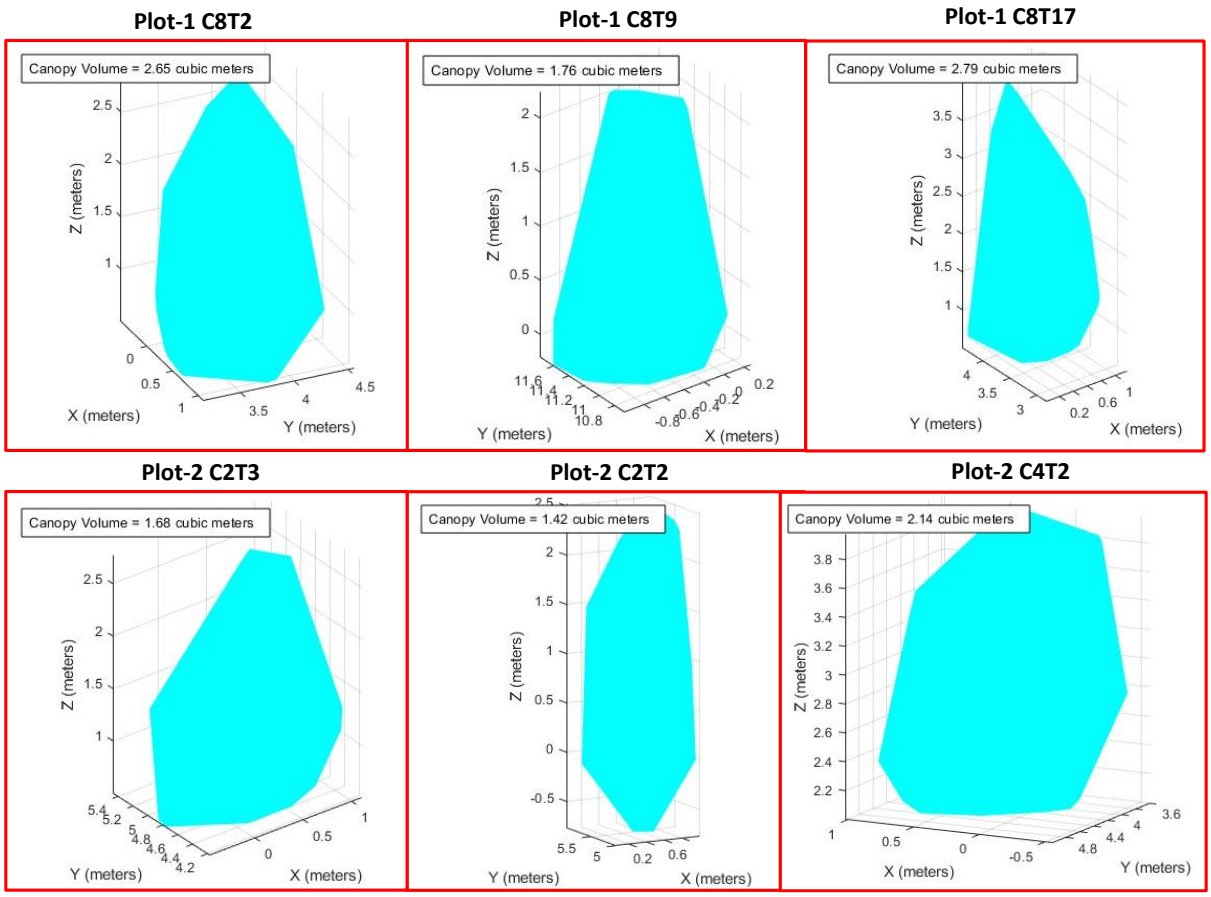

Figure 4.10. Canopy volume measurements of selected trees from Plot-1 and Plot-2 using Convex Hull. The top row represents trees from Plot-1: C8T2 (2.65 m³), C8T9 (1.76 m³), and C8T17 (2.79 m³). The bottom row represents trees from Plot-2: C2T3 (1.68 m³), C2T2 (1.42 m³), and C4T2 (2.14 m³). The convex hull method was used to estimate the canopy volumes, as visualized in 3D space.

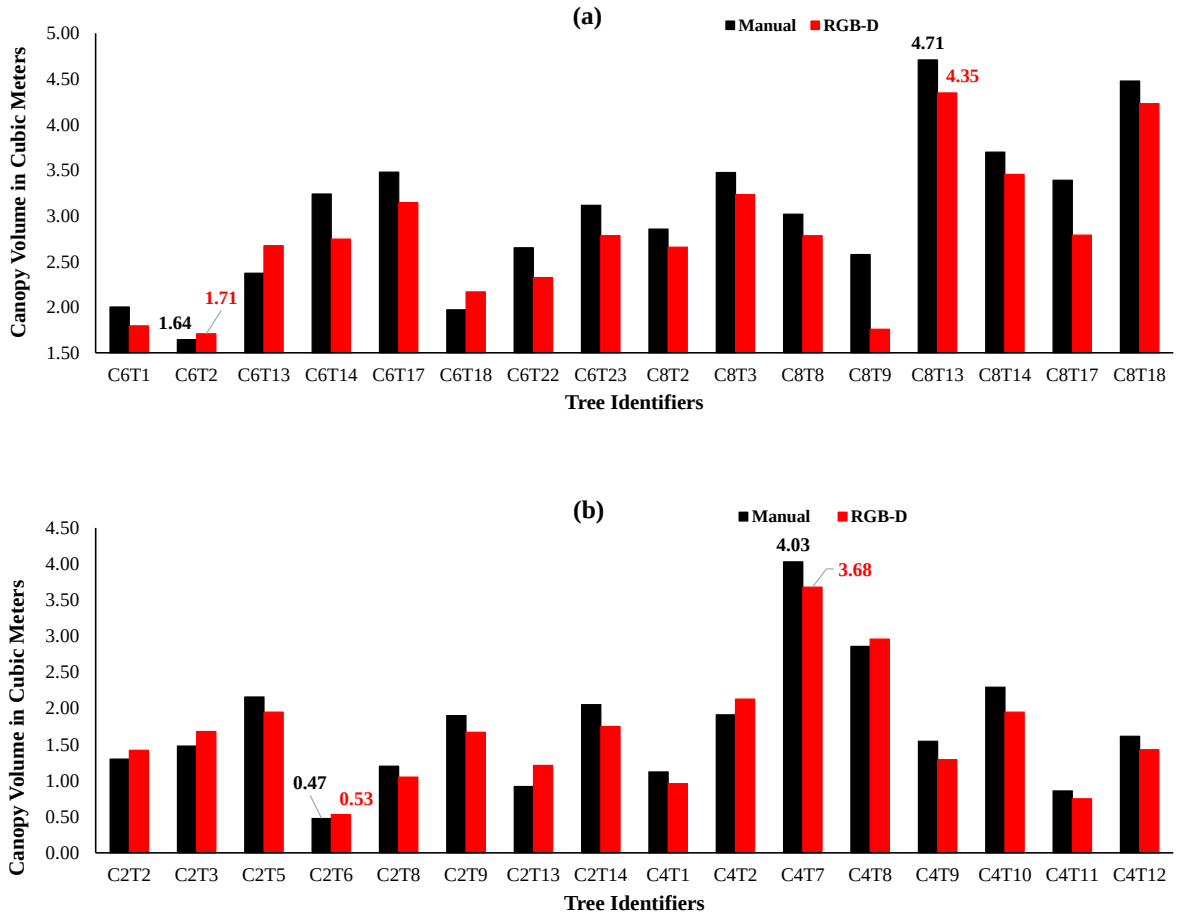

Figure 4.11. Comparison of canopy volume measurements obtained manually and using the LiDAR-based RGB-D system for trees in (a) Plot-1 and (b) Plot-2. In Plot-1, the lowest canopy volume was recorded for C6T2, with 1.64 m³ (manual) and 1.71 m³ (RGB-D). The highest canopy volume was observed for C8T13, with 4.71 m³ (manual) and 4.35 m³ (RGB-D). In Plot-2, the lowest canopy volume was recorded for C2T6, with 0.47 m³ (manual) and 0.53 m³ (RGB-D). The highest canopy volume was observed for C4T7, with 4.03 m³ (manual) and 3.68 m³ (RGB-D).

Table 4.2. Comparison of canopy volume measurements between manual and ground-based system (TLS) for oak trees in Plot-1 and Plot-2. The average absolute error for canopy volume measurements was 0.33 m³ (10.99%) for Plot-1 and 0.20 m³ (13.01%) for Plot-2.

Plot 1					Plot 2				
Tree ID	Canopy Volume (m^3)		Absolute Error		Tree ID	Canopy Volume (m^3)		Absolute Error	
	Manual	TLS	(m)	(%)		Manual	TLS	(m)	(%)
C6T1	2.00	1.80	0.21	10.37	**C2T2**	1.30	1.42	0.12	9.25
C6T2	1.64	1.71	0.06	3.92	**C2T3**	1.48	1.68	0.20	13.65
C6T13	2.37	2.67	0.30	12.71	**C2T5**	2.16	1.95	0.21	9.51
C6T14	3.24	2.75	0.49	15.25	**C2T6**	0.47	0.53	0.06	11.84
C6T17	3.48	3.15	0.33	9.58	**C2T8**	1.20	1.05	0.15	12.30
C6T18	1.97	2.17	0.20	9.98	**C2T9**	1.90	1.67	0.23	12.07
C6T22	2.65	2.32	0.33	12.32	**C2T13**	0.92	1.21	0.29	31.10
C6T23	3.12	2.78	0.33	10.62	**C2T14**	2.05	1.75	0.31	14.92
C8T2	2.86	2.65	0.21	7.21	**C4T1**	1.12	0.96	0.16	14.63
C8T3	3.47	3.23	0.24	6.91	**C4T2**	1.91	2.14	0.23	11.92
C8T8	3.02	2.78	0.23	7.76	**C4T7**	4.03	3.68	0.35	8.69
C8T9	2.58	1.76	0.82	31.68	**C4T8**	2.86	2.96	0.10	3.61
C8T13	4.71	4.35	0.36	7.71	**C4T9**	1.55	1.29	0.25	16.27
C8T14	3.70	3.45	0.24	6.62	**C4T10**	2.29	1.95	0.34	14.94
C8T17	3.39	2.79	0.60	17.69	**C4T11**	0.86	0.75	0.11	12.35
C8T18	4.48	4.23	0.25	5.53	**C4T12**	1.61	1.43	0.18	11.18
Avg.	**3.04**	**2.79**	**0.33**	**10.99**	**Avg.**	**1.73**	**1.65**	**0.20**	**13.01**

4.4.4 Tree Maturity

In Plot-1, a total of 10 trees were classified as mature, 1 tree was classified as semi-mature, and 5 trees as young. This distribution reflects the generally more advanced growth stage in Plot-1. In contrast, Plot-2 had fewer matured trees, with only 5 trees classified as matured, 1 tree as semi-mature, and 10 trees as young. This difference is likely from Plot-2's later planting date, resulting in younger growth stages, along with its steeper incline, which may have led to variable access to water and nutrients. These factors likely contributed to fewer matured trees and less uniform growth in Plot-2 as compared to the more level terrain in Plot-1. Fig. 4.12 shows the bar graphs for visualization of number of trees in each experimental column of each plot categorized based on their maturity.

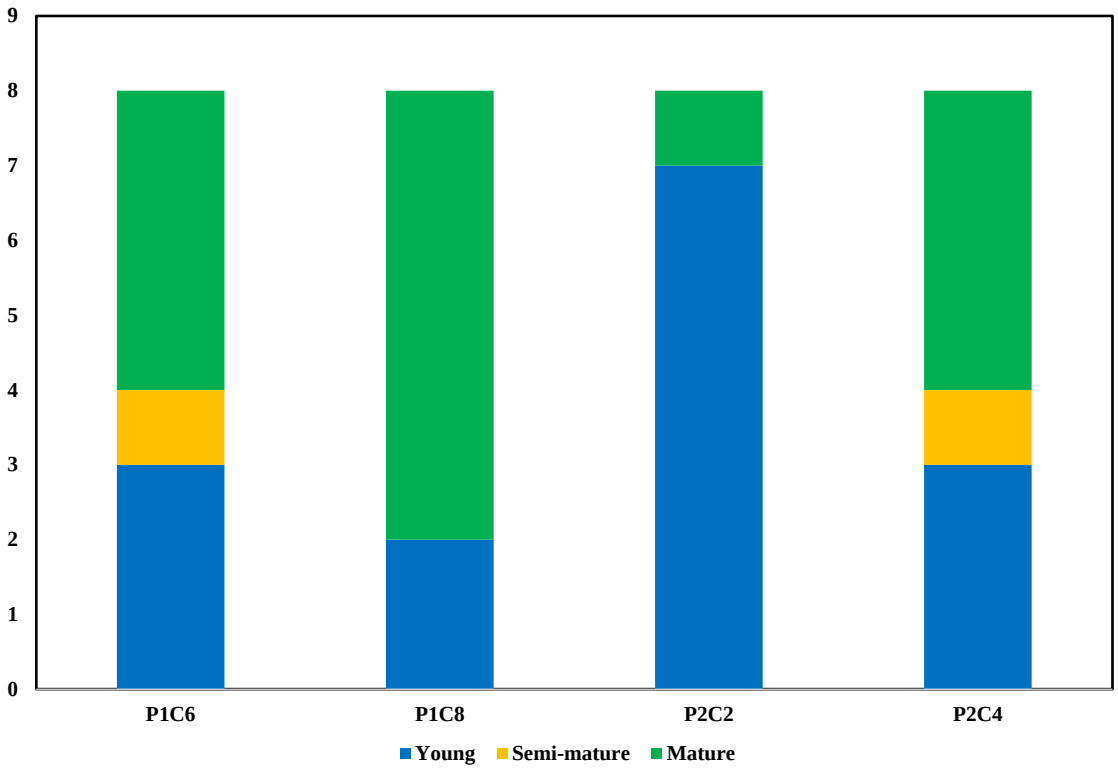

Figure 4.12. Classification of trees based on maturity levels (mature, semi-mature, and young) across experimental columns (P1C6 and P1C8 from Plot-1, and P2C2 and P2C4 from Plot-2). The classification is determined by trunk diameters measured at 15.24 cm (6 in) above ground, illustrating the distribution of tree maturity stages in each column.

4.4.5 Agrochemical Requirement

This study introduced the use of canopy volume as a critical parameter for determining the exact amount of agrochemicals required for ornamental trees. The agrochemical requirements for each experimental tree were calculated based on canopy volume data from Table 4.2. In Plot-1, the required agrochemical volumes ranged from 0.14 l for C6T1 to 0.35 l for C8T13, with an average volume of 0.22 l. In Plot-2, the requirements ranged from 0.04 l for C2T6 to 0.29 l for C4T7, with an average of 0.14 l, as visualized in Fig. 4.13. This method enabled a precise calculation of agrochemical needs, ensuring efficient resource usage based on the specific canopy volume of each tree. In future studies, these estimated amounts will be compared with actual application rates in nurseries using precision sprayers, adjusting volumes

based on canopy characteristics to assess the system's effectiveness in reducing chemical usage and improving tree management practices.

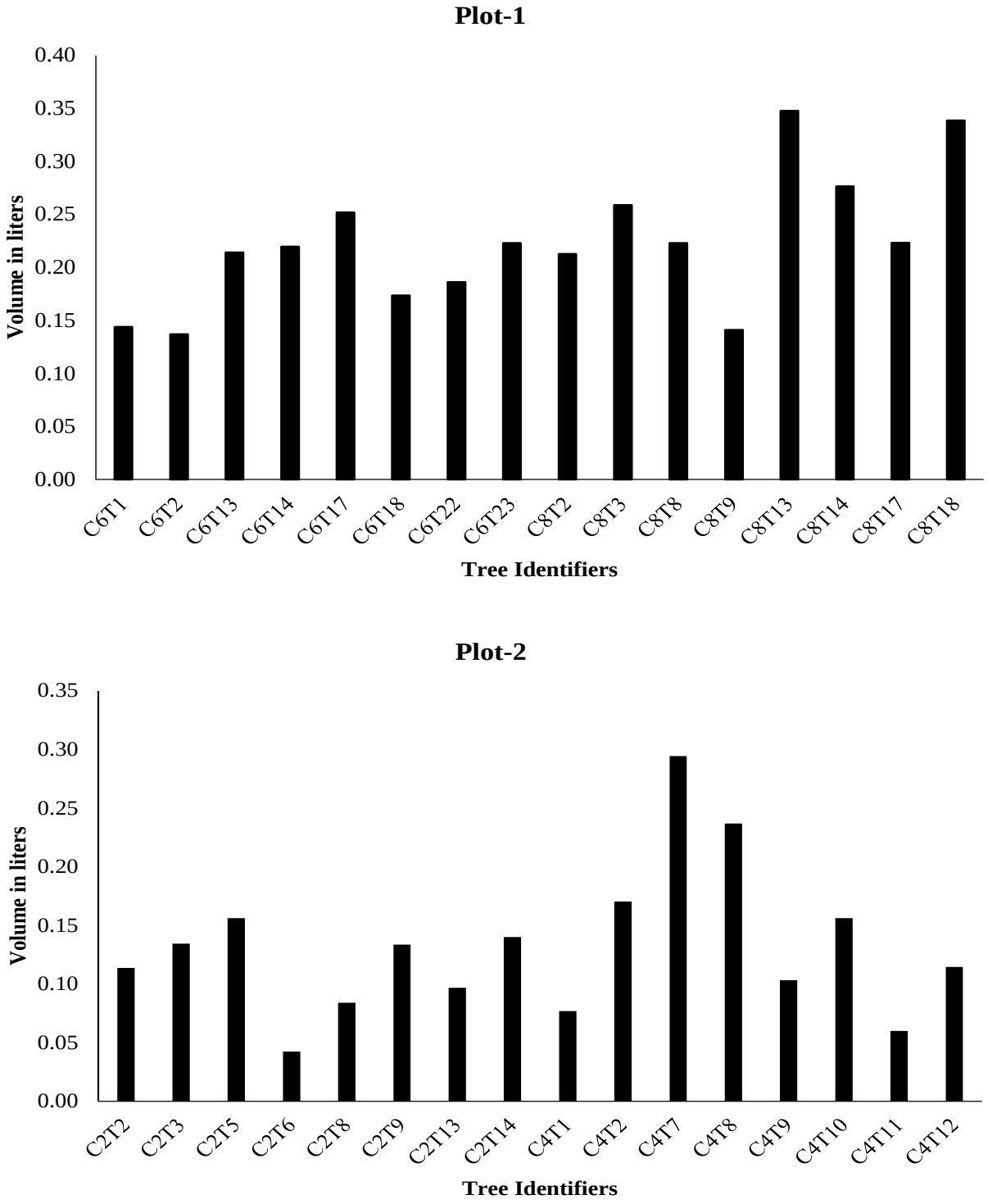

Figure 4.13. Volume of agrochemicals required for each experimental tree in Plot-1 and Plot-2. The graphs illustrate the estimated agrochemical volume in liters for individual trees based on their canopy volume.

4.5 Discussion and Future Directions

This study introduced a sensor-based approach for evaluating ornamental trees, focusing on 3D canopy volume and trunk diameter. This method provides a reliable solution for accurately calculating these parameters, tailored to the specific needs of ornamental trees in nursery settings, offering a granular understanding of agrochemical requirements at the individual tree level along with determining tree growth over time. The results demonstrated its effectiveness in determining agrochemical needs and assessing tree maturity in nurseries.

The methodology developed in this study offers a solid foundation for a precision sprayer system particularly suited for the woody ornamental industry. This system could calculate the exact amount of agrochemicals required for individual trees using a single scan, utilizing 3D canopy volume data to enable precise, targeted spraying. Such an approach has the potential to significantly reduce chemical waste. The successful trunk diameter estimation in this study also highlights the method's reliability, making it a dependable tool for accurate trunk diameter measurements. Richardson-Calfee et al. (2007) demonstrated that trunk diameter could be used as an indicator of crop maturity by tracking the seasonal growth patterns of roots, shoots, and trunks in sugar maples transplanted at different times.

A key challenge was the need to calculate canopy volume and trunk diameter individually for each tree, which proved time-consuming. Accurate results were heavily dependent on the proper placement of the LiDAR system. To capture the entire canopy structure, the LiDAR had to be positioned at a sufficient distance from the trees, which was sometimes difficult, particularly when trees are closely surrounded by others. In such dense environments, ensuring full canopy coverage without interference from neighboring trees requires careful sensor placement and planning. Furthermore, an adjustable tripod allowed the LiDAR to remain stable on sloped or uneven terrain, ensuring precise leveling and avoiding tilting that could compromise data accuracy. Processing techniques, including noise filtering

and managing partial occlusions, further enhanced data quality and precision, making it possible to overcome the spatial challenges in these complex nursery environments.

Unlike forests, where complex and dense vegetation can significantly complicate data collection, ornamental nurseries offer a more structured environment with trees typically planted in specific rows and maintaining consistent plant-to-plant distances. This organized layout reduces the challenges associated with data acquisition and allows for more straightforward sensor deployment. In such settings, TLS and depth cameras are likely sufficient to capture critical parameters such as canopy volume and trunk diameter with high accuracy. The regular spacing between trees facilitates easy placement of sensors and ensures minimal interference from surrounding vegetation, enabling more precise and focused measurements.

However, while stationary sensor systems like TLS and depth cameras are useful, they require manual setup and repositioning for each tree, which can be time-consuming, especially in large nurseries. To overcome this limitation, a more efficient approach would involve integrating both sensors into a mobile platform, such as an automated vehicle or robot, combined with additional sensors like IMU (Inertial Measurement Unit), GPS, and odometry sensors. Integrating sensors into a mobile platform provides a highly efficient and scalable solution for collecting tree measurements in large nurseries. The IMU provides detailed information on the platform's orientation, capturing roll, pitch, and yaw data, which is important for understanding the angle at which data is collected. It also helps maintain data consistency by compensating for tilts or movements due to uneven ground, enabling accurate point cloud generation for trees in sloped or variable terrain. GPS adds another layer of precision by recording the platform's exact geographical position, allowing for accurate location-based data collection and spatial alignment of tree measurements within the nursery. This is especially beneficial when revisiting the same trees over time to monitor growth or

perform longitudinal studies. Odometry sensors track the distance traveled and the speed of movement, further enhancing the platform's capability to adjust its navigation and sensor orientation in real-time. When combined, these sensors enable data fusion techniques that merge positional and orientation data to create a cohesive map of the nursery, with each tree accurately positioned and measured. This complements the system to seamlessly adjust for shifts in terrain, slopes, or obstructions, reducing errors in measurement due to platform tilt or positional inaccuracies. Tremblay et al. (2020) used mobile robots to measure tree diameters with an RMSE of 3.45 cm across the dataset and 2.04 cm in optimal conditions. This level of precision showcases the potential for mobile, sensor-equipped platforms to deliver accurate, reliable measurements in nursery environments.

During the data collection process using LiDAR and RGB-D cameras, additional data was gathered using the Husky A200™ (Clearpath Robotics, Kitchener, ON), a versatile unmanned ground vehicle (UGV) designed for a wide range of applications. The Husky's robust chassis, payload mounting framework, and onboard microcontroller are supported by three user power ports, making it adaptable to various sensor configurations. The setup integrated key sensors, including the Velodyne Puck (VLP-16) LiDAR (San Francisco, CA), SwiftNav Duro GPS/GNSS package (San Francisco, CA), and Open IMU UM7 (Xsens Technologies, Edisonstraat 10, 6902 PK, Zevenaar, Netherlands). To manage and process sensor data, the NVIDIA Jetson AGX Orin 64 GB Developer Kit (Santa Clara, CA) running on Ubuntu 20.04 was employed, facilitating real-time processing and visualization of the collected data. A comparison will be made in future studies between the datasets collected by LiDAR and RGB-D cameras to evaluate their performance and accuracy in capturing key tree attributes. This automated mobile robot setup is designed to create comprehensive maps of each tree and estimate essential parameters in a single pass. By automating the data collection process, this approach will minimize manual labor, improve accuracy, and enhance precision

in tree management and agrochemical application. Additionally, integrating Simultaneous Localization and Mapping (SLAM) technology will enable real-time mapping and tracking of tree positions within the nursery. This integration allows the system to gather detailed information on all trees at once, streamlining data processing and supporting more informed decision-making in nursery management.

Moving ahead, the approach applied in this study has the potential to lay the groundwork for future research in estimating tree attributes, particularly for ornamental and fruit trees grown in rows. By refining and enhancing the model and methodology from this study, it could be adapted for integration into an edge device, allowing for real-time nursery assessments. Such advancements would significantly boost the ornamental industry, improving precision, efficiency, and accuracy in estimating tree attributes.

4.6 Conclusions

Accurately estimating agrochemical requirements is essential for ornamental growers to optimize costs, reduce excessive chemical usage, and support sustainable agricultural practices. Meanwhile, trunk diameter measurements are critical for determining optimal market readiness, allowing growers to make informed decisions on when their trees are mature. This study leveraged LiDAR and depth camera to measure canopy volume and trunk diameter of young oak trees, respectively, with the goal of optimizing agrochemical application through precision spraying and accurately assessing tree maturity. LiDAR effectively captured the full canopy structure, providing detailed 3D models essential for calculating canopy volume, while the depth camera offered high-resolution data for precise trunk diameter measurements. This combined approach addressed several limitations of traditional methods, including variability and labor demands in manual measurements. The study implemented key methodologies such as sensor calibration, noise reduction through SOR, voxel grid filtering, and point cloud

processing to enhance the reliability and accuracy of measurements. These methods not only improved data quality but also demonstrated that advanced sensing technologies can effectively address the needs of ornamental nurseries. The results show strong agreement between sensor-derived and manual measurements, indicating that LiDAR and RGB-D systems are viable solutions for scalable, accurate assessments of tree characteristics in nursery settings. In addition, the study underlined the importance of advanced technology such as ground-based robots in nursery management. By implementing sensor-based measurements on a mobile platform, future work can aim to fully automate the data collection process, minimizing labor requirements and enabling large-scale adoption. The integration of SLAM technology and additional sensors, such as IMUs and GPS, can enhance real-time mapping and allow for continuous monitoring of tree growth, canopy development, and other vital characteristics over time. These advancements not only streamline the measurement process but also support more precise agrochemical application, contributing to sustainable agricultural practices and potentially transforming the ornamental nursery industry.

Acknowledgements

This study was supported in part by the USDA's NIFA Hatch Project (Accession No. 7007738) and the Startup and Institute for IIPA Seed Grant Funds from the University of Georgia.

CHAPTER 5

DEVELOPMENT OF A WEB APPLICATION FOR MONITORING DISEASE DYNAMICS AND SUPPORTING PRECISION SPRAYER SYSTEMS IN ORNAMENTAL CROPS [3]

---

[3] Rayamajhi, A. and M.S. Mahmud. To be submitted to a peer-reviewed journal.

Abstract

Spot anthracnose is a fungal disease that poses a significant threat to flowering dogwood trees, impacting their aesthetic appeal and decreasing market value. Fungicides are widely accepted as an effective management practice to manage spot anthracnose disease and minimize tree defoliation. This study aimed to develop SpotChecker, a user-friendly artificial intelligence-guided web application to evaluate disease severity of leafspots diseases like Spot Anthracnose quantitatively overtime. A total of 900 RGB images from six flowering dogwood trees were collected for training, validation, and testing of two deep learning models. Images were captured across different months (May, June, July) to represent various disease severity stages (mild, moderate, extreme) and under varying sunlight conditions using regular smartphones, ensuring dataset diversity and realism. The MaskFormer with Swin T exhibited an outstanding F1-Score (95.98%) while Mask RCNN with ResNet-50 backbone had F1-score of 92.03%. Moreover, MaskFormer model yielded an average IoU of 0.94 for canopy and 0.34 for leaf spots, while Mask RCNN model achieved an average IoU of 0.86 for canopy and 0.47 for leaf spots. The overall result suggested that for the task such as plant disease detection, especially when an object is tiny (leafspot) and objective is calculation of the percentage area of infection, MaskFormer with Swin T outperforms traditional Mask RCNN with ResNet-50. Consequently, the MaskFormer model was selected for web deployment which is capable of providing users with real-time analysis of the spot anthracnose severity in flowering dogwood canopies. Despite some challenges of computational speed, this project serves as a foundation for the development of a comprehensive real-time disease-detection system for monitoring dogwood tree health for all kinds of users.

Keywords: Disease Detection, Ornamentals, MaskFormer, Swin T, Mask R-CNN, Web Application.

5.1 Significance of the Study

This chapter addresses a critical gap in the development of precision sprayer systems by introducing a web-based tool for assessing the efficacy of reduced fungicide applications. Precision sprayers are designed to optimize agrochemical usage, reducing waste and minimizing environmental impact. However, their effectiveness hinges not only on accurate canopy volume measurements but also on ensuring that the reduced spray volumes are sufficient to manage diseases effectively. Currently, growers lack a quantifiable, real-time method to evaluate whether the applied fungicide rates achieve the desired disease control in ornamental crops. This study bridges that gap by developing *SpotChecker*, a user-friendly web application that utilizes advanced deep learning model to detect and quantify spot anthracnose severity on flowering dogwood canopies. By providing precise, real-time assessments of disease prevalence and treatment efficacy, this tool empowers growers to make informed decisions about the adequacy of fungicide applications, ensuring optimal disease management while supporting sustainable practices in ornamental crop production. Furthermore, it establishes a benchmark for integrating cutting-edge artificial intelligence technologies into accessible tools for the ornamental industry, paving the way for advancements in crop health monitoring and management.

5.2 Introduction

Flowering dogwood (*Cornus florida* L.) is a deciduous tree native to the eastern United States and Canada, known for its vibrant blooms and autumn leaves. Its aesthetic appeal attracts humans, while its vibrant red fruits serve as essential autumnal food for approximately forty bird species and numerous mammals Mitchell et al. (1988). The United States recorded around USD 31 million dogwood sales in 2019 alone (USDA, 2020), expressing the importance of woody ornamentals. However, this aesthetically important tree is listed as endangered in Maine

and threatened in Vermont in the northeastern United States (Call et al., 2016). It faces various biotic and abiotic stresses, making it susceptible to fungal infestations. Spot anthracnose, caused by the fungus *Elsinoe corni*, is one of the damaging diseases that affects the bracts and leaves of susceptible trees. Major symptoms include one to two millimeters of tiny brown spots with a red or purple border (Blake, 2009). To control the disease with fungicides, one should spray them when bracts start to open or have fallen and flower buds have formed (Hartman et al., 2017). Growers typically rely on visual inspection to assess the effectiveness of applied fungicides although this method lacks quantifiability, time-consuming, and laborious.

To address the challenge, computer vision technologies have emerged as a solution. These technologies encompass a wide range of methods and tools like deep learning that enable machines to interpret and understand visual information from the real world, relying on algorithms and computational models to analyze and extract meaningful information from images or video data (Chouhan et al., 2020; Hassaballah & Awad, 2020). Deep learning revolutionizes computer vision, empowering machines to perceive and interpret visual data with unparalleled accuracy and efficiency (Voulodimos et al., 2018). Computer vision techniques such as instance segmentation tackle the dual challenges of identifying individual objects within an image while also delineating their precise boundaries (Hafiz & Bhat, 2020). This method integrates object detection and semantic segmentation tasks, allowing for a comprehensive understanding of the visual scene by recognizing distinct objects and providing pixel-level segmentation to distinguish their exact shapes and positions within the image (Hafiz & Bhat, 2020). Building on these advancements, CNNs have achieved remarkable success across numerous computer vision applications, particularly in the realm of image classification and instance segmentation (Bello et al., 2019). Leveraging the capabilities of CNNs, Mask R-CNN (He et al., 2017) emerges as an effective instance segmentation technique, generating binary masks for each class independently. This approach typically outperforms previous

cutting-edge single-model outcomes on the COCO instance segmentation task, highlighting its superior performance (Lin et al., 2014). ResNet (Residual Network) (He et al., 2016), the default backbone of Mask RCNN, enhanced CNNs by increasing depth to 152 layers and reducing error by 3.75%. However, ResNet models may struggle with capturing global contextual information due to their design (Wang et al., 2022), leading researchers to explore alternative deep learning architectures. MaskFormer (Cheng et al., 2021) introduces a novel approach to instance segmentation, offering a unified solution for both semantic- and instance-level tasks. It exhibits compatibility with various backbone architectures, including ResNet and Swin T (Liu et al., 2021). By predicting binary masks linked with individual global class labels, MaskFormer simplifies segmentation while ensuring robust performance. Its transformative approach surpasses the performance of more intricate models, such as DETR (Detection Transformer) model (Carion et al., 2020) on COCO (Lin et al., 2014) and ADE20K (Zhou et al., 2017) datasets, achieving a new state-of-the-art performance on COCO with a PQ score of 52.7 (Cheng et al., 2021).

MaskFormer with transformer-based backbone, being a recent development, has been applied to limited studies in areas of agriculture and forestry (Fortin et al., 2022; Liu et al., 2024; Zhong et al., 2023), where it has showcased promising performance. However, there are some studies in agriculture where a traditional CNN backbone was replaced with a transformer-based backbone. For example, Cong et al. (2023) fused Mask RCNN with Swin T for greenhouse sweet pepper detection, which demonstrated the algorithm's effectiveness in accurately segmenting sweet peppers, achieving high detection and segmentation scores. The aforementioned studies provided evidence that Swin T performs better than traditional ResNet backbones in detecting diseases in agricultural crops. Some previous studies have also employed comparable deep learning models for spot anthracnose detection. For instance, Wang et al. (2022) introduced PAST-Net, a Path Aggregation Swin Transformer Network, which

employs Swin T as the backbone to enhance feature extraction from large lesions, leading to improved instance segmentation performance for spot anthracnose detection in crops. Rayamajhi and Mahmud (2023) developed a Mask R-CNN model, achieving a high F-1 score for detecting and segmenting spot anthracnose-infected leaves in flowering dogwoods. This study suggests that disease detection is possible for similar diseases in flowering dogwood leaves.

In agriculture, there is a demand for web-based applications for disease detection due to their remote accessibility. A few studies have explored real-time disease detection using deep learning algorithms and deploying detection models to web or mobile applications. For example, Islam, Adil, et al. (2023a) developed a web application using the ResNet-50 model to help farmers identify and classify plant diseases from leaf photos. Islam, Talukder, et al. (2023b) developed a web-based smart application for real-life disease prediction on cotton leaf utilizing the Xception model that achieved the highest accuracy rate of 98.70%. Tembhurne et al. (2023) developed an Android app, "Plantscape," with the aim of accurately detecting diseases. While many of these studies compared CNN architectures for accuracy, there's a lack of exploration into transformer-based models for web applications. Consequently, the ornamental industry lags in accessing such advanced tools for disease detection.

The primary goal of this study was to develop a web application - SpotChecker, using the deep learning model that performed best for spot anthracnose detection in flowering dogwood canopy images. MaskFormer with Swin T was trained for spot anthracnose detection and compared to Mask RCNN with ResNet-50. Superior results led to MaskFormer's deployment in a web-based application, SpotChecker, that detects and segments spot anthracnose in flowering dogwood canopies and precisely quantifies the existence of disease infection, enabling growers and researchers to analyze disease dynamics in real-time using the images of flowering dogwood canopies or leaves. This study will contribute to the ornamental

industry and benefit the growers and researchers of the flowering dogwood industry. Additionally, deploying deep learning models in accessible applications closes the gap between sophisticated research and practical, real-world use. In essence, the transition from model development to practical deployment validates the model's real-world applicability and ensures that cutting-edge research benefits users in their day-to-day farming and research activities. While many studies have developed efficient disease detection models, only a few have deployed them into practical tools like web-based or mobile applications.

The specific objectives of the study were: (a) development of an artificial intelligence model that detects and segments spot anthracnose in flowering dogwood canopies and gives an area of infection, (b) comparison of performance of (i) Mask R-CNN with ResNet101 and (ii) MaskFormer with Swin T (c) deployment of the model to a user-friendly web portal called SpotChecker for real-time assessment.

Among the main contributions of this study, the following stand out:

a. SpotChecker provides the area of infection of the disease, allowing the growers and researchers to analyze disease dynamics overtime.

b. The study assesses the efficacy of Swin T in MaskFormer over ResNet in Mask RCNN for disease diagnosis. By establishing a benchmark through this research, this study offers a valuable reference for future studies, providing researchers with a standard for conducting similar investigations.

c. SpotChecker is built with diverse images, which are similar to an image that a user with a regular smartphone may capture in the field for real-time assessment. It is targeted at farmers/growers as its main end users. The users need to simply upload a picture of a canopy suspected of disease, and the result will be available instantly.

5.3 Materials and Methods

5.3.1 Data Collection and Preparation

In the summer of 2023 (May to July), 3870 images of flowering dogwood canopies were captured using a smartphone (Google Pixel 5 with a 12.2-megapixel primary sensor with an f/1.7 aperture with autofocus). Six flowering dogwood trees planted at the Otis L Floyd Nursery Research Center (35°42′28.13″ N, 85°44′45.77″ W), Tennessee State University, McMinnville TN, were considered for data collection. An image included one or more leaves, stems, or bracts of the flowering dogwood along with the background. The images were captured at various times throughout the day to ensure a diverse range of lighting conditions, thereby adding to the overall diversity of the dataset (Fig. 5.1). The more diverse the dataset, the more robust the final model is (Rezk et al., 2022). The images were chosen in such a way that they were diverse in terms of lighting, severity of symptoms, background, and area of canopies involved. Images captured in early May exhibited minimal leafspots on the canopies, with both the size and number of spots gradually increasing towards the end of July, as illustrated in Fig. 5.1. Special care was taken to capture images from a specific distance from the canopies, ensuring that leafspots were clearly visible in the images. All the images were captured during the day between 8:00 AM and 4:00 PM. The weather was mostly sunny during the image collection.

Out of 3870 images, some of the images were blurry and not suitable for the training. Such images were filtered out. The dimensions of the images collected were 3024 × 4032 square pixels, and the format was JPG. The study used JPG format, considering that growers typically use smartphones to capture and upload images for disease assessment. The JPG is generally a default format for captured images captured using smartphones. A total of 900 images were selected for this study. For training and validation, 675 and 125 images were respectively allocated, ensuring a ratio of approximately 75% for training and 25% for testing

and validation. A total of 100 images were allocated for testing. The training and validation datasets were annotated using an online annotation tool - Makesense.ai. They were saved into JSON (JavaScript Object Notation) format with a COCO (Common Objects in Context) structure. Annotations were done manually using a Graphic Tablet (Huion HS611, Shenzen Huion Trend Technology Co. Ltd., Shenzhen, China). There were two classes: (i) canopy and (ii) leafspot. It was made sure the labeling was done properly with boundaries not crossing the objects. Polygons were used to create labels. The JSON files were used to train and validate the model.

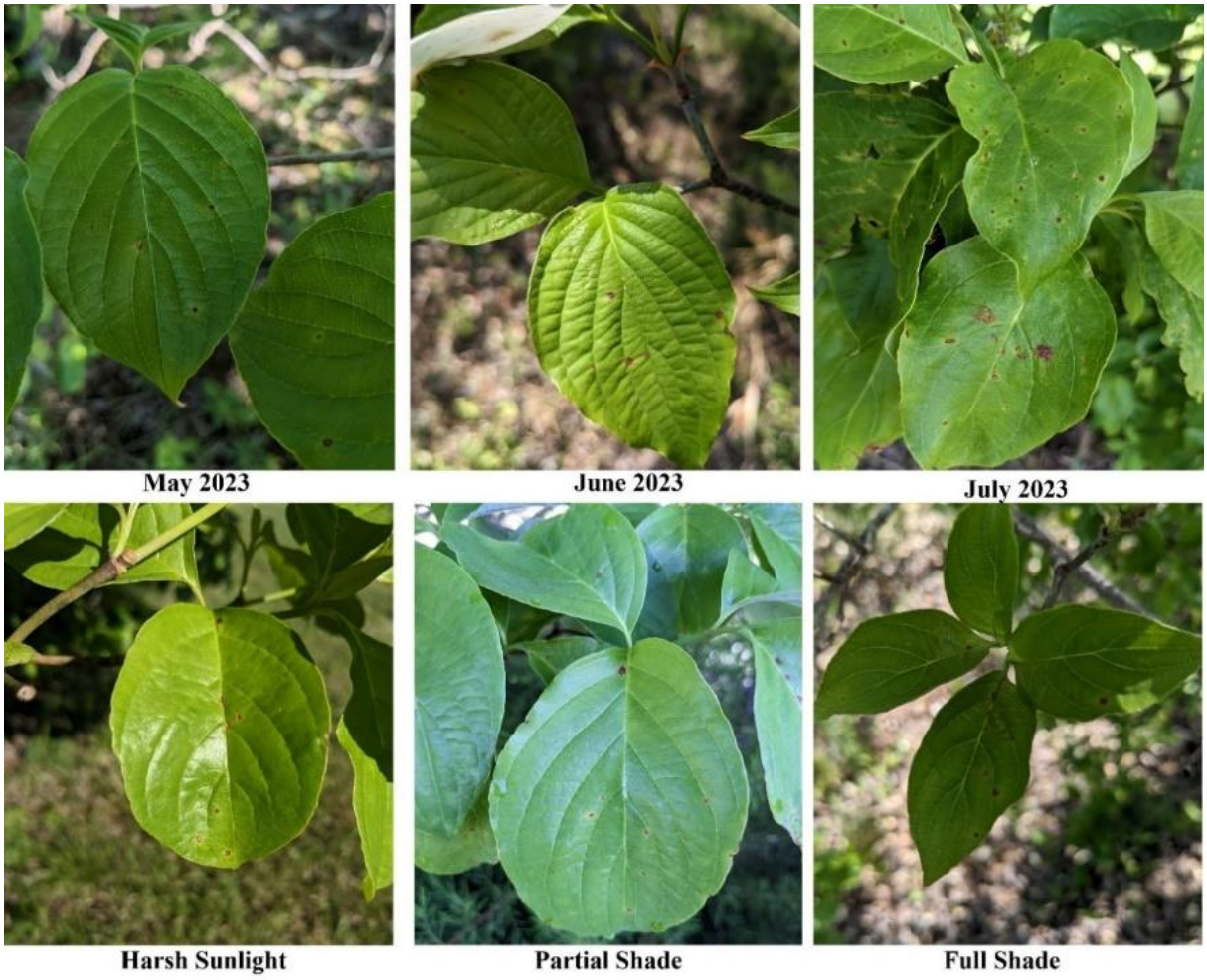

Figure 5.1. Sample images from the dataset collected across different months (May, June, and July 2023) and under varying sunlight conditions (harsh sunlight, partial shade, and full shade). These images illustrate the diversity in lighting and seasonal variations captured in the dataset.

5.3.2 SpotChecker Web-application Development

Deep Architecture Models

Recent advancements in deep neural networks have been extending the performance limits across various deep learning applications, including computer vision (West & O'shea, 2017). The performance of deep learning models is significantly influenced by the selection of architecture and hyperparameters. Although automatic hyperparameter optimization has been extensively studied for simple spaces, the exploration of complex spaces like deep architectures is still limited; consequently, architects rely on manual selection, often employing a slow trial-and-error process guided primarily by intuition (Negrinho & Gordon, 2017). In this plant disease detection project, focusing on spot anthracnose characterized by small spots as symptoms, two distinct models were utilized: Mask RCNN with ResNet-50 and MaskFormer with Swin T.

Mask RCNN

The first model, Mask R-CNN, was based on Matterport Inc.'s implementation, employing Python 3, Keras, and TensorFlow, with a ResNet-101 backbone and Feature Pyramid Network (FPN) architecture. However, in this implementation, an enhanced Mask R-CNN network model was developed utilizing the PyTorch 1.8.1 deep learning framework. In general, the backbone architecture of Mask RCNN typically employs ResNet-101, which consists of 101 network layers. However, using a network with too many layers can significantly slow down the processing speed. Since the task of extracting disease spots in this study is relatively straightforward and doesn't demand an extensive network layer count, the paper opts to utilize ResNet-50 instead. This decision was made to enhance the algorithm's execution speed while still fulfilling the requirements of the task. Fig. 5.2 provides a general architecture of Mask RCNN with ResNet-50 backbone. The initial step involves inputting the image into the pre-trained ResNet50 + FPN network model to extract features and generate

corresponding feature maps. Subsequently, a significant number of regions of interest (ROI) are obtained from the feature maps through the Region Proposal Network (RPN). Following this, binary classification of the foreground and background is carried out.

During the training of the Mask-RCNN model, a batch size of 4 was utilized along with the Stochastic Gradient Descent (SGD) optimizer. Each epoch is comprised of 168 iterations. The learning rate was set to 0.0001, and the backbone architecture chosen for feature extraction was ResNet-50. The hyperparameters and configurations were carefully selected to facilitate effective training, aiming to achieve accurate and robust performance in disease detection tasks for flowering dogwood canopies across various field conditions.

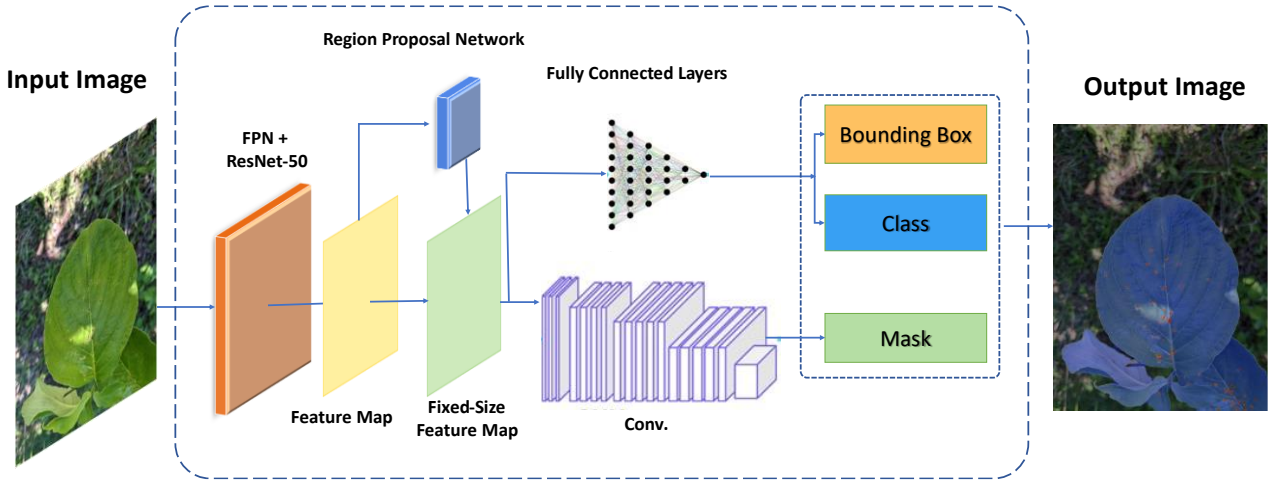

Figure 5.2. Illustration of the Mask R-CNN architecture with ResNet-50 as the backbone. The network takes an input image, and extracts feature maps using an FPN integrated with ResNet-50. The RPN generates region proposals, which are refined into fixed-size feature maps and processed through convolutional and fully connected layers to predict bounding boxes, classify objects, and generate segmentation masks for the regions of interest, providing a detailed output image with object detection and segmentation results.

MaskFormer

The second model, MaskFormer, was implemented based on Cheng et al.'s work (Cheng et al., 2021), which required Python version 3.6 or higher and PyTorch version 1.7 or higher, with torchvision matching the PyTorch installation. The architecture of MaskFormer consists of three main components: a backbone, a pixel decoder, and a Transformer decoder (Cheng et al., 2022). Fig. 5.3 gives a general architecture of the MaskFormer model with Swin T backbone.

The architecture components can be further explained:

A. Pixel-level Module: Took an image as input and used a backbone network to generate low-resolution image features. These features were then up-sampled by a pixel decoder to produce per-pixel embeddings.

B. Transformer Module: Employed a Transformer decoder that took image features and N learnable positional embeddings (queries) as inputs to produce N per-segment embeddings. These embeddings captured global information about each segment.

C. Segmentation Module: This module generated predictions from the per-segment embeddings. It used a linear classifier with SoftMax activation to produce class probability predictions for each segment. For mask prediction, a Multi-Layer Perceptron (MLP) transformed the per-segment embeddings into N mask embeddings, which were then used to obtain binary mask predictions through a dot product with per-pixel embeddings followed by a sigmoid activation.

During the training of the MaskFormer model, a batch size of 16 was employed along with a learning rate of 0.00001 and a weight decay of 0.02. The optimization process was conducted using the AdamW optimizer. Additionally, the backbone architecture chosen for feature extraction was Swin-Base. Careful selection was made of hyperparameters and

configurations to enable effective training, with the aim of achieving accurate and robust performance in disease detection tasks for flowering dogwood canopies across various field conditions.

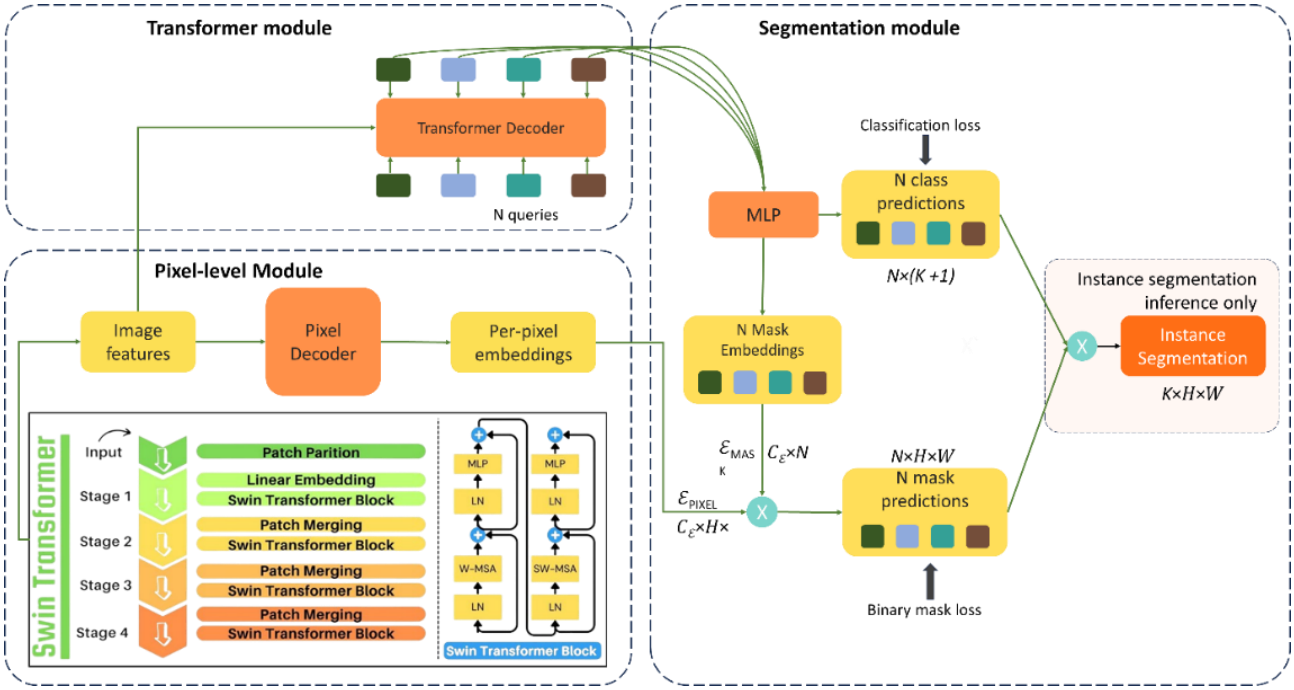

Figure 5.3. Architecture of MaskFormer with Swin T backbone, combining pixel-level feature extraction, transformer-based object-level embeddings, and a segmentation module for instance segmentation with classification and binary mask predictions.

Swin T Backbone

The Swin T block consists of two layers: Window-based Multi-Head Self-Attention (WMSA) and Shifted Window (SW) Multi-Head Self-Attention (Fig. 5.4). In WMSA, the input image is divided into windows, and attention is computed for patches within each window, occurring in the initial layer. The subsequent stage, Shifted Window MSA, mimics the sliding kernel concept from convolutional neural networks. It shifts the window by two patches, computing attention within these shifted windows. Swin T addresses a classic transformer limitation in visual tasks by introducing shifted windows. Traditionally, multi-head self-

attention is computationally intensive for images, requiring attention computation between all patches. Swin Transformer provides windows to divide the input image, enabling self-attention computation within the window while ignoring the remaining patches.

Swin T, used as a backbone, is comprised of four key components: patch partition, linear embedding, Swin T block, and patch merging (Fig. 5.4). The input image was first sent to the patch partitioning block, was divided into non-overlapping patches or tokens. A patch size 4x4 was used in the model. Each created patch was then linearly embedded into a c-dimensional vector, with c set to values such as 96, 128, or 192. In patch merging, neighboring 2x2 patches were combined through a linear layer, effectively reducing the number of patches by half and doubling the c dimension. This process was iteratively applied through the network's stages, leading to larger patch sizes at the end of each stage (e.g., 16x16 and 32x32).

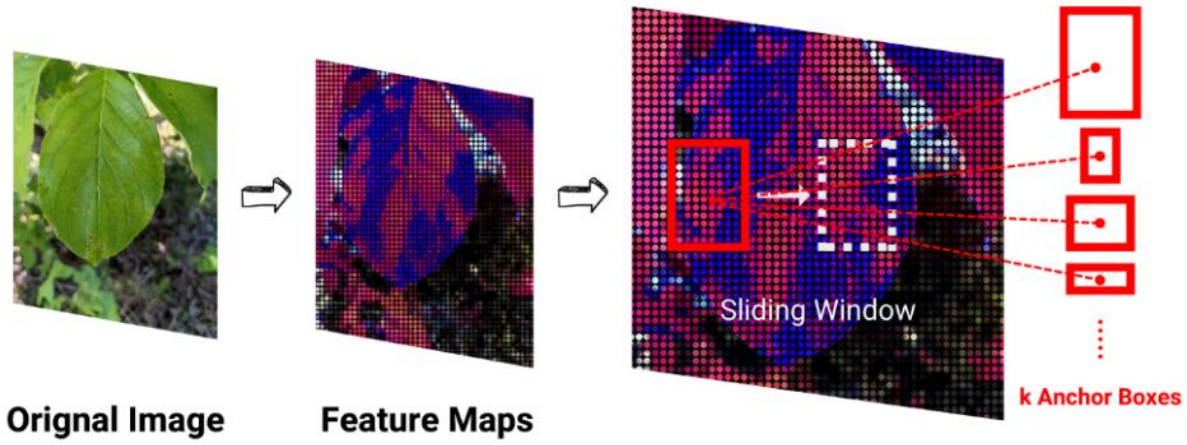

Figure 5.4. The architecture of the Swin T backbone, illustrating feature extraction from the original image through hierarchical feature maps and a sliding window mechanism with multiple anchor boxes for object detection.

5.3.3 Model Training and Validation

The training dataset, comprising 675 images, was employed to train the model, while the validation dataset, consisting of 125 images, was utilized for fine-tuning hyperparameters

and mitigating overfitting. In contrast, the testing dataset, containing 100 images, assessed the model's performance on unseen data. The images for training, validation and testing were randomly chosen from the dataset for the development of the detection model. The model was designed to classify two classes (canopy and leafspot) in addition to the background, generating masks of the same color for each class. Both models underwent training for 25 epochs using a pre-trained weight trained on the COCO dataset, facilitating transfer learning and significantly enhancing performance while reducing training time and resource expenditure.

Training and validation were conducted on a personal computer running Windows 11 Pro 64-bit, equipped with a 12th Gen Intel® Core™ i9-12900K processor (24 CPUs) clocked at ~3.2GHz and having 132 GB RAM. GPU mode was leveraged, employing an NVIDIA RTX A4500 20 Gb graphics card to optimize training speed. Employing state-of-the-art techniques and equipment ensured reliable and reproducible results, underpinning the accuracy and credibility of the findings. To verify the effectiveness of the disease detection model, two object detection algorithms, Mask RCNN with ResNet-50 and MaskFormer with Swin T, and one dataset were compared in this study. During the training of the Mask-RCNN model, a batch size of 4 was utilized along with the Stochastic Gradient Descent (SGD) optimizer. Each epoch was comprised of 168 iterations. The learning rate was set to 0.0001, and the backbone architecture chosen for feature extraction was ResNet-50. Likewise, in the case of MaskFormer, a batch size 16 was employed, along with a learning rate of 0.00001 and a weight decay of 0.02. The optimization process was conducted using the AdamW optimizer. Additionally, the backbone architecture chosen for feature extraction was Swin-Base. These hyperparameters and configurations for both models were carefully selected to facilitate effective training of both models, aiming to achieve accurate and robust performance in disease detection tasks for flowering dogwood canopies across various field conditions.

5.3.4 Model Performance Evaluation

Intersection over Union (IoU), Precision, Recall, and F1-score are common metrics used for evaluating the performance of algorithms in tasks such as object detection or segmentation. IoU measures the overlap between predicted and ground truth bounding boxes, with scores above 0.5 indicating acceptable detections.

$$IoU = |P \cap G| \; |P \cup G| \quad \text{(Eq 5.1)}$$

Where, "P" denotes the prediction bounding box, while "G" denotes the ground truth bounding box. Precision assesses the accuracy of positive predictions as a percentage. Recall quantifies the proportion of actual positives among all ground truths. F1-score represents the harmonic means of precision and recall, balancing their trade-offs.

The testing dataset was analyzed manually to evaluate the model's performance. Evaluation indexes like precision, recall, and F-1 score were calculated with Eq. 5.2, Eq. 5.3 and Eq. 5.4.

$$\text{Precision} = \frac{\boldsymbol{TP}}{\boldsymbol{TP + FP}} \quad \text{(Eq. 5.2)}$$

Where "TP" denotes True Positive, which is instances of the class correctly detected by the model and "FP" denotes False Positives, which instances wrongly detected as belonging to the class.

$$\text{Recall} = \frac{\boldsymbol{TP}}{\boldsymbol{TP + FN}} \quad \text{(Eq 5.3)}$$

Where "FN" denotes False Negatives, which are instances of the class that the model did not detect.

$$\text{F1-score} = 2\left(\frac{\boldsymbol{Precision \times Recall}}{\boldsymbol{Preision + Recall}}\right) \quad \text{(Eq 5.4)}$$

SpotChecker Web Application

To provide user-friendly and fast access to the upgraded instance segmentation model, the SpotChecker web application was developed. It was built using Flask, a web framework for building APIs with Python. Flask offers asynchronous support, ensuring efficient concurrent handling of multiple requests. The web application comprises two main components: the User Interface (UI) and the API endpoints. The UI is designed using HTML and JavaScript. HTML defines the basic structure and styling of the web page, while JavaScript handles the dynamic behavior related to file input and animations. The flow-chart of the SpotChecker web application is presented in Fig. 5.5.

The web app enables users to upload an image from their device. It then sends the image to the backend for processing and displays the resulting processed outputs. This entire process is achieved by the Flask end points, which trigger the SpotChecker Model for inference and returns the processed results to be published on the app. The SpotChecker Web App employs HTTP (Hypertext Transfer Protocol) for standard communication between the client and server. This ensures the seamless transfer of data and images. The mockup of SpotChecker is illustrated in Fig. 5.6.

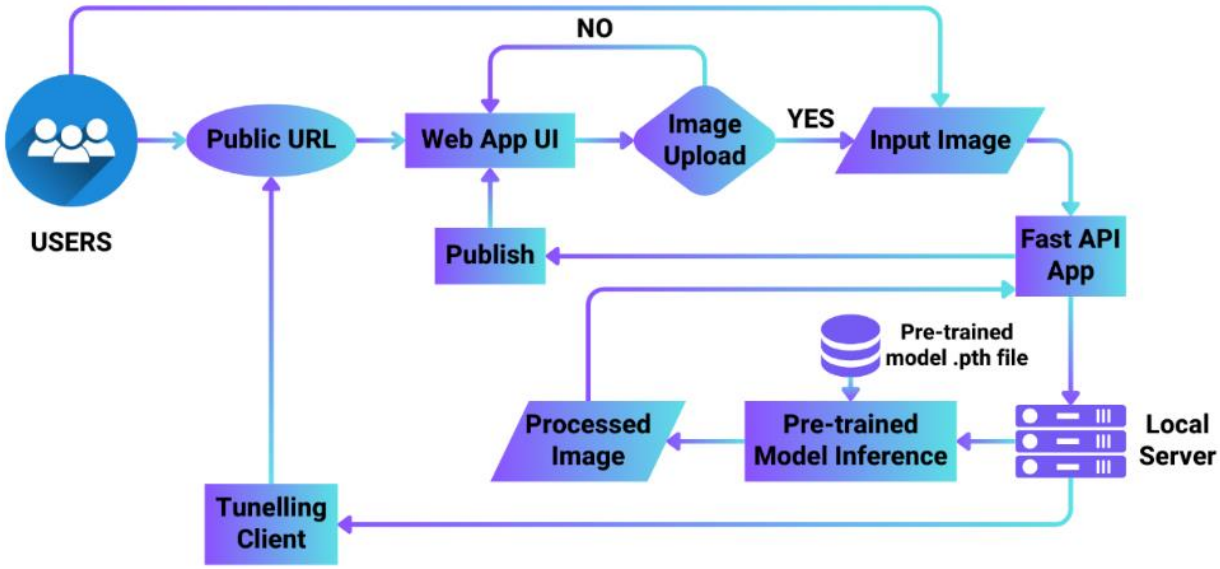

Figure 5. 5. Flowchart of the SpotChecker web application, illustrating the user interaction with the web app interface via a public URL for image upload, processing through a FastAPI application with a pre-trained model, and output publication through a tunneling client for visualization.

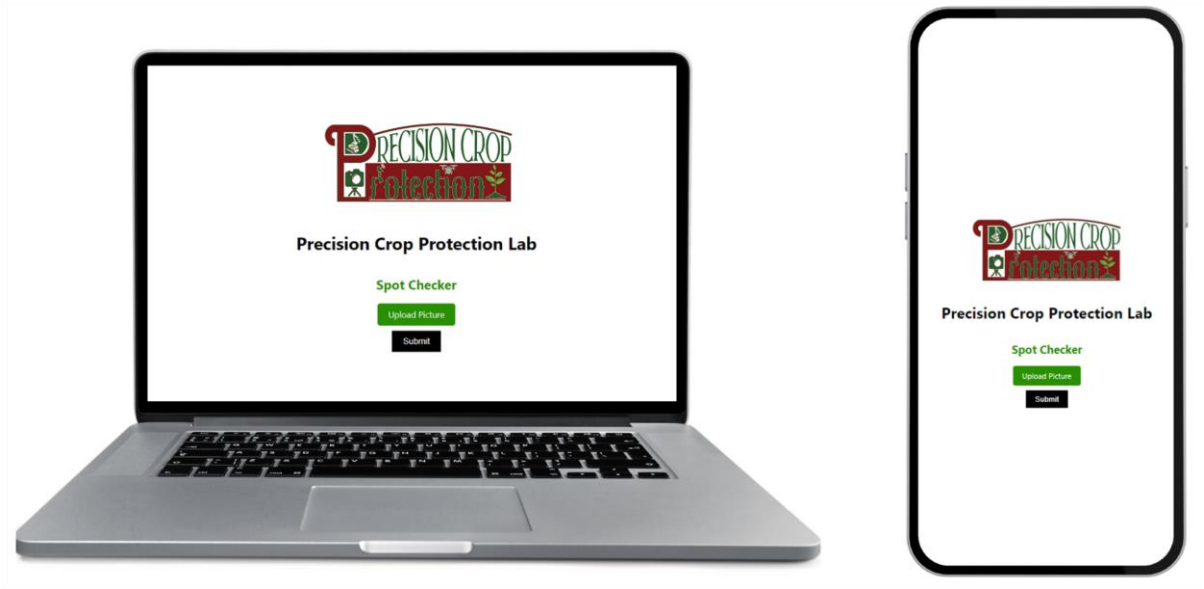

Figure 5.6. Mockup of the SpotChecker web application interface demonstrating its compatibility and responsiveness on both desktop and mobile devices.

5.3.5 Model Deployment and SpotChecker's Performance Evaluation

For the SpotChecker web app, the backend processing involving model inference takes place on the local server of the Precision Crop Protection Lab at the University of Georgia. To make the application publicly accessible, a secure external tunneling service was employed. This service established a protected tunnel from the public server URL to the local server, enabling external users to conveniently access the application. The /uploadfiles/ endpoint defined in the Flask web frame receives the uploaded image, runs it through the SpotChecker model, and returns the processed image. Upon uploading an image, the SpotChecker model is invoked on the backend to make an inference on the input image. Once the object detection is executed, the processing pipeline delineates objects of interest by applying masks on the image. The output is a refined image, where detected leafspots are highlighted with specific colors for easy interpretation. The SpotChecker model also quantifies the respective areas of canopies and leafspot instances. In this way, the total infected area percentage is calculated to aid precision agriculture practices.

$$Infected\ Area\ Percentage = \frac{Area\ of\ Leafspots}{Total\ Canopy\ Area} \times 100 \quad \text{(Eq. 5.5)}$$

5.4 Experimental Results and Analysis

5.4.1 Training and Validation Loss Comparison

The loss over epochs for both models across 25 epochs is illustrated in Fig. 5.7. Early stopping approach was incorporated on the models upon observing that the further training led to no significant improvement in the validation loss. MaskFormer with ResNet-50 exhibits superior performance in terms of training loss, significantly reducing from 0.20 to less than 0.06 within the 25 epochs. Conversely, the Mask RCNN model demonstrates a reduction in loss from approximately 5 to around 1.5 by the 25th epoch.

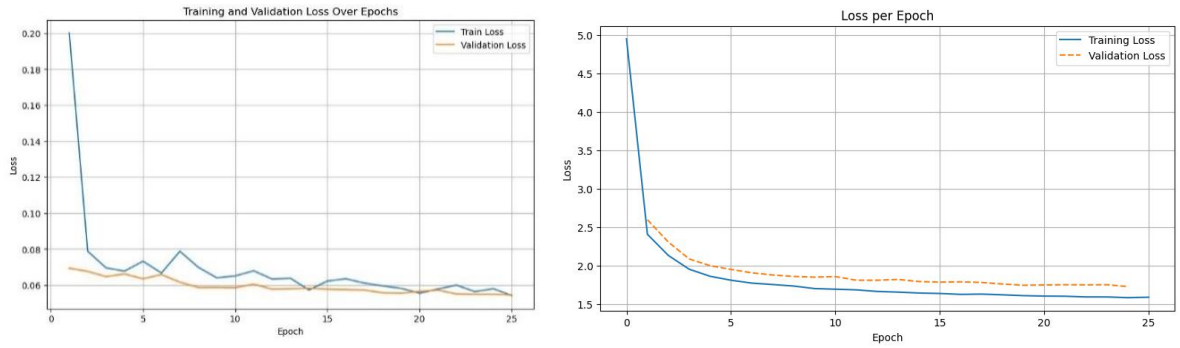

(i) **(ii)**

Figure 5.7. Loss curves for training and validation for (i) MaskFormer with Swin T and (ii) Mask RCNN with ResNet-50 backbone across 25 epochs.

5.4.2 Comparisons of Mask RCNN and MaskFormer Models

The state-of-the-art models were comprehensively evaluated, analyzing key metrics including Intersection over Union (IoU), precision, recall, and F-1 score. This comparative analysis was performed separately for both segmentation and detection tasks, providing information about the models' performance in accurately delineating objects and detecting instances within the images.

Detection

Upon examining the F-1 score for each model, Mask RCNN with ResNet-50 achieved a score of 92%, whereas MaskFormer with Swin T scored 96% (Table 5.1). The recall value is notably high for MaskFormer with Swin T, while Mask RCNN with ResNet-50 has a comparatively lower value. Additionally, the analysis of false negative and false positive occurrences in the test images reveals that MaskFormer demonstrates negligible false negatives compared to Mask RCNN, where false negatives are more prevalent. This suggests that MaskFormer is capable of detecting instances of canopies, potentially minimizing the risk of missing infected areas. Fig. 5.8 displays the results on two selected test images for both models.

The visualizations indicate that MaskFormer outperforms Mask RCNN in detecting both canopy and leafspots. Mask RCNN appears to encounter difficulties in generating accurate

masks for canopies and exhibits instances of false negatives. In contrast, MaskFormer demonstrates superior performance in detecting both canopy and leafspots, showcasing its ability to produce more accurate segmentation masks.

Table 5.1. Comparison of P, R, F1-score between state-of-the-art models: Mask RCNN with ResNet-50 and MaskFormer with Swin T for two classes (canopy and leafspot)

	Precision	**Recall**	**F-1 Score**
Mask RCNN with ResNet-50	0.992284	0.858007	0.920273
MaskFormer with Swin T	0.928056	0.993737	0.959774

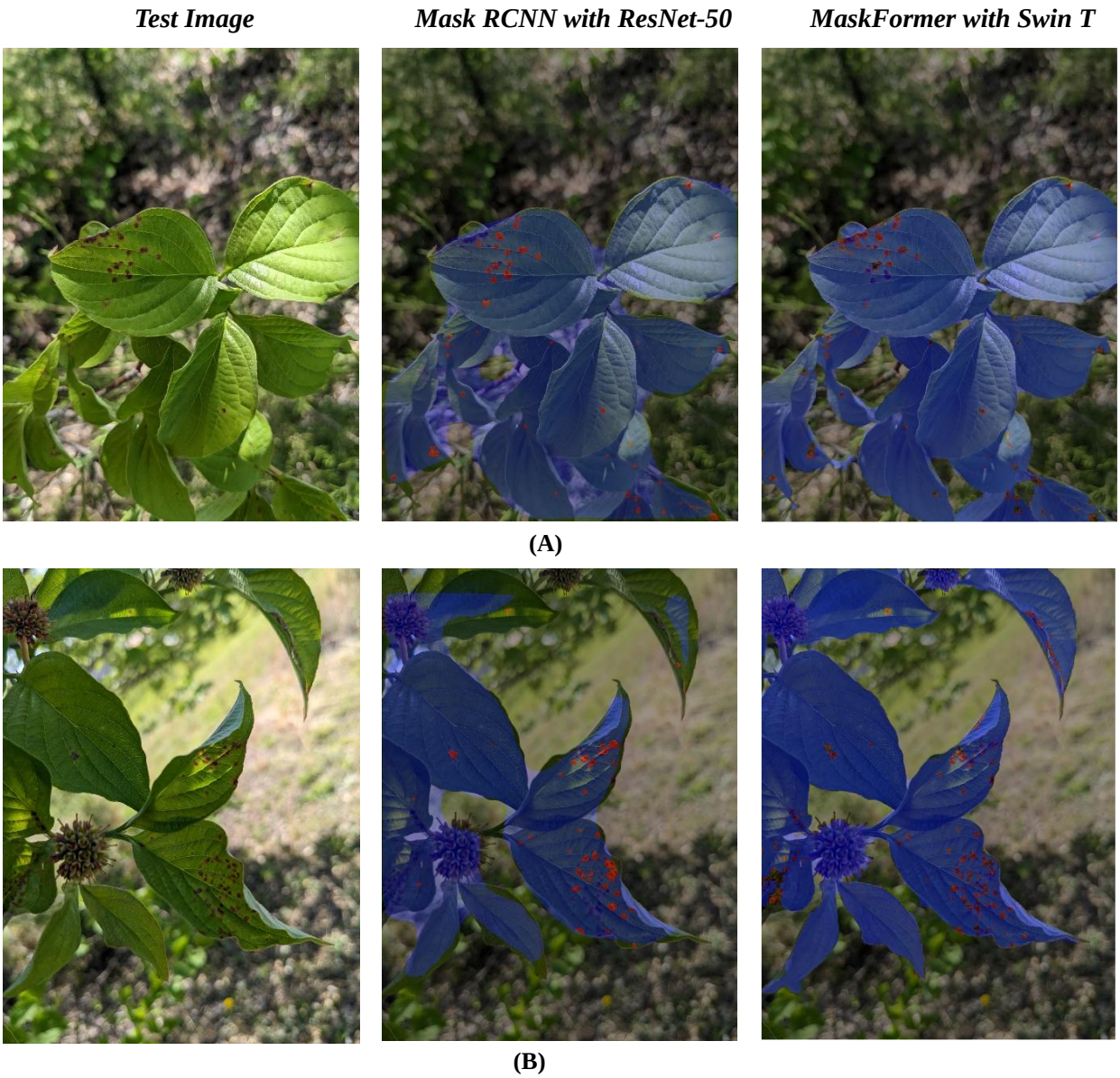

Figure 5.8. Comparison of segmentation results on two test images, (A) and (B), using Mask RCNN with ResNet-50 and MaskFormer with Swin T models. The images demonstrate differences in detection and segmentation accuracy between the models, with regions of interest marked in red for leafspot and blue for canopy for clear visualization.

Segmentation

The IoU was computed from ten out of the 100 test images for both canopy and leafspots, given their significance in determining the infection area percentage on the canopy. MaskFormer with Swin T yielded an average IoU of 0.94 for canopy and 0.34 for leafspots, while Mask RCNN with ResNet-50 achieved an average IoU of 0.86 for canopy and 0.47 for leafspots. Fig. 5.9 compares the predictions made by both models along with the ground truths.

The performance of MaskFormer with Swin T appears superior to that of Mask RCNN with ResNet-50, particularly in canopy detection. Mask RCNN exhibited missed detections in the bottom left and right sections of the canopy, which were accurately identified by MaskFormer. However, in terms of detecting leafspot, MaskFormer registers one false negative, whereas Mask RCNN successfully identifies instances of the disease. Based on its superior performance in both detection and segmentation tasks, MaskFormer with Swin T was selected for the spot anthracnose detection task. This model showed fewer false negatives compared to Mask RCNN, indicating its tendency to slightly overestimate disease counts, which is acceptable for disease assessment in this task. Conversely, Mask RCNN exhibited a notable number of false negatives, leading to potential underestimation of the disease. Moreover, MaskFormer demonstrated better canopy detection and segmentation, essential for precise area of infection calculation. Thus, its overall comprehensive performance in detection and segmentation aspects rendered it the preferred choice for the task at hand.

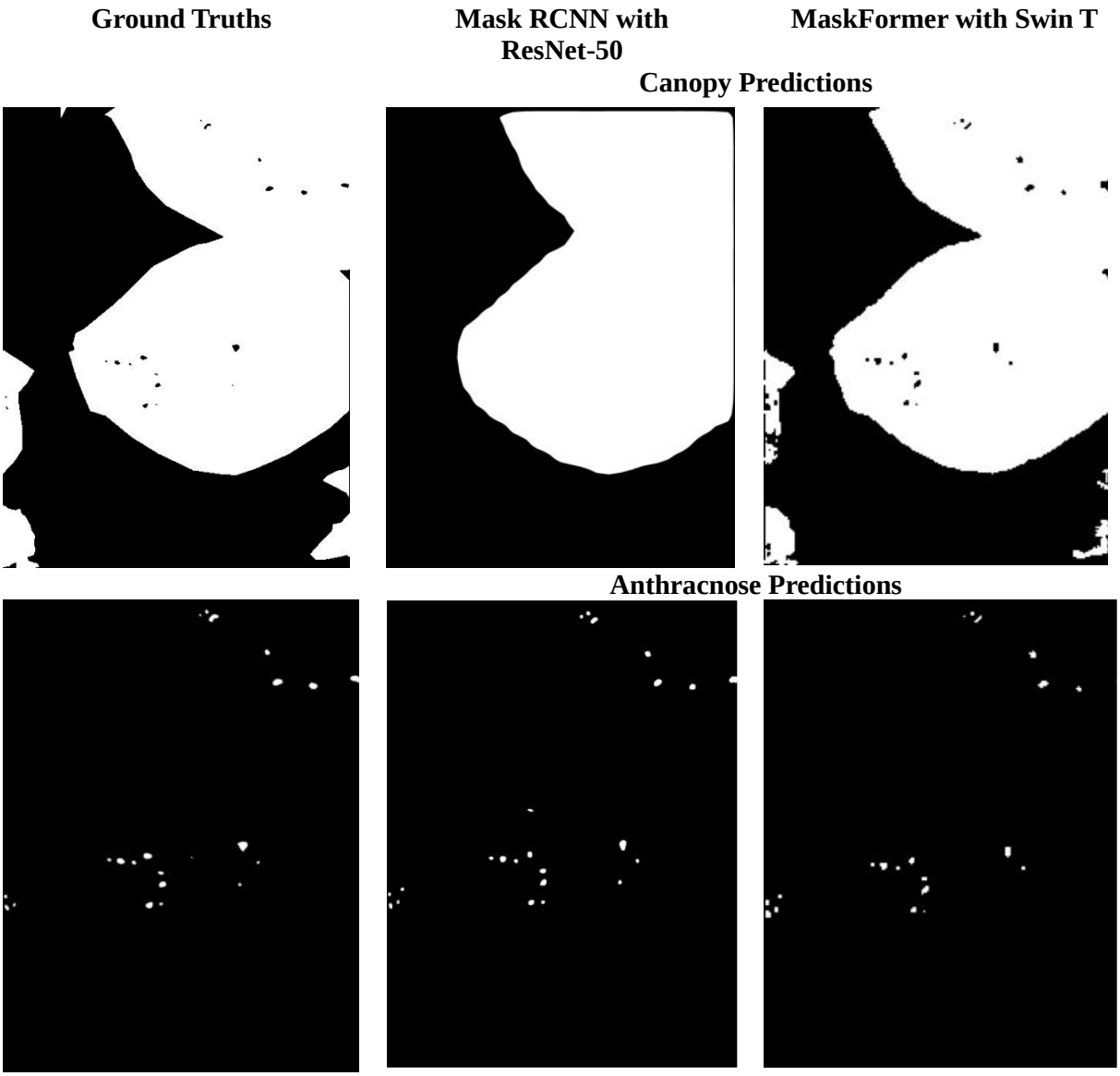

Figure 5.9. Results of Mask RCNN with ResNet-50 and MaskFormer with Swin T for canopy and disease predictions along with the ground truth on one of the test images. The white pixels indicate the object of interest while the black pixels indicate background.

5.4.3 SpotChecker Performance

Three different images of flowering dogwood canopy were tested with the SpotChecker. The results are illustrated on Fig. 5.10.

These images were categorized visually based on disease severity as less severe, medium severe, and extremely severe, resulting in three separate cases. In Case 1: Mild, where the symptoms were less severe, the SpotChecker detected a 0.24% infection area. In Case 2: Moderate, with medium-severe symptoms, it detected a 1.49% infection area, and in Case 3: Extreme, with extremely severe symptoms, it detected a 3.07% infection area. There was a gradual increase in the infection area with increased severity, indicating the efficacy of the SpotChecker. Additionally, the web app accurately identified and segmented the disease and canopy regions, providing fairly accurate percentages of the infection area.

5.5 Discussion

This study suggests that for the task of disease detection involving small objects, the MaskFormer model with Swin T as a backbone outperforms the Mask RCNN model with ResNet-50 backbone when tested with images. However, both models are expected to yield improved results with the inclusion of additional images in the training and validation datasets. Despite the dataset containing over 3000 images, the models were only trained on 675 images, indicating potential for further enhancement. Labeling presents a significant challenge due to its labor-intensive and repetitive nature, yet precision is essential for optimal performance. Despite this obstacle, endeavors will be made to retrain the models using a more extensive collection of training and validation images, enhancing their generalization capability. To tackle the time-consuming task of image annotation, alternative methods to manual labeling will be explored and implemented.

The Mask R-CNN model showed partial success in identifying instances of leafspots but had a notable number of false negatives. Conversely, the MaskFormer model demonstrated superior detection accuracy with fewer false negatives. However, it did produce some false positives in specific test images, suggesting an overestimation of spots. One of the challenges encountered by the MaskFormer model was distinguishing water droplets on leaves from spot anthracnose due to the glossy texture of the droplets, leading to misclassifications.

The web application operates swiftly and delivers excellent results. By providing instantaneous feedback on disease severity and treatment effectiveness, users can be empowered by SpotChecker to swiftly address issues, safeguarding the vitality of these trees. The next step involves performing outreach efforts like direct engagement with primary users (growers, stakeholders, and ornamental horticulturists) of this web tool, including hands-on training and soliciting valuable feedback to enhance its functionality. However, its usage is restricted to web browsers, and it has not yet been developed into a mobile application. This limitation detracts from its user-friendliness, as obtaining results requires more than one click. In the next phase, the plan involves deploying the model to a mobile application compatible with Android and iOS platforms. The mobile application will be available in at least two languages: English and Spanish. It will enable 91.3% population of the United States (according to 2022 American Community Survey, United States Census Bureau) to use the application.

For the mobile application model, additional investigation into deep learning models will be pursued to enhance accuracy while prioritizing computational speed and resource efficiency. It will include a recommendation section, a manual for site-specific management techniques, and various features to aid growers and researchers in comprehending diseases in flowering dogwood and similar ornamental crops. The application aims to function as a

comprehensive plant health guide. User feedback will be gathered through a survey, which will be utilized to enhance the features of the mobile application. Efforts will be dedicated to designing the application to be user-friendly and easily accessible for users from diverse backgrounds.

In the training of additional deep learning algorithms, the aim is to include more training images with more diversity. Additionally, additional disease symptoms and classes will be incorporated into the model through further studies so that it can provide comprehensive information on multiple diseases affecting flowering dogwood. This expanded scope can benefit growers in detecting and preventing the spread of plant diseases, contributing to the overall health and productivity of the flowering dogwood population along with an accurate analysis of disease dynamics.

.

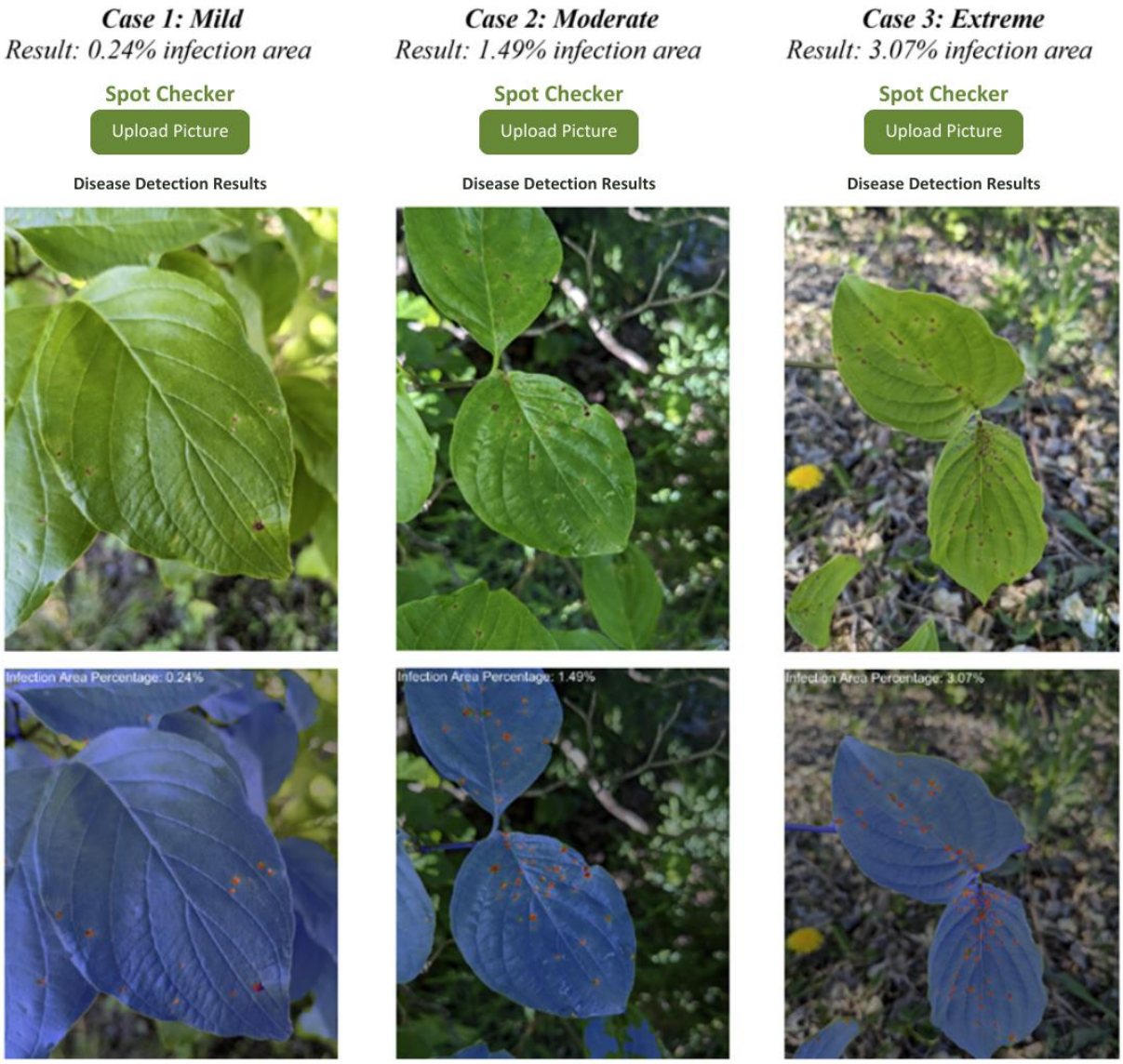

Figure 5.10. SpotChecker results in three different cases of severity of leafspots (mild, moderate, and extreme) on flowering dogwood. Case 1: Mild (result: 0.24%), Case 2: Moderate (result: 1.49%), Case 3: Extreme (result: 3.07%).

5.6 Conclusions

This study proposed SpotChecker, a web-based application for calculating the area of infection of spot anthracnose on flowering dogwood canopies. It compared two state-of-the-art models, Mask RCNN with ResNet-50 and MaskFormer with Swin T, for detecting and segmenting two classes – canopy and leafspot – across a diverse dataset. Results indicated that for such tasks, especially when dealing with tiny objects like leafspots, MaskFormer with Swin T backbone outperforms Mask RCNN with ResNet-50, achieving excellent F1-Score. As a result, the model was deployed on SpotChecker web application. The users can obtain real-time detection and area calculation results by simply uploading a picture of the leaf or canopy of flowering dogwood suspected of spot anthracnose on SpotChecker using a smartphone or computer. The application excels in predicting the extent of spot anthracnose infection on flowering dogwood canopy images. However, opportunities for improvement exist, including enlarging the dataset, introducing diversity, and enhancing the web application's functionality.

Acknowledgements

This study was supported by the Startup and Institute for Integrative Precision Agriculture (IIPA) funds from the University of Georgia. The authors would like to give special thanks to Otis L. Floyd Nursery Research Center and Smith Farm for providing field access and necessary resources.

CHAPTER 6
OVERALL CONCLUSIONS AND FUTURE DIRECTION

This study aimed to advance the field of precision spraying and management in ornamental plants, particularly woody ornamentals, by leveraging UAV and ground-based systems in conjunction with a disease detection web application. The primary objectives were to accurately estimate agrochemical requirements for individual trees, assess plant maturity through trunk measurements, and provide an accessible tool for real-time disease monitoring. Each of these objectives contributed to a comprehensive framework for optimizing resource use and enhancing disease control in ornamental nurseries.

The UAV-based system, equipped with high-resolution RGB camera, provided efficient large-scale canopy assessments. UAVs offered a valuable aerial perspective that enabled quick data collection across expansive nursery areas and allowed for estimating tree attributes such as tree height and canopy volume essential for planning agrochemical applications at a macro level. However, while UAVs excelled in efficiency and scalability, they were less precise for measurements of the tree characteristics as compared to ground-based system. UAV imagery lacked the fine-grained detail needed for tasks that required proximity to the tree, limiting its applicability in generating data for highly individualized agrochemical dosing.

Ground-based systems, using LiDAR sensor and depth camera, filled this gap by providing high-resolution data for close-range tree attributes, including precise measurements of trunk diameter and canopy structure. These systems captured intricate details essential for accurately estimating the agrochemical needs of each tree, enabling precision treatment that minimizes waste and maximizes efficacy. The ground-based approach proved especially

valuable in monitoring trunk diameter as an indicator of maturity, allowing growers to make informed decisions about harvesting and resource allocation. By offering a level of detail that UAVs cannot provide, ground-based systems proved to be ideal for individual tree management in precision agriculture.

However, the comparison between the two approaches revealed that while UAVs excelled in efficiency and scale, ground-based systems were superior for accuracy and detail. This distinction highlights the complementary nature of both approaches in a dual-system framework. UAVs are ideal for initial assessments and for tracking canopy-level characteristics over large areas, while ground-based systems are indispensable for high-resolution measurements that inform precise agrochemical needs at the individual tree level. Together, they form an integrated approach that combines the strengths of both broad canopy evaluation and fine-grained structural analysis, facilitating a comprehensive understanding of tree health and maturity. Additionally, this dual-system framework has significant practical applications for growers. By utilizing the drone-based system, growers can calculate the precise agrochemical requirements before spray operations. This enables them to mix the exact amount needed for each tree or plot, significantly reducing chemical wastage and associated costs.

An exciting direction for overcoming the time-intensive nature of ground-based assessments is the potential use of autonomous robotic platforms. Autonomous ground-based robots could be equipped with LiDAR, depth camera, and other sensors to navigate between trees and capture close-range data autonomously, freeing up labor and enabling frequent data collection. These robots would allow continuous, detailed monitoring without the manual effort currently required, making ground-based precision spraying feasible even for larger nursery operations.

The ultimate goal behind calculating canopy parameters is to integrate this information with other components of precision spraying technology, including variable-rate sprayers, sensor-based targeting systems, and automated dosing algorithms. For example, canopy volume data can be fed into variable-rate sprayers, allowing them to adjust the spray intensity and quantity in real-time, ensuring each tree receives the exact amount of agrochemical it needs. Sensor-based targeting systems can utilize the canopy shape and size information to focus on specific sections of the tree that require treatment, enhancing spray accuracy and reducing waste. Automated dosing algorithms can take this detailed canopy data and calculate the precise volume of chemical needed for a particular row or plot, streamlining the mixing process before the operation begins. This integration enables a precision-oriented approach, directly contributing to sustainable agricultural practices by cutting costs and reducing environmental impact. By ensuring agrochemicals are only applied where and when they are needed, this system supports holistic, data-driven management of each tree, aligning with the overarching objective of optimized resource use in ornamental horticulture.

In addition to canopy volume, other tree characteristics—such as height, trunk diameter, and tree count—are essential for efficient nursery management. Precise measurements of tree height and trunk diameter offer valuable insights into growth rates, enabling nursery managers to determine which trees are ready for market and which require further cultivation. Systematically tracking these parameters allows nurseries to manage inventory effectively, ensuring that each tree meets the quality standards required for specific ornamental species. A regularly updated tree count further supports nursery management by providing a clear view of stock health and progress, facilitating the scheduling of essential tasks like pruning, fertilization, and irrigation. Trunk diameter allows managers to forecast optimal harvest times and confirm that individual trees are resilient enough for transportation and transplanting. Additionally, maintaining records of harvested trees helps nurseries track sales trends, maintain

precise stock levels, and plan replanting schedules strategically. Together, these metrics empower nurseries to streamline operations, optimize resource allocation, and consistently provide a market-ready supply of high-quality ornamental trees that meet industry standards.

A significant innovation of this study was the development of a real-time disease detection web application, marking a major advancement in disease management for ornamental plants. Tailored specifically for growers and researchers, this application enabled immediate, field-ready insights into disease prevalence and severity using images, making it a highly practical and accessible tool. Currently focused on detecting a specific disease in flowering dogwoods, this technology offers a scalable foundation for future enhancements to identify multiple diseases, including leafspot conditions in hydrangeas, maples, and other ornamental species. By integrating advanced computer vision techniques, the application allows growers to assess disease dynamics over time, helping to minimize manual inspections while promoting efficient and consistent disease management practices. This approach not only optimizes time and resources but also empowers growers to make informed, real-time decisions that enhance the health and quality of their nursery stock. Future versions of SpotChecker will address current limitations, such as the need for broader disease datasets and enhanced accuracy under varying environmental conditions, by incorporating updated models and user feedback. Additionally, the application will feature a user-friendly interface with comprehensive instructions to ensure accessibility for all types of users, from novice growers to advanced practitioners.

In summary, this study provided a foundational framework for precision agriculture in the ornamental sector, particularly woody ornamentals. The integration of UAVs, ground-based systems, and real-time disease detection technologies offered a robust solution for managing agrochemical application and disease monitoring. Future directions for this work include refining autonomous robotic systems for ground-based measurements, expanding the disease

detection capabilities of the web application, and further integrating data-driven insights into nursery management practices. By addressing these avenues, the ornamental industry can continue to evolve towards a more precise, efficient, and sustainable approach to plant health and resource management, meeting the growing demands of both the market and environmental sustainability.

REFERENCES

Amin, M., & Islam, M. (2022). Effectiveness of some chemical pesticides against arthropod pests of ornamental plant.

Anderson, K., & Gaston, K. J. (2013). Lightweight unmanned aerial vehicles will revolutionize spatial ecology. *Frontiers in Ecology and the Environment*, *11*(3), 138-146.

Andújar, D., Dorado, J., Fernández-Quintanilla, C., & Ribeiro, A. (2016). An approach to the use of depth cameras for weed volume estimation. *Sensors*, *16*(7), 972.

Anifantis, A. S., Camposeo, S., Vivaldi, G. A., Santoro, F., & Pascuzzi, S. (2019). Comparison of UAV photogrammetry and 3D modeling techniques with other currently used methods for estimation of the tree row volume of a super-high-density olive orchard. *Agriculture*, *9*(11), 233.

Banu, S. (2015). Precision agriculture: tomorrow's technology for today's farmer.

Barber, D., Mills, J., & Smith-Voysey, S. (2008). Geometric validation of a ground-based mobile laser scanning system. *ISPRS journal of photogrammetry and remote sensing*, *63*(1), 128-141.

Bartholomeus, H., Calders, K., Whiteside, T., Terryn, L., Krishna Moorthy, S. M., Levick, S. R., Bartolo, R., & Verbeeck, H. (2022). Evaluating data inter-operability of multiple UAV–LiDAR systems for measuring the 3D structure of Savanna Woodland. *Remote Sensing*, *14*(23), 5992.

Bayraktar, E., Basarkan, M. E., & Celebi, N. (2020). A low-cost UAV framework towards ornamental plant detection and counting in the wild. *ISPRS journal of photogrammetry and remote sensing*, *167*, 1-11.

Bazi, Y., Malek, S., Alajlan, N., & AlHichri, H. (2014). An automatic approach for palm tree counting in UAV images. 2014 IEEE geoscience and remote sensing symposium,

Bello, I., Zoph, B., Vaswani, A., Shlens, J., & Le, Q. V. (2019). *Attention Augmented Convolutional Networks* IEEE/CVF international conference on computer vision,

Besl, P. J., & McKay, N. D. (1992). Method for registration of 3-D shapes. Sensor fusion IV: control paradigms and data structures,

Beverly, R. B., Florkowski, W., & Ruter, J. M. (1997). Fertilizer management by landscape maintenance and lawn care firms in Atlanta. *HortTechnology*, *7*(4), 442-445.

Bhakta, I., Phadikar, S., & Majumder, K. (2019). State-of-the-art technologies in precision agriculture: a systematic review. *Journal of the Science of Food and Agriculture*, *99*(11), 4878-4888.

Birdal, A. C., Avdan, U., & Türk, T. (2017). Estimating tree heights with images from an unmanned aerial vehicle. *Geomatics, Natural Hazards and Risk*, *8*(2), 1144-1156.

Blake, J. H. (2009). *Spot Anthracnose on Dogwood*. Clemson Cooperative Extension Home and Garden Information Center. https://hgic.clemson.edu/spot-anthracnose-on-dogwood/

Boatwright, H., Zhu, H., Clark, A., & Schnabel, G. (2020). Evaluation of the intelligent sprayer system in peach production. *Plant Disease*, *104*(12), 3207-3212.

Bonicelli, B., Naud, O., Rousset, S., Sinfort, C., De Rudnicki, V., Lescot, J.-M., Ruelle, B., Scheyer, L., & Cotteux, E. (2010). The challenge for precision spraying. AgEng 2010: International Conference on Agricultural Engineering,

Bornand, A., Rehush, N., Morsdorf, F., Thürig, E., & Abegg, M. (2023). Individual tree volume estimation with terrestrial laser scanning: Evaluating reconstructive and allometric approaches. *Agricultural and Forest Meteorology*, *341*, 109654.

Brack, C., Schaefer, M., Jovanovic, T., & Crawford, D. (2020). Comparing terrestrial laser scanners' ability to measure tree height and diameter in a managed forest environment. *Australian Forestry*, *83*(3), 161-171.

Business Research Insights. (2024). *Flower and Ornamental Plants Market Size, Share, Growth, And Industry Analysis By Type (Potted Plants and Cut Flowers) By Application (Home and Commercial), Regional Forecast To 2032* https://www.businessresearchinsights.com/market-reports/flower-and-ornamental-plants-market-103548

Byers, R., Lyons, C., Yoder, K., Horsburgh, R., Barden, J., & Donohue, S. (1984). Effects of apple tree size and canopy density on spray chemical deposit. *HortScience*, *19*(1), 93-94.

Call, A., Sun, Y. X., Yu, Y., Pearman, P. B., Thomas, D. T., Trigiano, R. N., Carbone, I., & Xiang, Q. Y. (2016). Genetic structure and post-glacial expansion of Cornus florida L.(Cornaceae): integrative evidence from phylogeography, population demographic history, and species distribution modeling. *Journal of Systematics and Evolution*, *54*(2), 136-151. https://doi.org/https://doi.org/10.1111/jse.12171

Carion, N., Massa, F., Synnaeve, G., Usunier, N., Kirillov, A., & Zagoruyko, S. (2020). End-to-end object detection with transformers. European conference on computer vision,

Carraro, A., Sozzi, M., & Marinello, F. (2023). The Segment Anything Model (SAM) for accelerating the smart farming revolution. *Smart Agricultural Technology*, *6*, 100367.

Carvalho, L. M., Souza, B., & de Sousa, A. L. V. (2019). Ornamental plants. *Natural Enemies of Insect Pests in Neotropical Agroecosystems: Biological Control and Functional Biodiversity*, 355-368.

Charania, I., & Li, X. (2020). Smart farming: Agriculture's shift from a labor intensive to technology native industry. *Internet of Things*, *9*, 100142.

Chen, F., Tsaftaris, S. A., & Giuffrida, M. V. (2024). GMT: Guided Mask Transformer for Leaf Instance Segmentation. *arXiv preprint arXiv:2406.17109*.

Chen, G., & Shang, Y. (2022). Transformer for tree counting in aerial images. *Remote Sensing*, *14*(3), 476.

Chen, J. (2021). Ornamental plant research inaugural editorial. *Ornamental Plant Research*, *1*(1), 1-2.

Chen, Y., & Medioni, G. (1992). Object modelling by registration of multiple range images. *Image and vision computing*, *10*(3), 145-155.

Cheng, B., Misra, I., Schwing, A. G., Kirillov, A., & Girdhar, R. (2022). Masked-attention mask transformer for universal image segmentation. Proceedings of the IEEE/CVF conference on computer vision and pattern recognition,

Cheng, B., Schwing, A., & Kirillov, A. (2021). Per-pixel classification is not all you need for semantic segmentation. *Advances in Neural Information Processing Systems*, *34*, 17864-17875.

Chouhan, S. S., Singh, U. P., & Jain, S. (2020). Applications of computer vision in plant pathology: a survey. *Archives of computational methods in engineering*, *27*, 611-632.

Chowdhuri, T. K., & Deka, K. (2019). Biodiversity and conservation of ornamental crops. *Conservation and Utilization of Horticultural Genetic Resources*, 139-216.

Cong, P., Li, S., Zhou, J., Lv, K., & Feng, H. (2023). Research on instance segmentation algorithm of greenhouse sweet pepper detection based on improved mask RCNN. *Agronomy*, *13*(1), 196. https://doi.org/https://doi.org/10.3390/agronomy13010196

Cunha, J. P. d., Sirqueira, M. A., & Hurtado, S. M. (2019). Estimating vegetation volume of coffee crops using images from unmanned aerial vehicles. *Engenharia Agrícola*, *39*(spe), 41-47.

da Cunha, J. P., Sirqueira, M. A., & Hurtado, S. (2019). Estimating vegetation volume of coffee crops using images from unmanned aerial vehicles. *Engenharia Agrícola*, *39*, 41-47.

Dalla Corte, A. P., Rex, F. E., Almeida, D. R. A. d., Sanquetta, C. R., Silva, C. A., Moura, M. M., Wilkinson, B., Zambrano, A. M. A., Cunha Neto, E. M. d., & Veras, H. F. (2020). Measuring individual tree diameter and height using GatorEye High-Density UAV-Lidar in an integrated crop-livestock-forest system. *Remote Sensing*, *12*(5), 863.

Dalponte, M., Ørka, H. O., Ene, L. T., Gobakken, T., & Næsset, E. (2014). Tree crown delineation and tree species classification in boreal forests using hyperspectral and ALS data. *Remote sensing of environment*, *140*, 306-317.

Demol, M., Calders, K., Verbeeck, H., & Gielen, B. (2021). Forest above-ground volume assessments with terrestrial laser scanning: a ground-truth validation experiment in temperate, managed forests. *Annals of Botany*, *128*(6), 805-819.

Eliopoulos, N. J., Shen, Y., Nguyen, M. L., Arora, V., Zhang, Y., Shao, G., Woeste, K., & Lu, Y.-H. (2020). Rapid tree diameter computation with terrestrial stereoscopic photogrammetry. *Journal of Forestry*, *118*(4), 355-361.

Fahlstrom, P. G., Gleason, T. J., & Sadraey, M. H. (2022). *Introduction to UAV systems*. John Wiley & Sons.

Farhan, S. M., Yin, J., Chen, Z., & Memon, M. S. (2024). A Comprehensive Review of LiDAR Applications in Crop Management for Precision Agriculture. *Sensors (Basel, Switzerland)*, *24*(16), 5409.

Fekry, R., Yao, W., Cao, L., & Shen, X. (2022). Ground-based/UAV-LiDAR data fusion for quantitative structure modeling and tree parameter retrieval in subtropical planted forest. *Forest Ecosystems*, *9*, 100065.

Fessler, L, D., Wright, W., Pietsch, G., Xiaocun, S., Yeary, W., Zhu, H., Bordeau, T., Russo, L., & Fulcher, A. (2022). Intelligent spray technology to control pests in nursery and

orchard systems with reduced pesticide application rates. XXXI International Horticultural Congress (IHC2022): III International Symposium on Mechanization, Precision Horticulture, and 1360,

Fisher, M. C., Henk, D. A., Briggs, C. J., Brownstein, J. S., Madoff, L. C., McCraw, S. L., & Gurr, S. J. (2012). Emerging fungal threats to animal, plant and ecosystem health. *Nature*, *484*(7393), 186-194.

Fortin, J.-M., Gamache, O., Grondin, V., Pomerleau, F., & Giguère, P. (2022). Instance segmentation for autonomous log grasping in forestry operations. 2022 IEEE/RSJ International Conference on Intelligent Robots and Systems (IROS),

Fu, C., Mertz, C., & Dolan, J. M. (2019). Lidar and monocular camera fusion: On-road depth completion for autonomous driving. 2019 IEEE Intelligent Transportation Systems Conference (ITSC),

Furness, G., Magarey, P., Miller, P., & Drew, H. (1998). Fruit tree and vine sprayer calibration based on canopy size and length of row: unit canopy row method. *Crop protection*, *17*(8), 639-644.

Gallardo-Salazar, J. L., & Pompa-García, M. (2020). Detecting individual tree attributes and multispectral indices using unmanned aerial vehicles: Applications in a pine clonal orchard. *Remote Sensing*, *12*(24), 4144.

Gao, S., Zhang, Z., & Cao, L. (2021). Individual tree structural parameter extraction and volume table creation based on near-field LiDAR data: a case study in a subtropical planted forest. *Sensors*, *21*(23), 8162.

Gavrilescu, M., & Chisti, Y. (2005). Biotechnology—a sustainable alternative for chemical industry. *Biotechnology advances*, *23*(7-8), 471-499.

Grella, M., Marucco, P., Balafoutis, A. T., & Balsari, P. (2020). Spray drift generated in vineyard during under-row weed control and suckering: evaluation of direct and indirect drift-reducing techniques. *Sustainability*, *12*(12), 5068.

Guimarães, N., Pádua, L., Marques, P., Silva, N., Peres, E., & Sousa, J. J. (2020). Forestry remote sensing from unmanned aerial vehicles: A review focusing on the data, processing and potentialities. *Remote Sensing*, *12*(6), 1046.

Hafiz, A. M., & Bhat, G. M. (2020). A survey on instance segmentation: state of the art. *International journal of multimedia information retrieval*, *9*(3), 171-189.

Hartman, J. R., M. L. Witt, W. M. Fountain, R. E. McNiel, M. F. Potter, & Jones, R. T. (2017). *The Flowering Dogwood*.

Hassaballah, M., & Awad, A. I. (2020). *Deep learning in computer vision: principles and applications*. CRC Press.

He, K., Gkioxari, G., Dollár, P., & Girshick, R. (2017). Mask r-cnn. Proceedings of the IEEE international conference on computer vision,

He, K., Zhang, X., Ren, S., & Sun, J. (2016). Deep residual learning for image recognition. Proceedings of the IEEE conference on computer vision and pattern recognition,

Henning, J. G., & Radtke, P. J. (2006). Detailed stem measurements of standing trees from ground-based scanning lidar. *Forest Science*, *52*(1), 67-80.

Hertz, T., & Zahniser, S. (2013). Is there a farm labor shortage? *American Journal of Agricultural Economics*, *95*(2), 476-481.

Hu, C., Pan, S., Zhang, H., & Li, P. (2020). Trunk model establishment and parameter estimation for a single tree using multistation terrestrial laser scanning. *IEEE Access*, *8*, 102263-102277.

Hu, V. M. (2023). *Tree Structure Retrieval for Apple Trees from 3D Pointcloud* UNSW Sydney].

Huylenbroeck, J. (2018). *Ornamental crops*. Springer.

Internacional, O. d. l. A. C. (2011). *Unmanned aircraft systems (UAS)*. Icao.

Islam, M. M., Adil, M. A. A., Talukder, M. A., Ahamed, M. K. U., Uddin, M. A., Hasan, M. K., Sharmin, S., Rahman, M. M., & Debnath, S. K. (2023). DeepCrop: Deep learning-based crop disease prediction with web application. *Journal of Agriculture and Food Research*, *14*, 100764.

Islam, M. M., Talukder, M. A., Sarker, M. R. A., Uddin, M. A., Akhter, A., Sharmin, S., Al Mamun, M. S., & Debnath, S. K. (2023). A deep learning model for cotton disease prediction using fine-tuning with smart web application in agriculture. *Intelligent Systems with Applications*, *20*, 200278.

Jacobs, M., Rais, A., & Pretzsch, H. (2020). Analysis of stand density effects on the stem form of Norway spruce trees and volume miscalculation by traditional form factor equations using terrestrial laser scanning (TLS). *Canadian Journal of Forest Research*, *50*(1), 51-64.

Jayathunga, S., Pearse, G. D., & Watt, M. S. (2023). Unsupervised Methodology for Large-Scale Tree Seedling Mapping in Diverse Forestry Settings Using UAV-Based RGB Imagery. *Remote Sensing*, *15*(22), 5276.

Jeon, H., & Zhu, H. (2023). Investigation of depth camera potentials for variable-rate sprayers.

Jin, D., Qi, J., Huang, H., & Li, L. (2021). Combining 3D radiative transfer model and convolutional neural network to accurately estimate Forest canopy cover from very high-resolution satellite images. *IEEE Journal of Selected Topics in Applied Earth Observations and Remote Sensing*, *14*, 10953-10963.

Kirillov, A., Mintun, E., Ravi, N., Mao, H., Rolland, C., Gustafson, L., Xiao, T., Whitehead, S., Berg, A. C., & Lo, W.-Y. (2023). Segment anything. *arXiv preprint arXiv:2304.02643*.

Kleunen, M., Essl, F., Pergl, J., Brundu, G., Carboni, M., Dullinger, S., Early, R., González-Moreno, P., Groom, Q. J., & Hulme, P. E. (2018). The changing role of ornamental horticulture in alien plant invasions. *Biological Reviews*, *93*(3), 1421-1437.

Kohyama, T. (1993). Size-structured tree populations in gap-dynamic forest--the forest architecture hypothesis for the stable coexistence of species. *Journal of Ecology*, 131-143.

Kozakiewicz, P., & McKinney, K. (2021). Study of selected properties of red maple wood (Acer rubrum) from the experimental plot of the forest arboretum in Rogów. *Annals of Warsaw University of Life Sciences-SGGW. Forestry and Wood Technology*, *115*.

Kulhandjian, H., Irineo, B., Sales, J., & Kulhandjian, M. (2024). Low-Cost Tree Health Categorization and Localization Using Drones and Machine Learning. 2024 International Conference on Computing, Networking and Communications (ICNC),

Kwong, I. H., & Fung, T. (2020). Tree height mapping and crown delineation using LiDAR, large format aerial photographs, and unmanned aerial vehicle photogrammetry in subtropical urban forest. *International Journal of Remote Sensing*, *41*(14), 5228-5256.

Kyriou, A., Nikolakopoulos, K., & Koukouvelas, I. (2021). How image acquisition geometry of UAV campaigns affects the derived products and their accuracy in areas with complex geomorphology. *ISPRS International Journal of Geo-Information*, *10*(6), 408.

Lambers, H., Chapin III, F. S., & Pons, T. L. (2008). *Plant physiological ecology*. Springer Science & Business Media.

Lamson, N. I. (1988). Precommercial Thinning and Pruning of Appalachian Stump Sprouts—10-Year Results. *Southern Journal of Applied Forestry*, *12*(1), 23-27. https://doi.org/10.1093/sjaf/12.1.23

Lance, R. (2004). *Woody plants of the southeastern United States: a winter guide*. University of Georgia Press.

Lassiter, H. A., Whitley, T., Wilkinson, B., & Abd-Elrahman, A. (2020). Scan pattern characterization of Velodyne VLP-16 lidar sensor for UAS laser scanning. *Sensors*, *20*(24), 7351.

Lee, K., & Ehsani, R. (2009). A laser scanner based measurement system for quantification of citrus tree geometric characteristics. *Applied Engineering in Agriculture*, *25*(5), 777-788.

Lee, K., Elliott, S., & Tiansawat, P. (2023). Use of Drone RGB Imagery to Quantify Indicator Variables of Tropical-Forest-Ecosystem Degradation and Restoration. *Forests*, *14*(3), 586.

Lefsky, M. A., Cohen, W. B., Parker, G. G., & Harding, D. J. (2002). Lidar remote sensing for ecosystem studies: Lidar, an emerging remote sensing technology that directly measures the three-dimensional distribution of plant canopies, can accurately estimate vegetation structural attributes and should be of particular interest to forest, landscape, and global ecologists. *BioScience*, *52*(1), 19-30.

Levoy, M., Pulli, K., Curless, B., Rusinkiewicz, S., Koller, D., Pereira, L., Ginzton, M., Anderson, S., Davis, J., & Ginsberg, J. (2000). The digital Michelangelo project: 3D scanning of large statues. Proceedings of the 27th annual conference on Computer graphics and interactive techniques,

Li, L., & Liu, C. (2019). A new approach for estimating living vegetation volume based on terrestrial point cloud data. *PloS one*, *14*(8), e0221734.

Liao, K., Li, Y., Zou, B., Li, D., & Lu, D. (2022). Examining the role of uav lidar data in improving tree volume calculation accuracy. *Remote Sensing*, *14*(17), 4410.

Lim, Y. S., La, P. H., Park, J. S., Lee, M. H., Pyeon, M. W., & Kim, J.-I. (2015). Calculation of tree height and canopy crown from drone images using segmentation. *한국측량학회지*, *33*(6), 605-613.

Lin, T.-Y., Maire, M., Belongie, S., Hays, J., Perona, P., Ramanan, D., Dollár, P., & Zitnick, C. L. (2014). Microsoft coco: Common objects in context. Computer Vision–ECCV 2014: 13th European Conference, Zurich, Switzerland, September 6-12, 2014, Proceedings, Part V 13,

Liu, S., Zhao, C., Zhang, H., Li, Q., Li, S., Chen, Y., Gao, R., Wang, R., & Li, X. (2024). ICNet: A Dual-Branch Instance Segmentation Network for High-Precision Pig Counting. *Agriculture*, *14*(1), 141.

Liu, Z., Lin, Y., Cao, Y., Hu, H., Wei, Y., Zhang, Z., Lin, S., & Guo, B. (2021). *Swin Transformer- Hierarchical Vision Transformer using Shifted Windows* IEEE/CVF international conference on computer vision,

López-Granados, F., Jurado-Expósito, M., Alamo, S., & Garcıa-Torres, L. (2004). Leaf nutrient spatial variability and site-specific fertilization maps within olive (Olea europaea L.) orchards. *European Journal of Agronomy*, *21*(2), 209-222.

Lovell, J., Jupp, D., Newnham, G., & Culvenor, D. (2011). Measuring tree stem diameters using intensity profiles from ground-based scanning lidar from a fixed viewpoint. *ISPRS journal of photogrammetry and remote sensing*, *66*(1), 46-55.

Maghsoudi, H., & Minaei, S. (2014). A review of applicable methodologies for variable-rate spraying of orchards based on canopy characteristics. *Journal of Crop Protection*, *3*(4), 531-542.

Mahmud, M. S., He, L., Heinemann, P., Choi, D., & Zhu, H. (2023). Unmanned aerial vehicle based tree canopy characteristics measurement for precision spray applications. *Smart Agricultural Technology*, *4*, 100153.

Matthews, G., Bateman, R., & Miller, P. (2014). *Pesticide application methods*. John Wiley & Sons.

Mazurowski, M. A., Dong, H., Gu, H., Yang, J., Konz, N., & Zhang, Y. (2023). Segment anything model for medical image analysis: an experimental study. *Medical Image Analysis*, *89*, 102918.

McQuilken, M. P., & Hopkins, K. (2004). Biology and integrated control of Pestalotiopsis on container-grown ericaceous crops. *Pest Management Science: formerly Pesticide Science*, *60*(2), 135-142.

Mekapogu, M., Jung, J.-A., Kwon, O.-K., Ahn, M.-S., Song, H.-Y., & Jang, S. (2021). Recent progress in enhancing fungal disease resistance in ornamental plants. *International Journal of Molecular Sciences*, *22*(15), 7956.

Miller, J., Morgenroth, J., & Gomez, C. (2015). 3D modelling of individual trees using a handheld camera: Accuracy of height, diameter and volume estimates. *Urban Forestry & Urban Greening*, *14*(4), 932-940.

Mitchell, W. A., Gibbs, P. A., & Martin, C. O. (1988). *Flowering dogwood (Cornus florida)*. US Army Corps of Engineers; July.

Nag, A., Chanda, P. R., & Nandi, S. (2023). Mobile app-based tomato disease identification with fine-tuned convolutional neural networks. *Computers and Electrical Engineering*, *112*, 108995.

Negrinho, R., & Gordon, G. (2017). Deeparchitect: Automatically designing and training deep architectures. *arXiv preprint arXiv:1704.08792*.

Nex, F., & Remondino, F. (2014). UAV for 3D mapping applications: a review. *Applied geomatics*, *6*, 1-15.

Palleja, T., Tresanchez, M., Teixido, M., Sanz, R., Rosell, J., & Palacin, J. (2010). Sensitivity of tree volume measurement to trajectory errors from a terrestrial LIDAR scanner. *Agricultural and Forest Meteorology*, *150*(11), 1420-1427.

Panagiotidis, D., Abdollahnejad, A., Surový, P., & Chiteculo, V. (2017). Determining tree height and crown diameter from high-resolution UAV imagery. *International journal of remote sensing*, *38*(8-10), 2392-2410.

Pascual, M., Villar, J., Rufat, J., Rosell, J., Sanz, R., & Arno, J. (2009). Evaluation of peach tree growth characteristics under different irrigation strategies by LIDAR system: Preliminary results. VI International Symposium on Irrigation of Horticultural Crops 889,

Patle, P., Kadu, P., Gabhane, A., Pharande, A., Bhagat, A., Bhoyar, S., Konde, N., & Rahangdale, M. (2019). Consequences provoked due to excess application of agrochemical on soil health deterioration–A review for Sustainable Agriculture. *Journal of Pharmacognosy and Phytochemistry*, *8*(2S), 63-66.

Pederi, Y., & Cheporniuk, H. (2015). Unmanned aerial vehicles and new technological methods of monitoring and crop protection in precision agriculture. 2015 IEEE International Conference Actual Problems of Unmanned Aerial Vehicles Developments (APUAVD),

Pedersen, S. M., & Lind, K. M. (2017). *Precision agriculture: Technology and economic perspectives*. Springer.

Pereira, P. C., Parente, C. E., Carvalho, G. O., Torres, J. P., Meire, R. O., Dorneles, P. R., & Malm, O. (2021). A review on pesticides in flower production: A push to reduce human exposure and environmental contamination. *Environmental Pollution*, *289*, 117817.

Pérez-Martín, E., Medina, S., Herrero-Tejedor, T., Pérez-Souza, M., de Mata, J., & Ezquerra-Canalejo, A. (2021). Assessment of tree diameter estimation methods from mobile laser scanning in a historic garden. Forests 2021, 12, 1013. In: s Note: MDPI stays neutral with regard to jurisdictional claims in published ….

Perry, A. S., Yamamoto, I., Ishaaya, I., & Perry, R. Y. (2013). *Insecticides in agriculture and environment: retrospects and prospects*. Springer Science & Business Media.

Poblete-Echeverría, C., Olmedo, G. F., Ingram, B., & Bardeen, M. (2017). Detection and segmentation of vine canopy in ultra-high spatial resolution RGB imagery obtained from unmanned aerial vehicle (UAV): A case study in a commercial vineyard. *Remote Sensing*, *9*(3), 268.

Polo, J. R. R., Sanz, R., Llorens, J., Arnó, J., Escola, A., Ribes-Dasi, M., Masip, J., Camp, F., Gracia, F., & Solanelles, F. (2009). A tractor-mounted scanning LIDAR for the non-destructive measurement of vegetative volume and surface area of tree-row plantations: A comparison with conventional destructive measurements. *Biosystems engineering*, *102*(2), 128-134.

Puliti, S., Ørka, H. O., Gobakken, T., & Næsset, E. (2015). Inventory of small forest areas using an unmanned aerial system. *Remote Sensing*, *7*(8), 9632-9654.

Punja, Z. K. (2006). Recent developments toward achieving fungal disease resistance in transgenic plants. *Canadian Journal of Plant Pathology*, *28*(S1), S298-S308.

Rayamajhi, A., & Mahmud, M. S. (2023). Detection and Segmentation of Anthracnose Leaf Spots in Flowering Dogwood Using Deep Learning for Site-Specific Management. 2023 ASABE Annual International Meeting,

Rezk, E., Eltorki, M., & El-Dakhakhni, W. (2022). Improving skin color diversity in cancer detection: deep learning approach. *JMIR Dermatology*, *5*(3), e39143.

Richardson-Calfee, L. E., Harris, J. R., & Fanelli, J. K. (2007). Posttransplant root and shoot growth periodicity of sugar maple. *Journal of the American Society for Horticultural Science*, *132*(2), 147-157.

Roşca, S., Suomalainen, J., Bartholomeus, H., & Herold, M. (2018). Comparing terrestrial laser scanning and unmanned aerial vehicle structure from motion to assess top of canopy structure in tropical forests. *Interface focus*, *8*(2), 20170038.

Salachna, P. (2022). Trends in ornamental plant production. In (Vol. 8, pp. 413): MDPI.

Salamí, E., Gallardo, A., Skorobogatov, G., & Barrado, C. (2019). On-the-fly olive tree counting using a UAS and cloud services. *Remote Sensing*, *11*(3), 316.

Salazar-García, S., & Lazcano-Ferrat, I. (2003). Site specific fertilization increased yield and fruit size in 'Hass' avocado. *Better Crops International*, *17*(1), 12-15.

Sankaran, S., Mishra, A., Ehsani, R., & Davis, C. (2010). A review of advanced techniques for detecting plant diseases. *Computers and Electronics in Agriculture*, *72*(1), 1-13.

Sankari, P. (2022). Automated Trunk Diameter Measurement.

Santoro, F., Tarantino, E., Figorito, B., Gualano, S., & D'Onghia, A. M. (2013). A tree counting algorithm for precision agriculture tasks. *International Journal of Digital Earth*, *6*(1), 94-102.

Sanz-Cortiella, R., Llorens-Calveras, J., Escolà, A., Arnó-Satorra, J., Ribes-Dasi, M., Masip-Vilalta, J., Camp, F., Gràcia-Aguilá, F., Solanelles-Batlle, F., & Planas-DeMartí, S. (2011). Innovative LIDAR 3D dynamic measurement system to estimate fruit-tree leaf area. *Sensors*, *11*(6), 5769-5791.

Sanz-Cortiella, R., Llorens-Calveras, J., Rosell-Polo, J. R., Gregorio-Lopez, E., & Palacin-Roca, J. (2011). Characterisation of the LMS200 laser beam under the influence of blockage surfaces. Influence on 3D scanning of tree orchards. *Sensors*, *11*(3), 2751-2772.

Shanwad, U., Patil, V., & Gowda, H. H. (2004). Precision farming: dreams and realities for Indian agriculture. *Map India*.

Shinoda, R., Kataoka, H., Hara, K., & Noguchi, R. (2023). Transformer-based ripeness segmentation for tomatoes. *Smart Agricultural Technology*, *4*. https://doi.org/10.1016/j.atech.2023.100196

Siefen, N., McCormick, R., Vogel, A., & Biegert, K. (2023). Effects of laser scanner quality and tractor speed to characterise apple tree canopies. *Smart Agricultural Technology*, *4*, 100173.

Singh, V. K., Singh, Y., & Kumar, P. (2012). Diseases of ornamental plants and their management. *Eco-friendly innovative approaches in plant disease management*, 543-572.

Sishodia, R. P., Ray, R. L., & Singh, S. K. (2020). Applications of remote sensing in precision agriculture: A review. *Remote Sensing*, *12*(19), 3136.

Solanelles, F., Escolà, A., Planas, S., Rosell, J., Camp, F., & Gràcia, F. (2006). An electronic control system for pesticide application proportional to the canopy width of tree crops. *Biosystems engineering*, *95*(4), 473-481.

Srinivasan, S., Popescu, S. C., Eriksson, M., Sheridan, R. D., & Ku, N.-W. (2015). Terrestrial laser scanning as an effective tool to retrieve tree level height, crown width, and stem diameter. *Remote Sensing*, *7*(2), 1877-1896.

Stafford, J. V. (2000). Implementing precision agriculture in the 21st century. *Journal of agricultural engineering research*, *76*(3), 267-275.

Stovall, A. E., MacFarlane, D. W., Crawford, D., Jovanovic, T., Frank, J., & Brack, C. (2023). Comparing mobile and terrestrial laser scanning for measuring and modelling tree stem taper. *Forestry: An International Journal of Forest Research*, *96*(5), 705-717.

Sui, R., Thomasson, J. A., Hanks, J., & Wooten, J. (2008). Ground-based sensing system for weed mapping in cotton. *Computers and Electronics in Agriculture*, *60*(1), 31-38.

Sutton, T., & Unrath, C. (1984). Evaluation of the tree-row-volume concept with density adjustments in relation to spray deposits in apple orchards. *Plant disease*, *68*(6), 480-484.

Team, R. D. C. (2010). R: A language and environment for statistical computing. *(No Title)*.

Tembhurne, J. V., Gajbhiye, S. M., Gannarpwar, V. R., Khandait, H. R., Goydani, P. R., & Diwan, T. (2023). Plant disease detection using deep learning based Mobile application. *Multimedia Tools and Applications*, 1-26.

Thai, H.-T., Tran-Van, N.-Y., & Le, K.-H. (2021). Artificial cognition for early leaf disease detection using vision transformers. 2021 International Conference on Advanced Technologies for Communications (ATC),

Thompson, N. M., Bir, C., Widmar, D. A., & Mintert, J. R. (2019). Farmer perceptions of precision agriculture technology benefits. *Journal of Agricultural and Applied Economics*, *51*(1), 142-163.

Torres-Sánchez, J., López-Granados, F., Borra-Serrano, I., & Peña, J. M. (2018). Assessing UAV-collected image overlap influence on computation time and digital surface model accuracy in olive orchards. *Precision Agriculture*, *19*, 115-133.

Torres-Sánchez, J., López-Granados, F., Serrano, N., Arquero, O., & Peña, J. M. (2015). High-throughput 3-D monitoring of agricultural-tree plantations with unmanned aerial vehicle (UAV) technology. *PloS one*, *10*(6), e0130479.

Traversari, S., Cacini, S., Galieni, A., Nesi, B., Nicastro, N., & Pane, C. (2021). Precision agriculture digital technologies for sustainable fungal disease management of ornamental plants. *Sustainability*, *13*(7), 3707.

Tremblay, J. F., Béland, M., Gagnon, R., Pomerleau, F., & Giguère, P. (2020). Automatic three-dimensional mapping for tree diameter measurements in inventory operations. *Journal of Field Robotics*, *37*(8), 1328-1346.

Ul Haq, I., Sarwar, M. K., Faraz, A., & Latif, M. Z. (2020). Synthetic chemicals: Major component of plant disease management. *Plant disease management strategies for sustainable agriculture through traditional and modern approaches*, 53-81.

USDA. (2020). *2019 census of horticultural specialties*.

Van der Zande, D., Hoet, W., Jonckheere, I., van Aardt, J., & Coppin, P. (2006). Influence of measurement set-up of ground-based LiDAR for derivation of tree structure. *Agricultural and Forest Meteorology*, *141*(2-4), 147-160.

Vinci, A., Brigante, R., Traini, C., & Farinelli, D. (2023). Geometrical characterization of hazelnut trees in an intensive orchard by an unmanned aerial vehicle (UAV) for precision agriculture applications. *Remote Sensing*, *15*(2), 541.

Voulodimos, A., Doulamis, N., Doulamis, A., & Protopapadakis, E. (2018). Deep learning for computer vision: A brief review. *Computational intelligence and neuroscience*, *2018*.

Wang, C., Yang, G., Huang, Y., Liu, Y., & Zhang, Y. (2023). A transformer-based mask R-CNN for tomato detection and segmentation. *Journal of Intelligent & Fuzzy Systems*(Preprint), 1-11.

Wang, Y., Wang, S., Ni, W., & Zeng, Q. (2022). An Instance Segmentation Method for Anthracnose Based on Swin Transformer and Path Aggregation. 2022 7th International Conference on Image, Vision and Computing (ICIVC),

Watt, P. J., & Donoghue, D. N. (2005). Measuring forest structure with terrestrial laser scanning. *International Journal of Remote Sensing*, *26*(7), 1437-1446.

Wei, X., & Khachatryan, H. (2021). Analyzing growers' pest management decisions in the US ornamental horticulture industry. *Journal of Cleaner Production*, *312*, 127788.

Weiss, M., Jacob, F., & Duveiller, G. (2020). Remote sensing for agricultural applications: A meta-review. *Remote sensing of environment*, *236*, 111402.

West, N. E., & O'shea, T. (2017). Deep architectures for modulation recognition. 2017 IEEE international symposium on dynamic spectrum access networks (DySPAN),

Winkelmann, T., Braun, P., Dhooghe, E., & Van Huylenbroeck, J. (2020). Advances in conventional breeding techniques for ornamentals. In *Achieving sustainable cultivation of ornamental plants* (pp. 119-148). Burleigh Dodds Science Publishing.

Wu, F., Wu, B., & Zhao, D. (2023). Real-time measurement of individual tree structure parameters based on augmented reality in an urban environment. *Ecological Informatics*, *77*, 102207.

Xun, L., Campos, J., Salas, B., Fabregas, F. X., Zhu, H., & Gil, E. (2023). Advanced spraying systems to improve pesticide saving and reduce spray drift for apple orchards. *Precision Agriculture*, *24*(4), 1526-1546.

Yao, L., Liu, T., Qin, J., Lu, N., & Zhou, C. (2021). Tree counting with high spatial-resolution satellite imagery based on deep neural networks. *Ecological Indicators*, *125*, 107591.

Yin, X., McClure, M. A., Jaja, N., Tyler, D. D., & Hayes, R. M. (2011). In-season prediction of corn yield using plant height under major production systems. *Agronomy Journal*, *103*(3), 923-929.

Young, D. J., Koontz, M. J., & Weeks, J. (2022). Optimizing aerial imagery collection and processing parameters for drone-based individual tree mapping in structurally complex conifer forests. *Methods in Ecology and Evolution*, *13*(7), 1447-1463.

Yrttimaa, T., Saarinen, N., Kankare, V., Viljanen, N., Hynynen, J., Huuskonen, S., Holopainen, M., Hyyppä, J., Honkavaara, E., & Vastaranta, M. (2020). Multisensorial close-range sensing generates benefits for characterization of managed Scots pine (Pinus sylvestris L.) stands. *ISPRS International Journal of Geo-Information*, *9*(5), 309.

Zaman, Q., Schumann, A., & Miller, W. (2005). Variable rate nitrogen application in Florida citrus based on ultrasonically-sensed tree size. *Applied Engineering in Agriculture*, *21*(3), 331-335.

Zhang, S., Wang, C., & Chan, S.-C. (2015). A new high resolution depth map estimation system using stereo vision and kinect depth sensing. *Journal of Signal Processing Systems*, *79*, 19-31.

Zhong, B., Wei, T., Luo, X., Du, B., Hu, L., Ao, K., Yang, A., & Wu, J. (2023). Multi-Swin Mask Transformer for Instance Segmentation of Agricultural Field Extraction. *Remote Sensing*, *15*(3), 549.

Zhou, B., Zhao, H., Puig, X., Fidler, S., Barriuso, A., & Torralba, A. (2017). Scene parsing through ade20k dataset. Proceedings of the IEEE conference on computer vision and pattern recognition,

Zhou, J., Cui, M., Wu, Y., Gao, Y., Tang, Y., Jiang, B., Wu, M., Zhang, J., & Hou, L. (2024). Detection of maize stem diameter by using RGB-D cameras' depth information under selected field condition. *Frontiers in plant science*, *15*, 1371252.

Zhou, L., Meng, R., Tan, Y., Lv, Z., Zhao, Y., Xu, B., & Zhao, F. (2022). Comparison of UAV-based LiDAR and digital aerial photogrammetry for measuring crown-level canopy height in the urban environment. *Urban Forestry & Urban Greening*, *69*, 127489.

Zhou, W., Li, M., & Achal, V. (2024). A comprehensive review on environmental and human health impacts of chemical pesticide usage. *Emerging Contaminants*, 100410.

Zhou, X., Wang, H., Chen, C., Nagy, G., Jancso, T., & Huang, H. (2023). Detection of Growth Change of Young Forest Based on UAV RGB Images at Single-Tree Level. *Forests*, *14*(1), 141.

Zhu, H., Derksen, R., Guler, H., Krause, C., & Ozkan, H. (2006). Foliar deposition and off-target loss with different spray techniques in nursery applications. *Transactions of the ASABE*, *49*(2), 325-334.

Zhu, H., Jeon, H. Y., Gu, J., Derksen, R. C., Krause, C. R., Ozkan, H. E., Chen, Y., Reding, M. E., Ranger, C. M., & Cañas, L. (2010). Development of Two Intelligent Spray Systems for Ornamental Nurseries©. *Proceedings of the International Plant Propagators' Society, Miami, FL, USA*, *60*, 322.

Zwertvaegher, I., Foqué, D., Dekeyser, D., Van Weyenberg, S., & Nuyttens, D. (2017). Comparison of spray configurations in a spray cabin design for ornamental potted plants: A proof-of-concept study. *Transactions of the ASABE*, *60*(3), 647-656.

APPENDIX

A. List of Abbreviations and Acronyms

1. 3D - Three-Dimensional
2. AdamW - Adam Optimizer with Weight Decay
3. AI - Artificial Intelligence
4. API - Application Programming Interface
5. AR - Augmented Reality
6. BMP - Bitmap
7. CAGR - Compound Annual Growth Rate
8. CNN - Convolutional Neural Network
9. COCO - Common Objects in Context
10. CWFID - Crop/Weed Field Image Dataset
11. DEM - Digital Elevation Model
12. DSM - Digital Surface Model
13. DTM - Digital Terrain Model
14. FAIR - Facebook AI Research
15. FOV - Field of View
16. FPN - Feature Pyramid Network
17. GPS - Global Positioning System
18. GSD - Ground Sample Distance
19. HD2K - High Definition 2K
20. HTTP - Hypertext Transfer Protocol
21. IMU - Inertial Measurement Unit
22. IoU - Intersection over Union

23. IIPA - Institute for Integrative Precision Agriculture

24. JPG - Joint Photographic Experts Group

25. JSON - JavaScript Object Notation

26. LiDAR - Light Detection and Ranging

27. MAE - Mean Absolute Error

28. MAPE - Mean Absolute Percentage Error

29. MLS - Mobile Laser Scanning

30. MLP - Multi-Layer Perceptron

31. NDVI - Normalized Difference Vegetation Index

32. NIFA - National Institute of Food and Agriculture

33. NMS - Non-Maximum Suppression

34. PA - Precision Agriculture

35. PCAP - Packet Capture

36. PCD - Point Cloud Data

37. PQ - Panoptic Quality

38. RCNN - Region-based Convolutional Neural Network

39. RGB - Red-Green-Blue

40. RGB-D - Red-Green-Blue-Depth

41. RMSE - Root Mean Squared Error

42. ROI - Region of Interest

43. RTK - Real-Time Kinematic

44. SAM - Segment Anything Model

45. SfM - Structure-from-Motion

46. SGD - Stochastic Gradient Descent

47. SLAM - Simultaneous Localization and Mapping

48. SOR - Statistical Outlier Removal

49. SW - Shifted Window

50. Swin T - Swin Transformer

51. SZ DJI - Shenzhen DJI (Company Name)

52. TLS - Terrestrial Laser Scanning

53. TRV - Tree Row Volume

54. UAV - Unmanned Aerial Vehicle

55. UGV - Unmanned Ground Vehicle

56. UI - User Interface

57. USD - United States Dollar

58. USDA - United States Department of Agriculture

59. VHSR - Very High Spatial Resolution

60. ViT - Vision Transformer

61. VLP-16 - Velodyne-16

62. WMSA - Window-based Multi-Head Self-Attention